Operational Modal Analysis, Model Updating and Response Prediction Bridge under the 2014 Napa Earthquake

by

Omar Alcazar Pastrana

BEng, Universidad Popular del Estado de Puebla, 2012

A THESIS SUBMITTED IN PARTIAL FULFILLMENT OF

THE REQUIREMENTS FOR THE DEGREE OF

MASTER OF APPIELD SCIENCE

in

THE FACULTY OF GRADUATE AND POSTDOCTORAL STUDIES

(Civil Engineering)

THE UNIVERSITY OF BRITISH COLUMBIA

(Vancouver)

September 2016

Abstract

Bridges constitute a critical and important part of the infrastructure of many cities' transportation network. They are expensive to build and maintain, and the consequences of a sudden failure are very severe. Therefore, bridges are expected to have a high degree of reliability, which means that they have to perform above a life safety criterion under earthquake excitations. In a continuous effort to improve design guidelines, it is imperative to understand the behavior of existing bridges that are subjected to severe shaking. For this reason, continuous monitoring of bridges has become essential: not only to help determine if a bridge has been damaged but also to understand their response to strong earthquake motions.

The work reported here includes an in-depth analysis of the behavior of the Vallejo- Hwy 37 Napa River Bridge during the 2014 California, Napa earthquake (M 6.0). The bridge located in Vallejo California connects Sears Point Road and Mare Island to Vallejo. It was built in 1967. The bridge was instrumented with 12 accelerometers on the superstructure and 3 accelerometers at a free-field site. An analysis of the recorded data of the accelerometers on the superstructure was carried out to determine the maximum displacement at mid-span, and to get the fundamental frequencies of the bridge during the excitation. A finite element (FE) model was developed based on the as-built drawings and model updaitng was perform. Finally, the updated model was used with the recorded ground motion of the 2014 Napa Earthquake to perform a time history analysis. The results were compared to the recorded data of the sensors located on the bridge. The peak displacement at mid-span in the longitudinal and transverse directions of the FE had a good match to the recorded peak displacement. It can be concluded that the updated FE model can capture the peak displacement at the bridge mid-span. It also shows that having a strong

motion network can help engineers to better understand the behavior of structures under earthquake loading, by looking at the recorded data and identifying peak values of acceleration, velocity and displacement.

Preface

The research presented here was completed by Omar Alcazar-Pastrana under the supervision of Dr. Carlos Ventura and Dr. Anoosh Shamsabadi. The literature review, model development and analysis were done by the author.

Part of Chapter 3 was presented at the 5th Tongji-UBC Symposium on Earthquake Engineering in Shanghai China, in May 2015. All the analysis work was done under the supervision of Dr. Carlos Ventura and Dr. Anoosh Shamsabadi. The complete findings of Chapter 5 will be published and presented at the 8th International Operational Modal Analysis Conference in May 2017.

Table of Contents

List of Tables

List of Figures

Acknowledgements

First and foremost, I would like to thank my supervisor Dr. Carlos Ventura for his guidance, encouragement and support. He has a great passion for innovations in earthquake engineering problems. I would also like to thank Dr. Anoosh Shamsabadi for his mentoring and guidance during this research. He has great knowledge and passion in bridge engineering, and motivated me during this project.

I would like to also thank all the EERF team and Dr. Carlos Ventura research group for all their help. In particular I would like to thank Dr. Yavuz Kaya and Mr. Felix Yao for providing technical support and valuable input into my research.

I would also like to thank my family, friends and especially my wife Veronica Simpon-Montero. I would have not been able to complete this master's without her support and encouragement. She has always been my motivation and inspiration.

Finally, I would like to thank al Consejo Nacional de Ciencia y Technologia (CONACYT) for partially funding this master's.

Dedication

To my wife

Chapter 1: Introduction

Long-span bridges are a critical part of a city's transportation systems, and they are essential in the economic growth and development of many cities. Therefore, they should have a high degree of reliability (Chen Y., 1996). If a sudden earthquake hits a city and damages its bridges, leading to bridge closures, neighboring cities would see economic hardship. Many cities have implemented multi-phase assessment procedures for long-span bridges. These procedures are not only focused on meeting live safety criterion (no collapse), but seek to meet better performance objectives, such as post-earthquake functionality for emergency routes and life-line bridges (Caltrans, 2015). In order to meet better performance criteria, it is imperative to understand the behavior of bridges during severe shaking. For this reason, continuous monitoring of bridges has become essential: not only to detect the damage on the bridge, but also to have a more profound understanding of the bridge response to earthquake loading.

On August 24 2014, a magnitude 6.0 earthquake hit the city of Napa and nearby cities. The earthquake caused some minor damage to the infrastructure network in the region. In Vallejo, California, the Hwy 37 Napa River Bridge is located about 11 km off the epicenter (CESMD, 2014). The bridge was built in 1967. It connects Sears Point Road and Mare Island to Vallejo in California. The bridge consists of 33 spans of precast girders supported on flexible 2-column piers and stiff 4-column piers. The bridge had rocker bearings at the expansion joints.

The bridge was retrofitted in 1996. The columns were encased in steel jackets to improve their ductility. The foundations were retrofitted by enlarging the pile caps and by adding more pile to the foundations. To improve the continuity of the bridge deck, bolsters around the end of

the diaphragms were added, as well as transverse prestressing with pipe seat restraints at the hinges.

In 2001, the bridge was instrumented with strong motion sensors. They consist of 12 accelerometers on the bridge deck and 3 accelerometers free-field in a geotechnical array that records the bridge acceleration and the ground acceleration respectively.

A detailed investigation of the response of the HWY 37 Napa River Bridge to the 2014 M6.0 Napa earthquake has been conducted by the author of this thesis. Given the limitations of the instrumentation, the dynamic characteristics of the bridge were obtained. These characteristics were used to conduct model updating to a finite element model developed using the bridge's as-built drawings. Eventually, the model was subjected to the recorded motion of the earthquake to simulate the peak displacements of the recorded data from the sensors located on the bridge deck.

1.1 Scope

A finite element model was developed to predict the maximum displacements recorded during the 2014 M6.0 Napa earthquake in California. It is acknowledged that the total response of the bridge may be captured with this finite element model. However, Caltrans guidelines specified that seismic analysis should capture the maximum displacements at distinct locations on the bridge deck. To have a better prediction of the entire recorded data a more refined model should be developed, which is beyond the scope of this work.

1.2 Motivation

Structural health monitoring has become an important tool for transportation networks to understand the response and behavior of bridges during their lifetime, especially during earthquakes in high seismic areas. Recognizing the importance of health monitoring, the California Department of Transportation (Caltrans) and the California Geological Survey (CGS) have developed a strong motion program for bridges for over 40 years (Hipley and Huang, 1997). This was started after some major earthquake events in the 1970s, where many bridges that were built in the 1960s suffered damage. Caltrans had to repair, retrofit and begin to instrument their bridges with strong motion sensors. The strong motion instrumentation consisted of implementing sensors on bridges. These sensors were located on the superstructure, bents caps, bottom of the columns, pile caps and pile foundation to capture the kinematic response of the support elements, along with the dynamic response of the entire superstructure of a bridge (CSMIP, 2012). All this instrumentation depended on the complexity of the bridge and its pile foundation. It is important to note that not all long-span bridges have this detailed instrumentation. Some bridges are partially instrumented and do not possess sensors at the base of the columns, pile caps and pile foundation. Such is the case for the Hwy 37 Napa River Bridge that connects Sears Point Road and Mare Island to Vallejo, California.

The Hwy 37 Napa River Bridge is located in Vallejo, California, 11km away from the epicenter of the M6.0 2014 Napa earthquake. The bridge is approximately 999 m (3230 ft.) long with 33 spans of precast I-girders supported on flexible 2-column piers and stiff 4-column piers. It has 12 strong motion sensors at the bridge deck and 3 sensors in a geotechnical array. However, the bridge has limited sensors as only half of the bridge is instrumented. These

limitations may not provide enough data to conduct a full system identification to obtain accurate mode shapes of the entire bridge. Furthermore, the sensors are all located on the superstructure and none one of them at the substructure. The lack of data at the base of the columns and at the pile caps brings about the challenge of what input motion can be used in a finite element model to simulate the bridge behavior under earthquake conditions.

Based on the previously mentioned limitation, a finite element model of the bridge was developed that could give a better understanding of the dynamic characteristics of the bridge during the 2014 Napa earthquake – a model that captures the peak displacement of the bridge deck during severe earthquake shaking. Ideally, the model needed to incorporate the contribution of the foundation and the nonlinearities of the structure elements. This is not incorporated in the finite element developed, but opens up further research that goes beyond the work done for this thesis project.

1.3 Purpose of the Study

The goal of this research is to develop a realistic finite element model of the Hwy 37 Napa River Bridge using Caltrans 2015 Seismic guidelines that can help engineers understand the bridge behavior during seismic events. This is achieved through:

- a detailed investigation of the recorded data during the 2014 M6.0 Napa earthquake in California
- conducting Preliminary Fourier Analyses of the recorded data
- conducting the system identification of the bridge using the recorded data of the 2014 Napa earthquake and different identification techniques;

- developing a finite element model that captures the peak displacements of the recorded data of the 2014 Napa earthquake
- creating a benchmark model of the bridge with the program CSI Bridge 2016 (Computer and Structures Inc. 2016)
- correlating the recorded data and the finite element model
- identifying the sensitivity of parameters such as column stiffness, girder mass and stiffness of the elastomeric bearings of the finite element model
- calibrating the finite element model to identified properties of the recorded data by modifying the dynamic properties of the FE model
- response-predicting the peak displacement of the deck at the sensor location of the bridge subjected to the 2014 Napa earthquake.

1.4 Thesis Outline

This section provides a brief description of the content that is included in each chapter.

Chapter (2): includes a literature review of system identification techniques, previous model updating studies and Caltrans guidelines for seismic analysis and design. The two main system identification techniques presented are Enhanced Frequency Domain Decomposition and Stochastic Subspace Identification. Chapter 2 shows what the bases of the techniques are and how they differ from each other. Similarly, previous model updating studies are summarized. It shows the range of techniques used and the purpose of the updating in each case. Finally, a description of the seismic guidelines provided by Caltrans in bridge modeling and design are presented. It shows what analysis techniques are acceptable and how to carry them out.

Chapter (3): presents a description of the Hwy 37 Napa River Bridge. This chapter describes the main structural components of the bridge, its location and its seismic region. It presents how the bridge is instrumented by California's strong motion network. It describes how the finite element model was developed.

Chapter (4): describes the system identification of the bridge. First, a preliminary Fourier analysis is performed on the data recorded during the 2014 Napa earthquake to identify the dominant frequencies of the bridge deck. Then, using the Enhanced Frequency Domain Decomposition and the Stochastic Subspace Identification techniques, the structural frequencies and damping are identified.

Chapter (5): presents the FE model updating and the acceleration, velocity and displacement comparison between the recorded data during the 2014 Napa earthquake and the FE model prediction. First, the developed FE model is compared to the identified mode shape and frequencies to determine if any model updating is needed. Second, sensitivity studies are performed on the column stiffness, girder mass and equivalent stiffness of the elastomeric bearing to understand how these properties affect the dynamic properties of the bridge. Model updating is then performed to match the modal frequencies. Finally, using the recorded ground motion data from the 2014 Napa earthquake and the updated finite element model, the peak displacements of data recorded by the sensors at mid-span are compared with the results provided by the FE model.

Chapter (6): presents a summary of the research findings and the recommendation for possible future work.

Chapter 2: Literature Review

2.1 Overview

In this chapter a literature review is presented on the modal identification techniques implemented in this research. It also presents some similar studies to this research done previously. Finally, it summarizes Caltrans' guidelines for modeling of bridges.

2.2 System Identification Techniques

In this section two important system identification techniques are discussed, the Frequency Domain Decomposition (FDD) and the Stochastic Subspace Identification (SSI) techniques. The FDD technique analyzes data in the frequency domain, while the SSI processes data in the time domain. The techniques are only briefly described, as their complex mathematics are beyond the scope of this research.

2.2.1 Frequency Domain Decomposition and Enhanced Frequency Domain Decomposition

Frequency Domain Decomposition (FDD) was introduced by Brincker, Zhang and Andersen (2000). It is an extension of the classical frequency domain approach often referred to as the peak picking technique or the Basic Frequency Domain (BFD) technique. The technique uses singular value decomposition to decompose the power spectral density function matrix. This allows one to decompose the spectral response into a set of single degree of freedom systems, which correspond to individual modes.

To identify the power spectral density function around the peak, a comparison between the singular vector frequencies around the peak and the mode shape estimate was performed. As long as the mode shape estimate and the found singular vector have a high Modal Assurance Criteria (MAC) value, the corresponding singular value belongs to a single degree of freedom density function. MAC values correlate the shape of two modes to determine their relation (Pastor, Binda and Harcarik, 2012). Figure 2.1 shows an example of a singular value power density plot of a two-story building (Brincker, Zhang and Anderson, 2000). The robustness of this technique allows it to be used for different applications. Large peaks appear on the plots to indicate the identified mode shape. The simplicity allows for intuitive use of the technique.

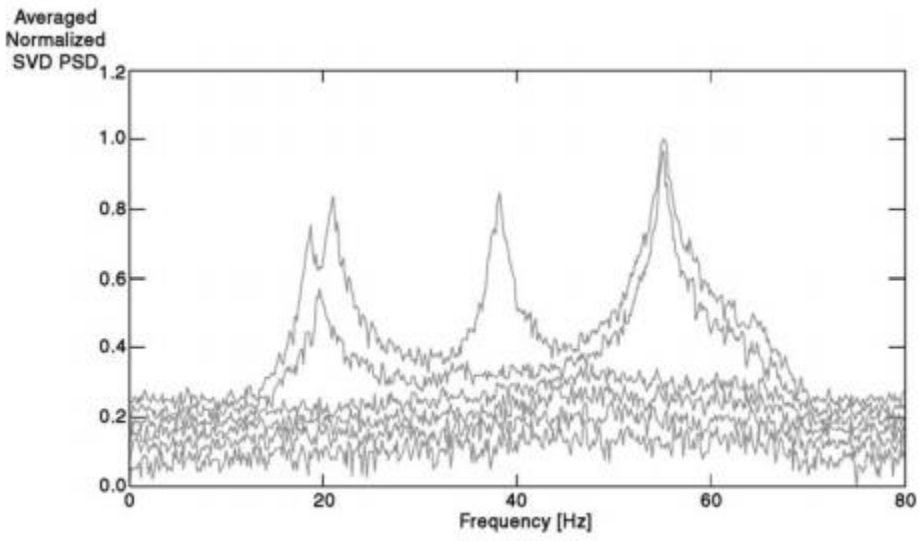

Figure 2.1 Singular value power spectral density plot example (Brincker, Zhang and Andersen 2000)

Enhanced Frequency Domain Decomposition (EFDD) is an extension of the FDD technique that gives an improved estimate of the modal shapes and frequencies of a system,

including damping. It allows for identifying harmonic components close to modal frequencies, thereby having a more accurate estimate (Jacobsen, Andersen and Brincker, 2006).Figure 2.2 shows the identified harmonic component using linear interpolation. The EFDD Technique is used in this research.

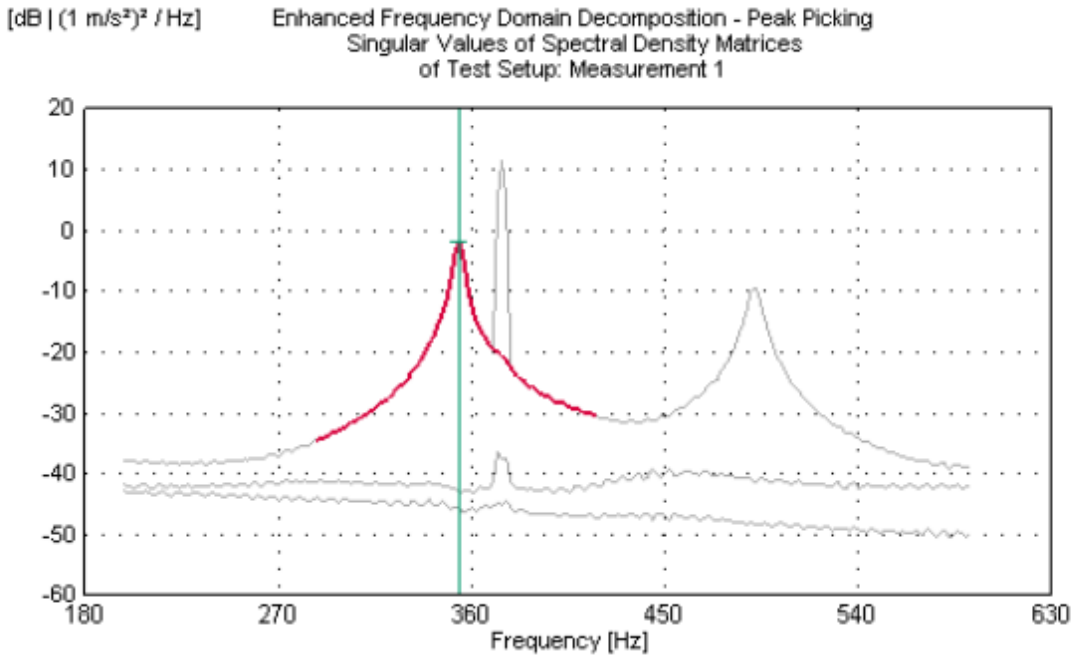

Figure 2.2 Example of a harmonic component removal by linear interpolation of an SDV plot (J. Jacobsen, P. Andersen and R. Brinker, 2006)

2.2.2 Stochastic Subspace Identification

Stochastic Subspace Identification (SSI) is one of the most powerful techniques for analyzing data in the time domain (Brincker and Andersen, 2006). It identifies mode shapes using the time domain data. The technique takes the time series data and fits it to a parametric model to correlate the predicted response and the measured response. This is done by choosing

the number of state space models that then select the number of parameters of the parametric model. It is important to have a balanced state space, not to be too large or too small. Once the model order is chosen, the eigenvalue for each state space is shown in a stabilization diagram (Brincker and Andersen, 2006). Figure 2.3 shows an example of a stabilization diagram with a y-axis showing the dimensions of the available state space model and an x- axis representing the frequency values.

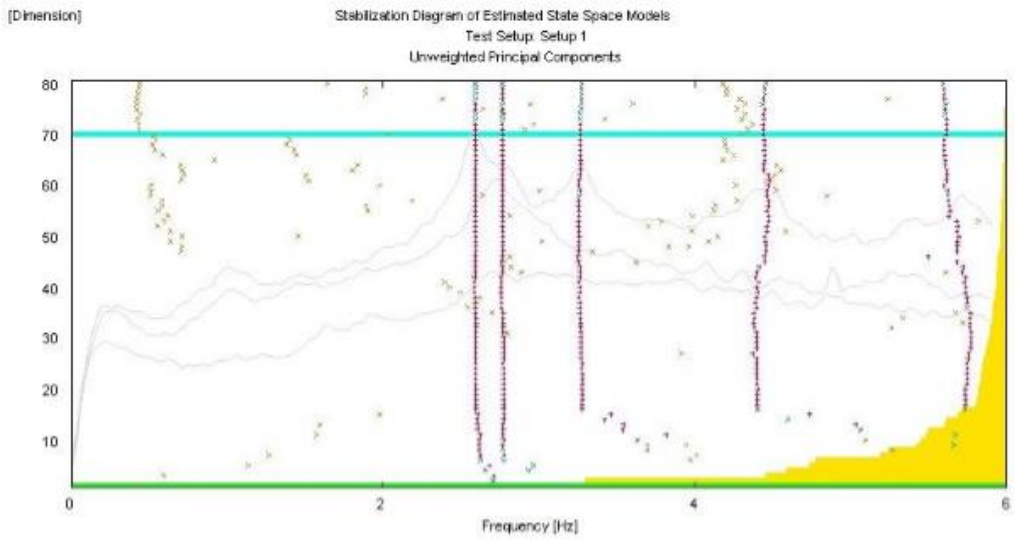

Figure 2.3 Example of stabilization diagram, SSI technique (ARTeMIS, 2016)

The stabilization diagram is meant to capture repeated trends of the state space model that can represent a structural model at resonance frequency. In order to have good results, the user needs to make judgments on how to set the stabilization criteria. Usually these criteria involve damping ratio, MAC between two state space models or maximum deviation of frequency. This would allow for distinction between stable, unstable and noise modes. For a detailed explanation of this technique see Brincker and Andersen (2006).

2.3 Literature of Model Updating

Model updating has been implemented in many civil engineering structures, such as buildings, towers, dams, bridges, steel frame and reinforced concrete structures. It has been around for many years, since the early 1970s (Mottershead and Friswell, 1993). The main purpose of model updating is to judiciously modify the mass, stiffness, damping parameter, boundary condition and modulus of elasticity of a numerical model in order to get a good comparison between experimental results. Modifying these structural parameters that have physical significance is the preferred route (Brownjohn and Xia 2000).

Most model updating studies focus on modifying material properties such as the modulus of elasticity and mass density. Sevim, Bayraktar and Altunisik (2009) conducted model updating to a concrete arch dam by manually modifying the modulus of elasticity and mass density parameters. They were able to calibrate eight mode shapes of the dam. Alves and Hall (2006) also manually updated an arch dam to calibrate it using earthquake records and force vibration test records. They modified the modulus of elasticity of concrete and rock until a good calibration of the first two mode shapes was obtained. Arslan and Durmus (2013) updated a model of an in-filled reinforced concrete frame by modifying the modulus of elasticity and mass density of the concrete, rebar and brick. They were able to reduce frequency errors from 39% to 8%. Ribeiro et al (2012) performed model updating of a bowstring-arch railway bridge using a genetic algorithm. By modifying the modulus of elasticity and mass density of the concrete and steel, they were able to reduce frequency to 3% compared to the experimental data. Ventura et al (2001) performed an automated model updating procedure to a 15-story reinforced concrete

shear wall building. The modulus of elasticity, mass density, moment of inertia of the columns and cladding thickness were updated to get good matching results to experimental test data.

Different researchers have published different model updating techniques. J. Garcia-Palencia (2008) implemented a frequency response function model-updating algorithm to address the issue of the assessment of bridges. He applied his method to a lab specimen and to a full-scale test. Yang and ZhongDong (2012) updated a prestressed concrete bridge averaging a 5% error between experimental and numerical frequencies using a fuzzy finite element method, in which the updating parameters were deemed fuzzy-variables.

Model updating has been also used for damage detection applications. In 2004, Teughels and De Roeck updated a prestress concrete bridge to localize the damage on the bridge if settlement in the foundation occurred. They lowered the piers at the desired location and were able to quantify and localize the damage in the simulation. Jie, ZhouHong and FuPeng (2015) identified cracking severity and location in the Xinyihe Bridge, by using response surface model updating and an energy damage index. In 2014, Türker and Bayrakta detected damaged members of a reinforced concrete building by correlating the first three mode shapes and by varying the moment of inertia.

Some studies compared the seismic response of structures before and after model updating. Bayraktar, Can Altunisik et al (2009) investigated the effect of running a seismic analysis before and after updating an arch-type steel footbridge. They found that the principal stresses decreased and the maximum displacement increased after model updating was

performed. Bayraktar, Sevim, et al (2010) investigated the effect of fluid-structure interaction under earthquake loading on a storage tank by updating the modulus of elasticity. It was found that the principal stress remained about the same while the displacement increased after the update. Sevim, Bayraktar and Can Altunisik et al (2011) built two finite element models of a masonry arch bridge in ANSYS to compare the response under earthquake loading before and after updating. They found that after model updating was conducted, the principal stresses were much lower than the original model. This shows an over-estimation of the un-calibrated model in line with engineering practice.

Similarly, Altunisik and Bayraktar (2014) studied the structural performance (forces, displacements and stress) of the Birecik Highway Bridge in Turkey. They applied only one ground motion and found a 20-30% reduction in displacement and forces with respect to the un-calibrated model. These results may not be as reliable since only one ground motion was used. It would have been a better approach if a whole set of different ground motions were implemented, because this would capture a better range of frequencies and more conclusions could have been observed. Similarly, McDonald (2016) conducted model updating of the Port Mann cable-stayed bridge in Canada, to compare the response under different ground motions (crustal, subcrustal and subduction) before and after updating. He found differences in the response quantities depending on the scale motion used. The displacement was found to increase to 79% at mid-span under the Chi Chi ground motion compared to the original model, with only a 0.2% decrease in displacement using the Olympia scale motion.

There are some studies done with large-scale bridges. Turek, Ventura, and Dascotte (2010) performed model updating to the Ironworkers Memorial Second Narrows Bridge. They

updated the bridge in several steps, both manually and automated. The longitudinal stiffness of the bearings was first updated to match the second frequency. Then, the modulus of elasticity and the moment of inertia of various trusses were updated until good results were obtained. Similarly, Hao Wang et al (2010) conducted model updating to the Runyang suspension bridge in China. They performed the updating in two phases, done during the two phases of construction on the bridge.

There is little research for nonlinear effects of model updating. El-Borgi et al (2008) conducted a study where he proposed a methodology for structural assessment using finite model updating and nonlinear analysis for reinforced concrete bridges. The methodology is then proven with a case study of an eight-span concrete bridge.

There have been some studies where model updating is used to calibrate the FE models to strong motion data. Taylor (2007) performed model updating to the Marga Marga Bridge in Chile. He used the recorded data from earthquakes in 2004, 2005 and 2006 to identify the mode shapes and frequencies of the bridge and calibrate them for a linear elastic finite element model in SAP2000. Once the model was calibrated to the obtained frequencies, time history analyses of the ground motions were carried out. It was observed that the peak displacement of the bridge deck at different locations had a good match to the recorded transverse displacements and not so good for the longitudinal direction, where there was a 43% error between the recorded data and simulated results. This error could be contributed to the simplification of the linear model and the fixed foundation used for modeling. In 2013, Vanegas-Bravo conducted a similar study to the Marga Marga Bridge. He calibrated a linear and nonlinear model to the recorded data on the

Marga Marga Bridge during the 2010 El Maule earthquake. He modeled the bridge in OpenSees, where he used fiber sections for the columns and linear elements for the steel girder beams, modeled the bridge bearings nonlinearly and assumed a fixed foundation. Once the models were updated, he ran nonlinear time history and compared the deck displacements to the recorded displacement during the 2010 El Maule earthquake. It was observed that the bridge underwent nonlinear behavior. For this reason, the nonlinear model gave a better representation of the behavior of the bridge during the earthquake. On the other hand, the linear model overestimated the displacements of the bridge deck. It was also noted that the bridge required better instrumentation to obtain more data for better calibration purposes.

Taciroglu, Shamsabadi et al (2014) did another study where model updating was conducted on the Eureka-Samoa Channel Bridge. The bridge was updated with ambient vibration surveys and recorded data from weak and strong earthquakes. The finite element model included the contribution of the foundation by modeling it with springs. Two types of model were used: a direct model, where the pile foundations and the soil were modeled with springs with the respective p-y curves; and an indirect model, created by reducing the stiffness matrices of the foundation for computational time efficiency. The two models were subjected to the recorded motion at the pile tips for the 2007, 2010 and 2014 Ferndale earthquakes, the 2008 Willow Creek earthquake and the 2008 Trinidad earthquake. The results of the model updating showed a good match of the peak displacement at mid-span of the bridge for the all recorded earthquakes. It was also observed that the model with reduced foundation matrices gave good results. However if better results were desired, the direct model that included all the foundation and soil springs should be used.

When doing model updating it is important to do it with caution, until it can truly be physically validated (Atamturktur and Laman, 2012). Modifying model parameters of a finite element model needs to be realistic, in order to avoid unrealistic mass and stiffness matrices.

2.4 Caltrans Seismic Design Criteria (2015)

An overview of the seismic analysis requirements implemented by the California Department of Transportation (Caltrans) is presented here. Important clauses are directly quoted from the guidelines, as the correct wording is desired. According to the minimum requirements of the Seismic Design Criteria (SDC), ordinary bridges should remain standing but can suffer sufficient damage for the design earthquake. The following sections and criteria of the SDC should be used to represent the seismic demands.

2.1 Ground Motion Representation

For structural applications, seismic demand is represented using an elastic 5% damped response spectrum. In general, the Design Spectrum (DS) is defined as the greater of:

(1) a probabilistic spectrum based on a 5% in 50 years probability of exceedance (or 975-year return period);

(2) a deterministic spectrum based on the largest median response resulting from the maximum rupture (corresponding to MMax) of any fault in the vicinity of the bridge site;

(3) a statewide minimum spectrum defined as the median spectrum generated by a Magnitude 6.5 earthquake on a strike-slip fault located 12 km from the bridge site.

A detailed discussion of the development of both the probabilistic and deterministic design spectra as well as possible adjustment factors is given in Appendix B.

The analysis objectives of the SDC are used only to assess the force and deformation demands of the structural system and components of Ordinary Standard Bridges. Equivalent static analysis and linear dynamic analysis are sufficient enough to predict the displacement demands of these types of bridges. Similarly, a static nonlinear analysis is sufficient to predict the deformation capacities of the bridge components. These analyses are described in SDC in its corresponding section, as follows:

5.2.1 Equivalent Static Analysis (ESA)

Equivalent Static Analysis (ESA) can be used to estimate displacement demands for structures where a more sophisticated dynamic analysis will not provide additional insight into behavior. ESA is best suited for structures or individual frames with well-balanced spans and uniformly distributed stiffness, where the response can be captured by a predominant translational mode of vibration.

The seismic load shall be assumed as an equivalent static horizontal force applied to individual frames. The total applied force shall be equal to the product of the ARS and the tributary weight. The horizontal force shall be applied at the vertical center of mass of the superstructure and distributed horizontally in proportion to the mass distribution.

In this analysis method, the initial stiffness of each bent is obtained from a pushover analysis of a simple model of the bent in the transverse direction or a bridge frame in the longitudinal

direction (abutment stiffness is included in the model). The initial stiffness shall correspond to the slope of the line passing through the origin and the first structural plastic hinge on the force–displacement curve. The bent and/or frame stiffness is then used to obtain the period $T=0.32\sqrt{(K/W)}$ (where W is the weight in kip and K is the stiffness in kip/in) in the transverse and longitudinal directions, respectively. The displacement demand corresponding to the period in each direction is then obtained from the design response spectrum.

5.2.2 Elastic Dynamic Analysis (EDA)

Elastic Dynamic Analysis (EDA) shall be used to estimate the displacement demands for structures where ESA does not provide an adequate level of sophistication to estimate the dynamic behavior. A linear elastic multi-modal spectral analysis utilizing the appropriate response spectrum shall be performed. The number of degrees of freedom (DOF) and the number of modes considered in the analysis shall be sufficient to capture at least 90% mass participation in the longitudinal and transverse directions. A minimum of three elements per column and four elements per span shall be used in the linear elastic model.

In this analysis method, the normalized modal displacements at each DOF are multiplied by participation factors and spectral responses. These products are summed together using the Complete Quadratic Combination 3 (CQC3) method [23] – see Section 2.1.2-1 – or the Square Root of Sum of Squares (SRSS) procedure to obtain the maximum response at each DOF. The CQC3 method is preferred to the SRSS method for practical bridge design because it is a more computationally efficient way of finding the maximum response at each DOF.

Elastic Dynamic Analysis based on design spectral accelerations will likely produce stresses in some elements that exceed their elastic limit. However, it should be noted that EDA is used in the present context for purposes of estimating the demand displacement and not the design forces.

Sources of nonlinear response that are not captured by EDA include the effects of the surrounding soil, yielding of structural components, opening and closing of expansion joints, and nonlinear restrainer and abutment behavior. EDA modal results shall be combined using the CQC3 method.

Multi-frame analysis shall include a minimum of two boundary frames, or one frame and an abutment beyond the frame under consideration.

5.2.3 Inelastic Static Analysis (ISA)

Inelastic Static Analysis (ISA), commonly referred to as "push over" analysis, shall be used to determine the reliable displacement capacities of a structure or frame as it reaches its limit of structural stability. ISA shall be performed using expected material properties of modeled members. ISA is an incremental linear analysis, which captures the overall nonlinear behavior of the elements, including soil effects, by pushing them to initiate plastic action. Each increment pushes the frame laterally, through all possible stages, until the potential collapse mechanism is achieved. Because the analytical model accounts for the redistribution of internal actions as components respond inelastically, ISA is expected to provide a more realistic measure of behavior than can be obtained from elastic analysis procedures.

These guidelines were used to develop the linear elastic model of the Hwy 37 Napa River Bridge. They provide the type of analysis that can be performed on the model in this work.

However, these analyses may not be sufficient to model more complex components of the bridge and a nonlinear time history analysis is necessary, which is beyond the scope of this study.

Chapter 3: Hwy 37 Napa River Bridge Background

3.1 HWY 37 Napa River Bridge Background

The Hwy 37 Napa River Bridge is located in Vallejo, California (38.1205°N, 122.2801°W) connecting Sears Point Road and Mare Island to Vallejo (Figure 3.1). The bridge is approximately 999 m (3230 ft) long and 20.3 m (67 ft) wide. Figure 3.2 shows an elevation view of the bridge. It was constructed in 1967 and in 1996 an extensive retrofit program was implemented after the 1989 Loma Prieta earthqauke.

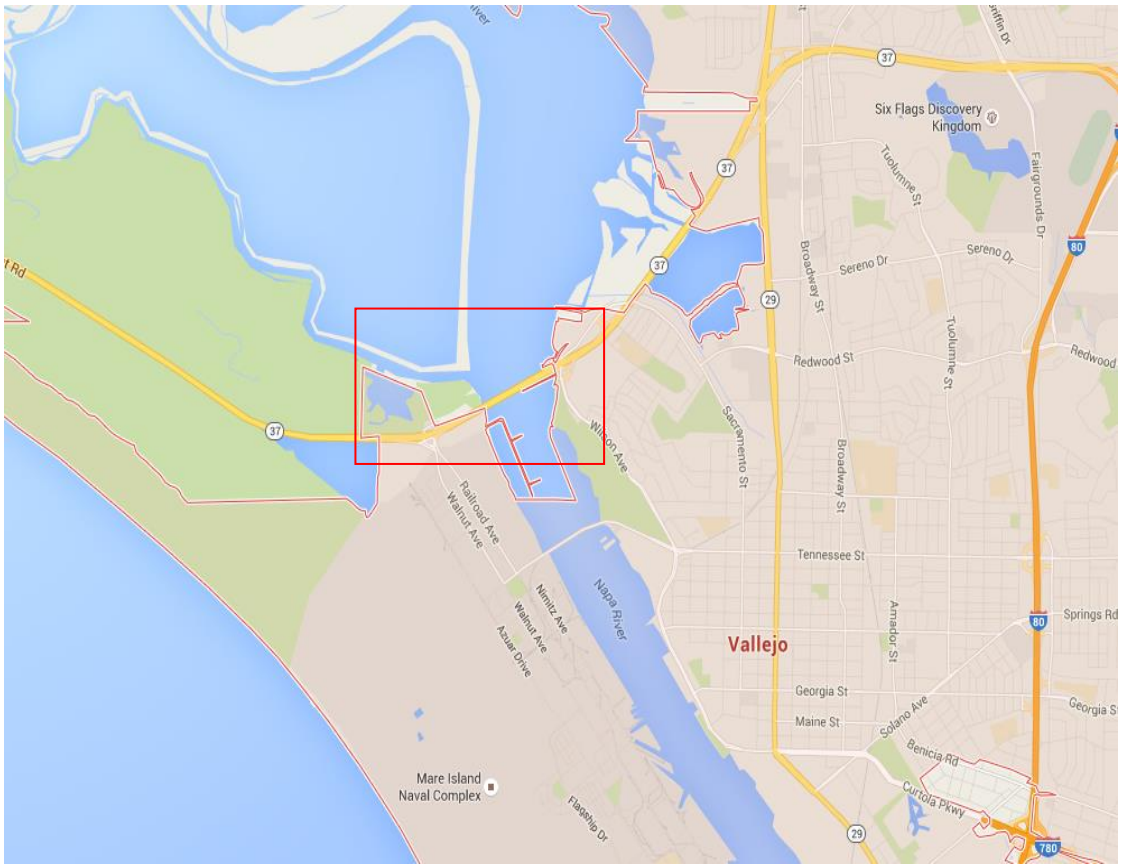

Figure 3.1 Satellite view of the location of the HWY 37 Napa River Bridge

Figure 3.2 Napa River Bridge elevation view (solanoopenspace).

The superstructure of the bridge consists of a 6.1 in-thick (15.5 cm) concrete deck with intermediate diaphragms on 10 precast I-girders. The girders are supported on concrete bent-caps and square concrete flexible 2-column piers and stiff 4-column piers. The columns in the pier are connected through concrete beams (Figure 3.4). The bridge consists of 33 spans with a typical length span of 120 ft (366.6 m) and a main span of 188 ft (57.3 m), as shown in Figure 3.3. After the 1989 Loma Prieta earthquake the bridge was repaired extensively. The connections were not well designed, and the girders were not continuous so as to protect the superstructure and forced plastic hinging in the columns. Many girders were pulled out at the end of the diaphragms (Yashinsky et al, 2014). The Napa Bridge was retrofitted in 1996. The retrofit consisted of encasing all the columns in steel jackets, enlarging the pile cap and adding more piles to the foundations. To make the girders continuous, bolsters around the end of the diaphragms were

added, as well as transverse prestressing with seat width and pipe seat restrainers at the hinges (Yashinsky et al, 2014). Figure 3.4 shows a bridge pier before and after the retrofit.

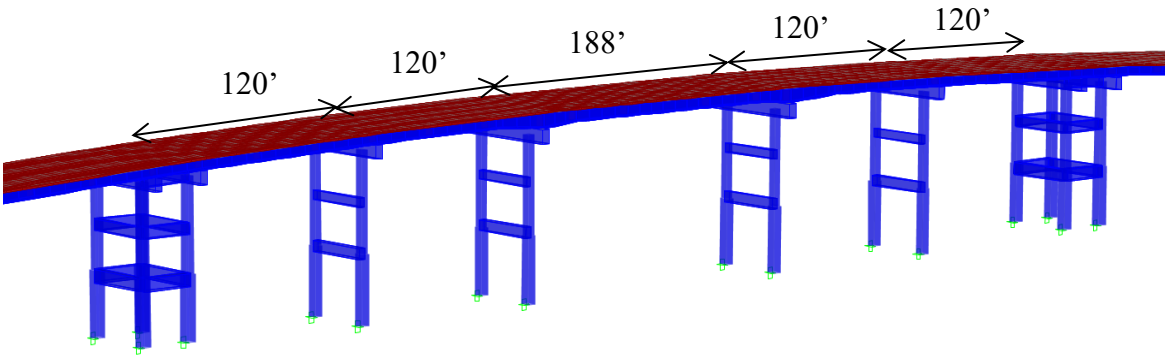

Figure 3.3 Typical and maximum span of the Napa River Bridge.

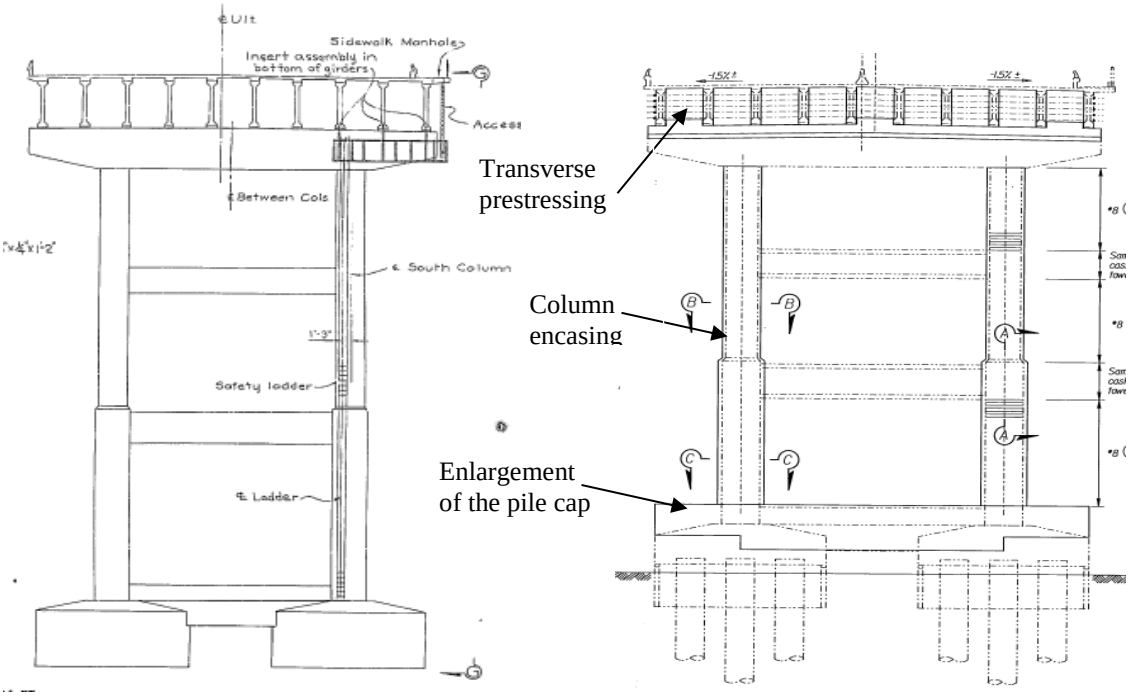

Figure 3.4 Pier Elevation as-built and retrofit case (Caltrans, 1967 and 1998).

3.2 Seismicity of the Region

The principal fault near Napa River Bridge is the San Andreas Fault. The San Andreas system contains many right-lateral strike-slip faults that form the boundary between the Pacific and North American tectonic plates (Brocher, Thomas M., et al. 2015). The movement of these plates has generated other secondary faults such as the Hayward fault and the Calaveras fault (Figure 3.5), which can cause significant earthquakes with magnitudes 6 or higher.

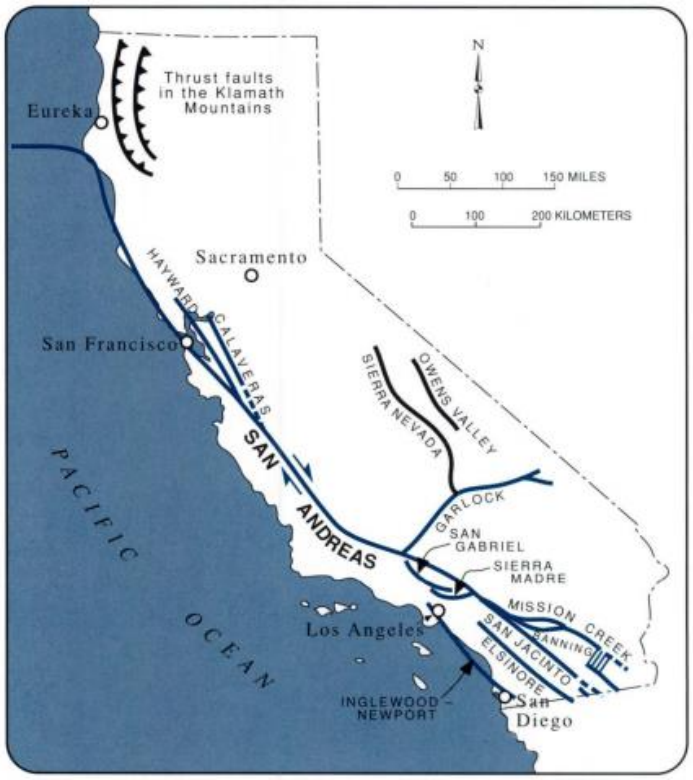

Figure 3.5 Seismicity map of California (Pridmore and Frost, 1992)

California has suffered several high intensity and high magnitude earthquakes that have severely damaged their bridge infrastructure. In 1971, the M6.6 San Fernando earthquake damaged several bridges. Similarly, the 1980 M7.2 Trinidad earthquake caused the collapse of one of the two Field's Landing Bridges and damaged other bridges. The M5.9 1987 Whittier

Narrows earthquake in Los Angeles moderately damaged existing bridges near the affected area. The 1989 M6.9 Loma Prieta earthquake occurred, causing even more damage, and in 1994 the M6.7 Northridge earthquake was observed to have caused severe damage on bridges (Chen, W. F., & Duan, L., 2014).

3.3 Instrumentation of the Napa River Bridge

The Napa River Bridge is instrumented with 12 accelerometers on the superstructure and 3 at free-field for continuous monitoring. The 12 permanent accelerometers record the acceleration at different locations and directions of the bridge deck: transverse, longitudinal and vertical directions.

Table 3.1 and Figure 3.6 show the location of the sensors along the bridge.

Table 3.1 Sensor number, location and recorded direction of the Napa River Bridge

Sensor Number	Location	Measure Direction
1	Mid-Span	Transverse (NS)
2	Mid-Span	Vertical
3	Mid-Span	Longitudinal (EW)
4	Tower 16	Vertical
5	Tower 16	Transverse (NS)
6	Pier 18	Transverse (NS)
7	Tower 20	Transverse (NS)
8	Tower 20	Longitudinal (EW)
9	Pier 23	Transverse (NS)
10	Ramp	Vertical
11	Ramp	Transverse (NS)
12	Ramp	Longitudinal (EW)

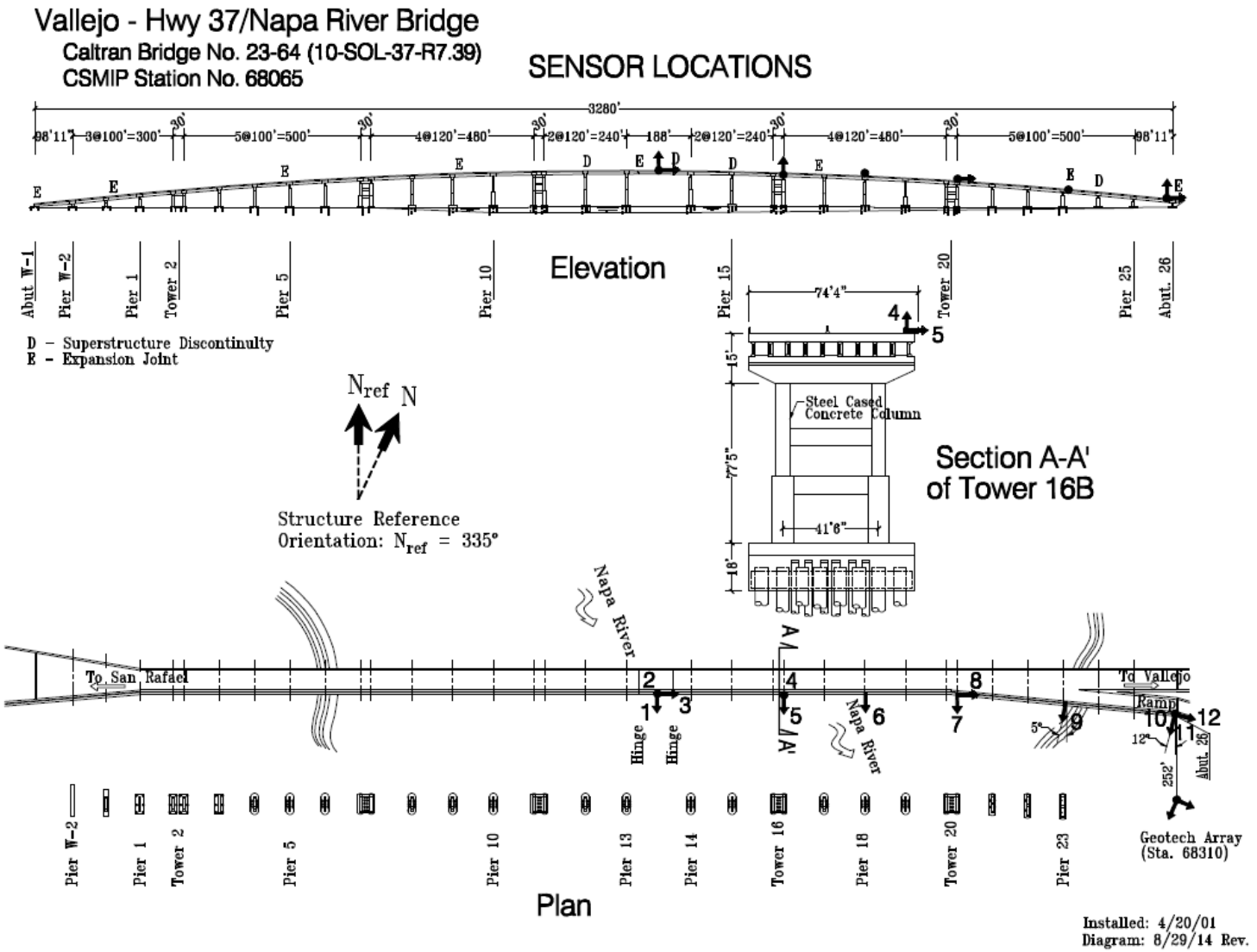

Figure 3.6 Napa River Bridge sensor layout (NCESMD)

Figure 3.6 identifies the instrumentation on the bridge. The arrows show the direction in which the sensors record data. The dots indicate that there is a sensor but its direction is vertical, or into the plane of the figure. As can be seen, only the right side of the bridge is instrumented. Sensors are located from the mid-span toward abutment 26. This is an important aspect to take into consideration when performing the system identification of the bridge. Only a few mode shapes can be extracted from the corresponding layout. Furthermore, there are no sensors located at the base of the columns, at the pile caps or in the pile foundation. By not having sensors at the different locations of the piles caps, there are no exact input motions to use in the FE model at different locations of the bridge. The primary soil conditions are soft and stiff clays throughout the length of the bridge. Based on USGS standards from pier 15 towards abutment 26 the soil can be classified as Class C, whereas from pier 14 toward abutment W-1 it can be considered as class E. This shows the importance of having more sensors located in the foundation to be able to obtain more information about how the waves propagate and are amplified at different location of the bridge.

3.4 Finite Element Model

A detailed finite element model of the Napa River Bridge with fixed foundations was created with CSI Bridge 2016 software. Using the available as-built drawings, the model is shown in Figure 3.7. A linear elastic model of the bridge was developed. To simplify the model, the exiting ramps were excluded from the modeling; only their contributed mass was added to their corresponding piers. Appendix A shows how the extra mass was calculated.

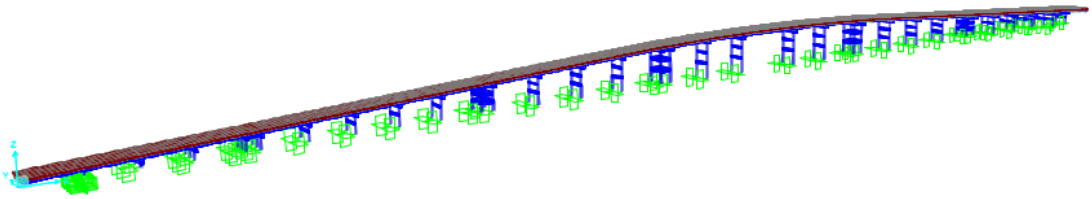

Figure 3.7 Hwy 37 Napa River Bridge model in CSI Bridge software

3.4.1 Modeling Components

The concrete elements were modeled using the specified concrete of 5,000 psi. For the base model, no modification was done to the material properties, to determine if the model needed any updating. The deck of the bridge was modeled using the bridge wizard model option in CSI Bridge. The concrete deck and precast I-girders are modeled together as shown in Figure 3.8. The concrete deck was modeled using shell elements and the I-girders were modeled with frame elements.

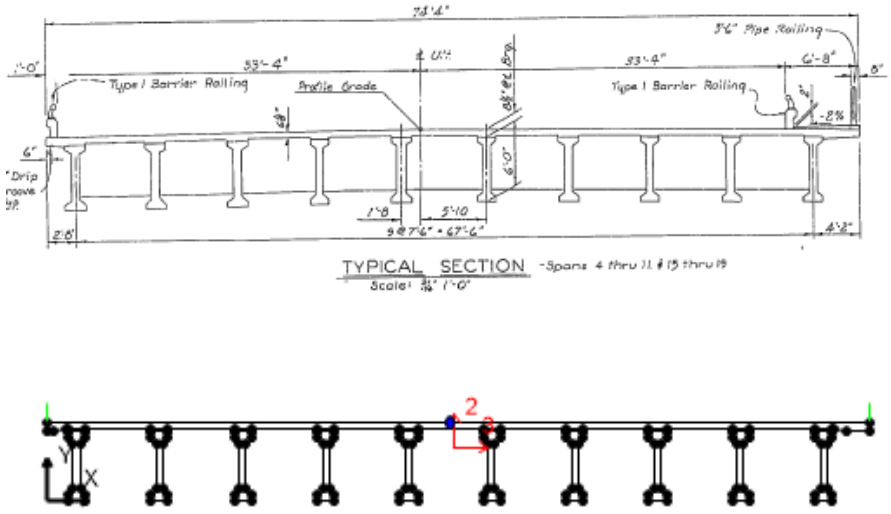

Figure 3.8 Modeling of the bridge deck compared to as-built drawings

The column piers, the bent caps and the column bents were modeled using frame elements (Figure 3.9). The columns at piers 7 to 20 have varying sections. The bottom half is noted as section 1 and the top half as section 2. Since the columns were retrofitted by encasing them in steel jackets, the column's concrete was considered as confined concrete. Steel jackets provide more confinement and more ductility to the columns (Priestly et al, 1994). A summary of the key properties used to model the bridge components are shown in Table 3.2.

Table 3.2 Values used to model the bridge components

Component	I_2 (m^4)	I_3 (m^4)	Area (m^2)	E (MPa)	Mass Density ρ(kg/m^3)	Poisson's ratio, ν
Girder	$4.6x10^{-3}$	0.18	0.46	27789.40	2.40	0.20
Bent A	0.72	1.84	3.71			
Bent B	0.49	1.36	3.14			
PW3-P6	0.23	0.36	1.85			
Section 1 P7,P11,P16,P20	0.93	0.93	3.34			
Section 2 P7,P11,P16,P20	0.45	0.45	2.32			
Section1 P8,P9,P10,P12,P13 P14,P15,P17,P18,P19	0.54	0.78	2.79			
Section2 P8,P9,P10,P12,P13 P14,P15,P17,P18,P19	0.23	0.35	1.86			
P21-P25	0.23	0.35	1.86			

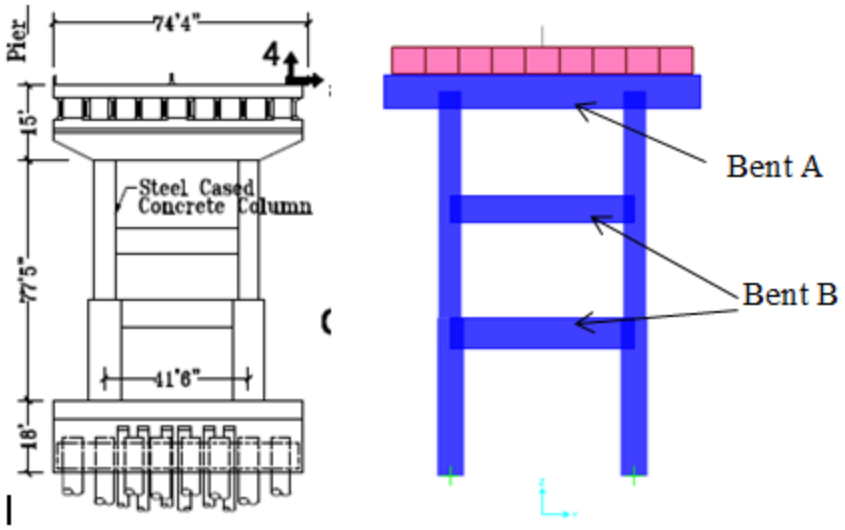

Figure 3.9 Model and as-built drawing comparison of Tower 16

The girders are supported on elastomeric bearing pads to allow movement at the expansion joints. The locations of these expansion joints are shown in Figure 3.10. These bearings were modeled with springs of equivalent stiffness, as no details of the bearing pads were obtained. For this reason, a preliminary assumption of the lateral equivalent stiffness was made. The equivalent stiffness use for the original model was 1500 KN/m for both the longitudinal and transverse directions, and fixed for the vertical direction. These values were assigned based on a previous study (Akogul, C., & Celik, O. C., 2008) of a bridge with similar bearing pad dimensions.

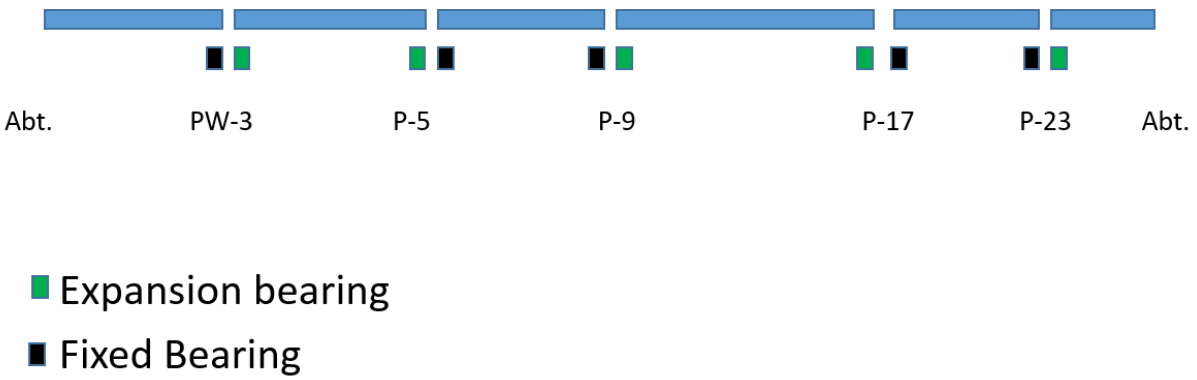

Figure 3.10 Location of the expansion joints along the bridge

At mid-span the bridge has a hinge that allows movement as an expansion joint. Based on the details of the structural drawings, the hinge was modeled as a roller. This would allow the deck to move longitudinally and rotate about three axes. Figure 3.11 shows the location of the hinge at the bridge's mid-span and its detail from the structural drawing. The abutments were modeled as pins, and the foundation was considered fixed. Modeling the foundation was beyond the scope of this study. However, remarks on the importance of including the foundation and modeling the soil with springs are noted in Chapter 5, based on the results obtained.

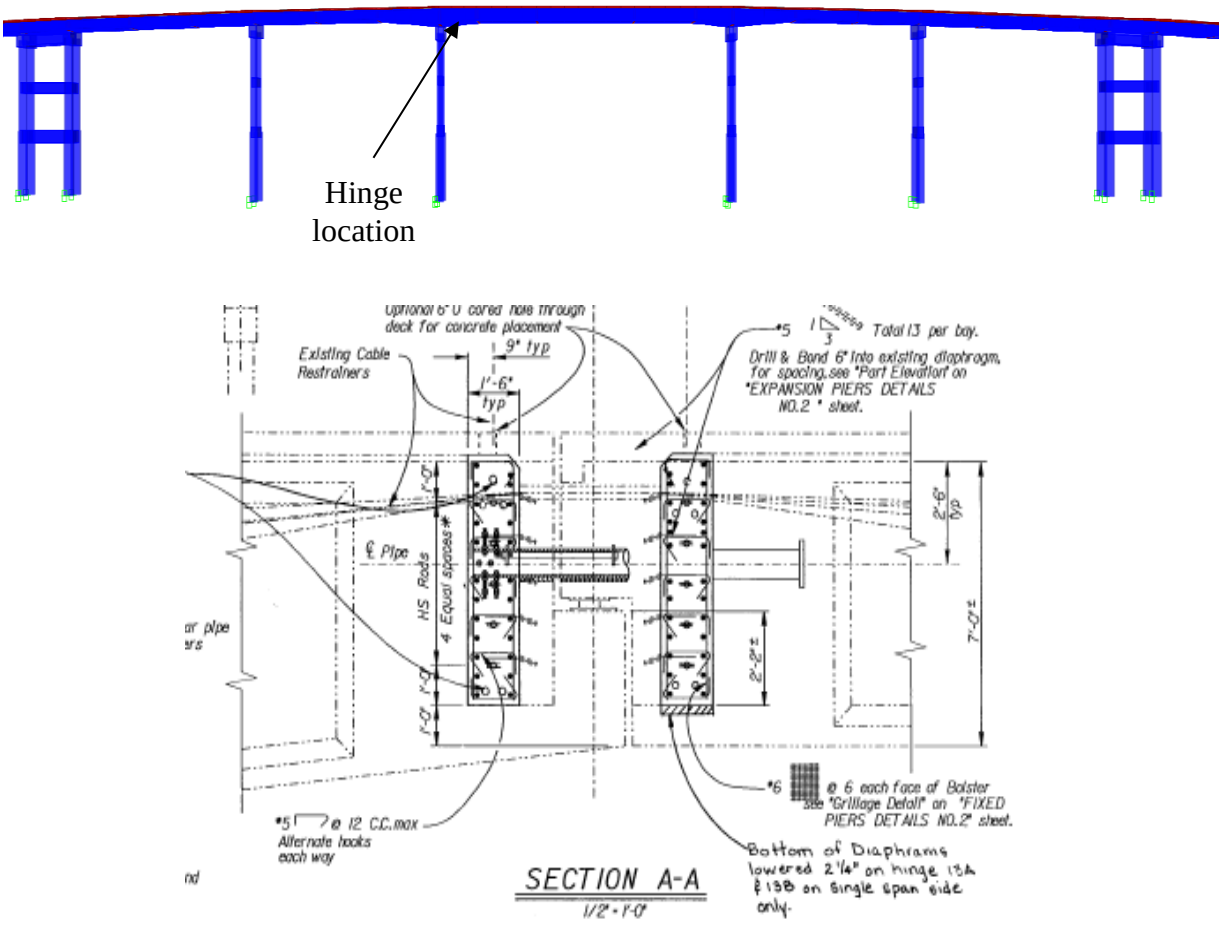

Figure 3.11 Location of the hinge at mid-span and detail from structural drawings

Chapter 4: Record Analysis of the Napa River Bridge during the 2014 Napa Earthquake

In this chapter a detailed evaluation is carried out on the records of the Hwy 37 Napa River Bridge during the 2014 Napa earthquake. In the first part the original recorded data is presented, with the observations done by an inspection team after the earthquake. This is followed by a preliminary analysis of the records gained by performing a Fourier analysis to get the modal frequencies of the bridge. Finally, a detailed system identification is carried out using the frequency domain decomposition and stochastic subspace identification techniques. The modal frequencies and mode shapes are identified to eventually perform a modal updating of the finite element model of the bridge.

4.1 Hwy 37 Napa River Bridge Recorded Data and Damage Observed after the 2014 Napa Earthquake

The recorded data by the sensor layout of the Hwy 37 Napa River Bridge during the 2014 Napa earthquake is presented here. Maximum accelerations, velocities and displacements are shown followed by the observations found by an inspection team conducting a survey of the damage suffered by the bridge during the earthquake.

4.1.1 Recorded Data by the Sensor Layout of the Napa River Bridge

On August 24 2014, a magnitude 6.0 earthquake hit the city of Napa and nearby cities in California. The Hwy 37 Napa River Bridge is located 11 km from the epicenter (USGS). The

bridge is part of the strong motion instrumentation network that Caltrans has implemented in its infrastructure. The sensors recorded the bridge acceleration and displacements at different locations of the bridge deck and geotechnical array (see Chapter 3 for sensor location). Figure 4.1, Figure 4.2 and Figure 4.3 show the acceleration, velocity and displacement records of the sensors located on the bridge, respectively. Table 4.1 shows a summary of the peak acceleration velocity and displacement of each recorded channel. The processed records were downloaded from the strong motion instrumentation database CSMIP and the data was plotted with ViewWave software (copyrighted). No modifications were made to the process records. The record of 90 seconds was obtained using a sampling rate of 100 samples per second with a frequency band of 0-100 Hz. As observed from the displacement time history records (Figure 4.3), the biggest displacement of the bridge during the earthquake occurred at the bridge's mid-span for the transverse and longitudinal directions.

In the acceleration time history (Figure 4.1) the acceleration figures do not seem to have smooth plots between 25 seconds and 35 seconds. The accelerations show a drastic change in direction when the bridge is going through the big pulse of the earthquake, suggesting that the bridge suffered damage during this pulse. This implication does not mean that the bridge had nonlinear behavior. It could have only suffered some minor damage at different locations of the bridge.

Furthermore, as observed in these time history plots, the earthquake pulse only lasts about 15 seconds, after which the bridge goes into free vibration. Using logarithmic decrement,

an estimate of bridge damping can be calculated. Through Equation 1 (Eq. 1), the damping of the bridge was calculated using the accelerations records of channels 1 and 3 respectively.

$$\zeta = \frac{1}{2\pi j} \ln\left(\frac{u_i}{u_{i+1)}}\right) \qquad \text{Eq.1}$$

Where j is the number of cycles, ui is the first acceleration or displacement at time i and ui+1 is the acceleration or displacement at time i+1. The damping of the bridge in the transverse direction was calculated to be 3.2%, and 3.8% in the longitudinal direction. These values can be compared to the damping obtained in the system identification section.

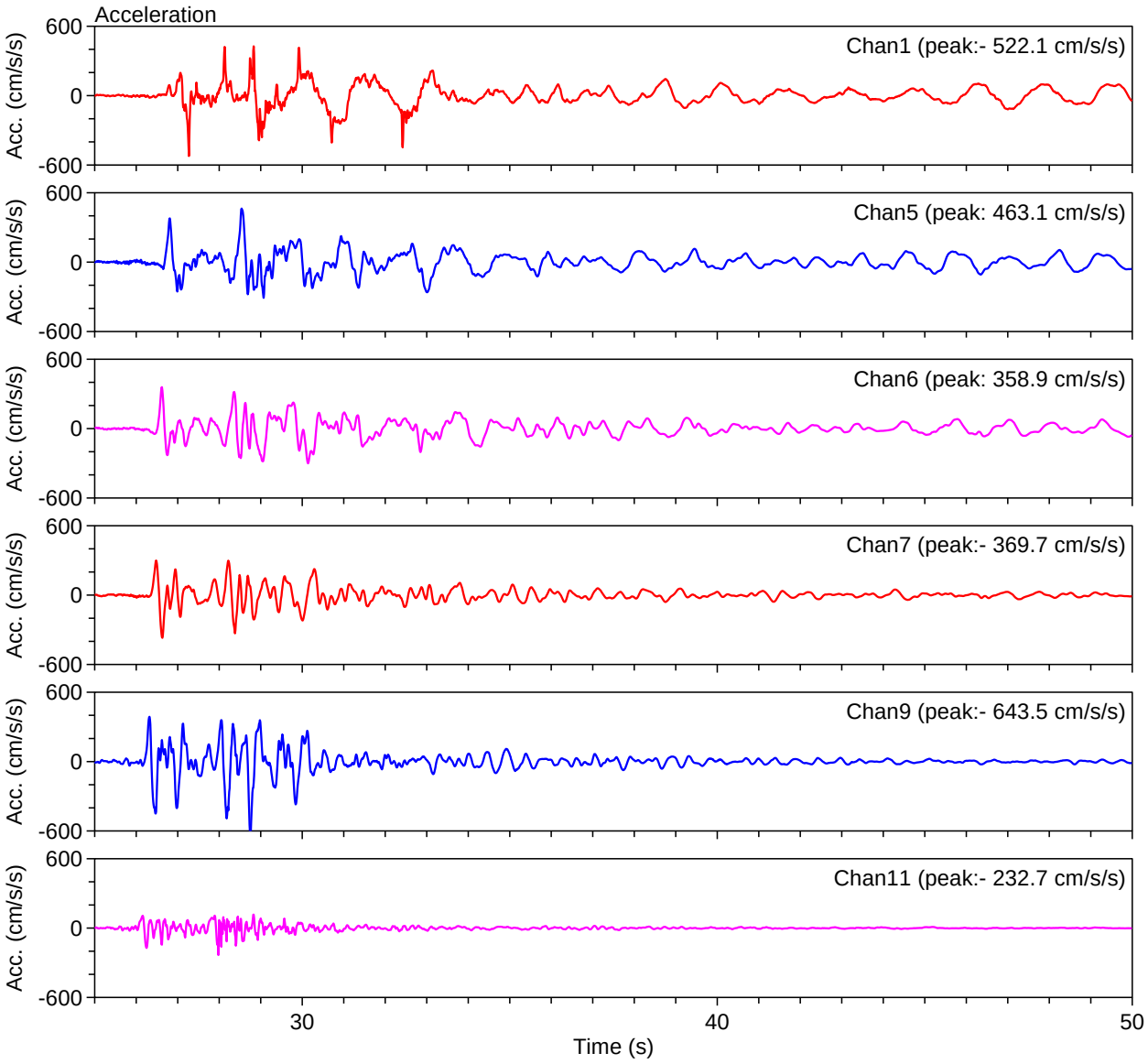
Acceleration
Chan1 (peak:- 522.1 cm/s/s)
Chan5 (peak: 463.1 cm/s/s)
Chan6 (peak: 358.9 cm/s/s)
Chan7 (peak:- 369.7 cm/s/s)
Chan9 (peak:- 643.5 cm/s/s)
Chan11 (peak:- 232.7 cm/s/s)
Acc. (cm/s/s)
600
0
-600
30
40
50
Time (s)

(a)

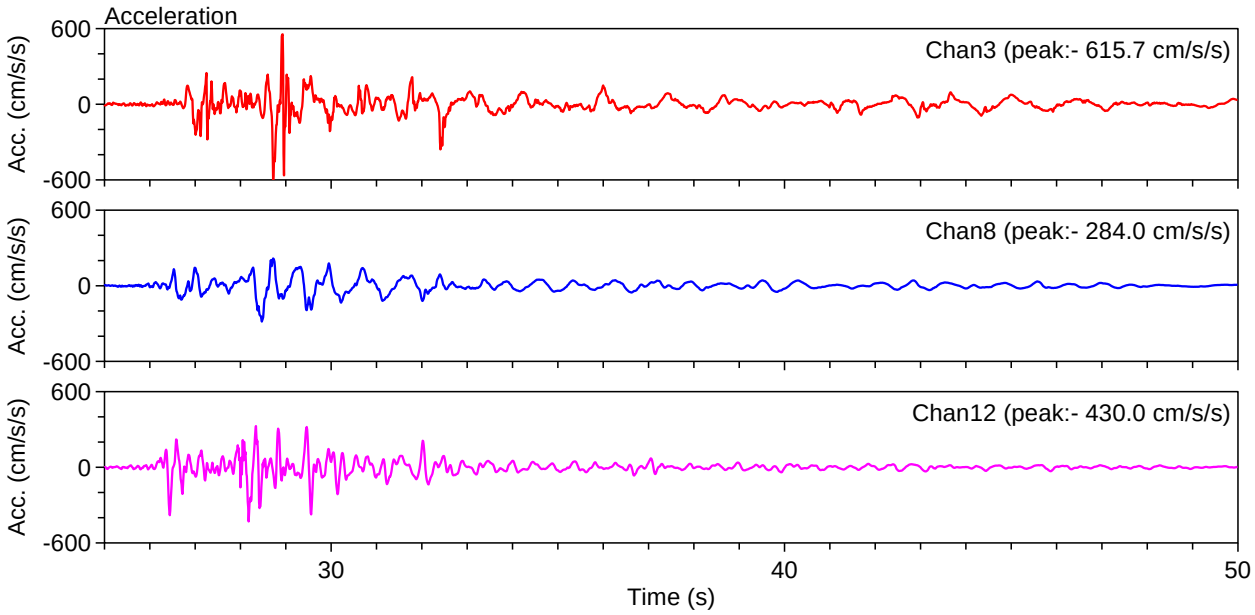

(b)

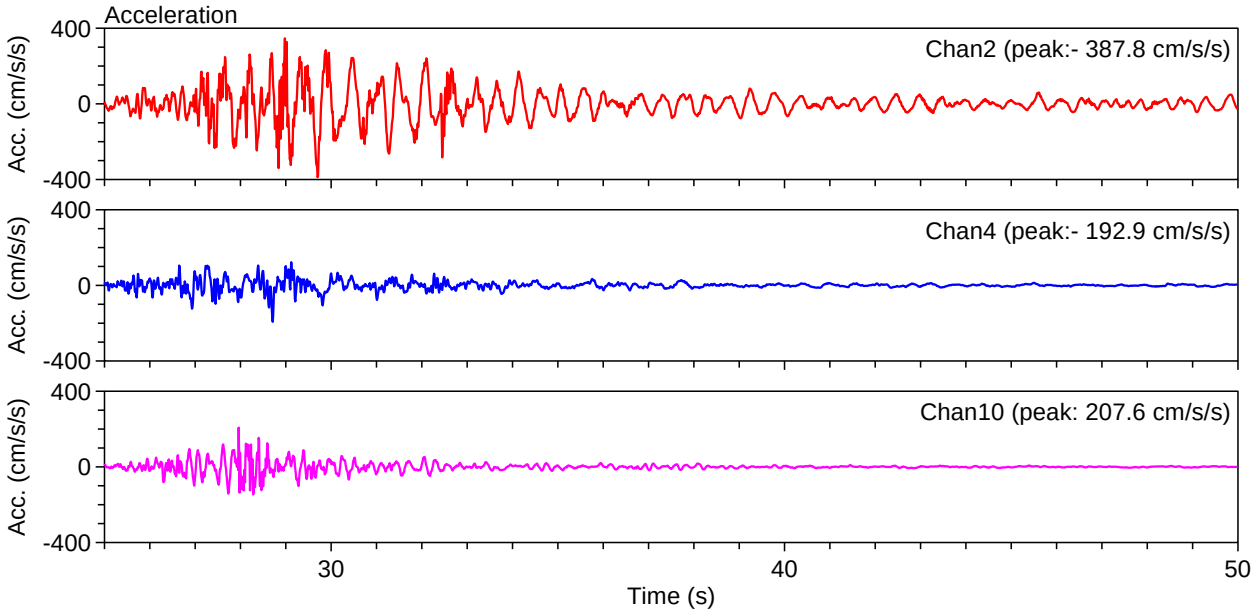

(c)

Figure 4.1 Acceleration time history of the sensors located on the Napa River Bridge under the 2014 Napa earthquake (a) transverse direction (b) longitudinal direction (c) vertical direction

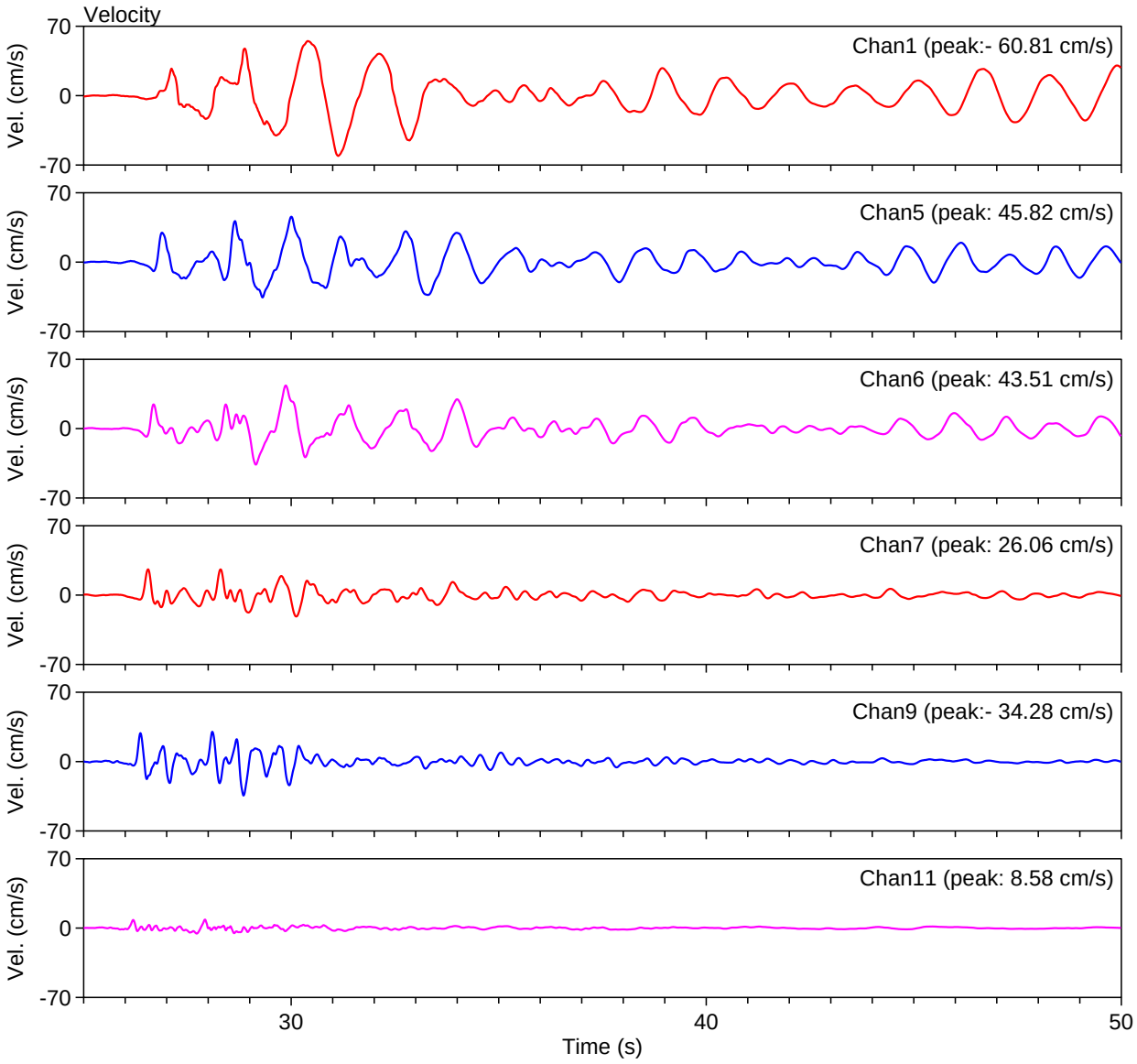
Velocity
Chan1 (peak:- 60.81 cm/s)
Chan5 (peak: 45.82 cm/s)
Chan6 (peak: 43.51 cm/s)
Chan7 (peak: 26.06 cm/s)
Chan9 (peak:- 34.28 cm/s)
Chan11 (peak: 8.58 cm/s)
Vel. (cm/s)
70
0
-70
30
40
50
Time (s)

(a)

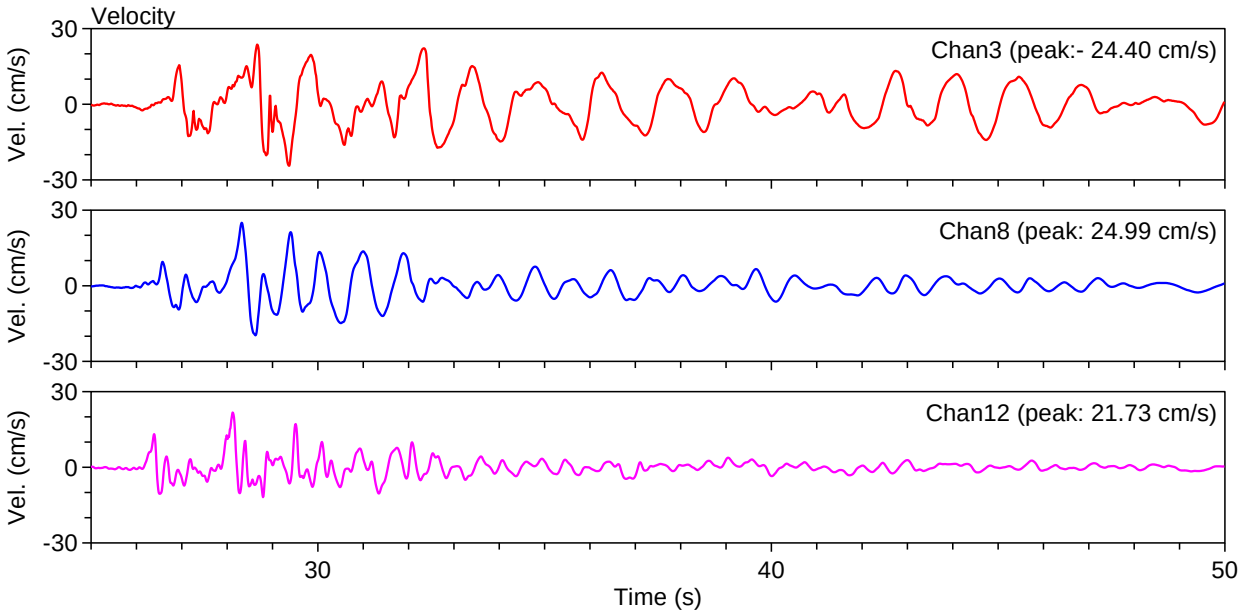

(b)

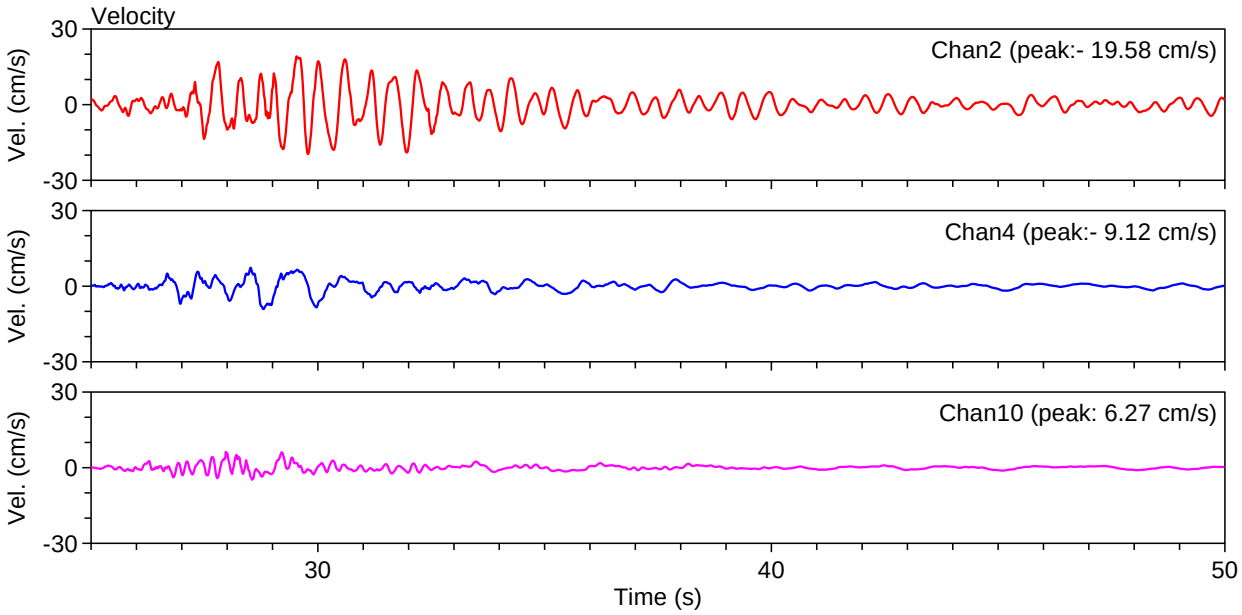

(c)

Figure 4.2 Velocity time history of the sensors located on the Napa River Bridge under the 2014 Napa earthquake (a) transverse direction (b) longitudinal direction (c) vertical direction

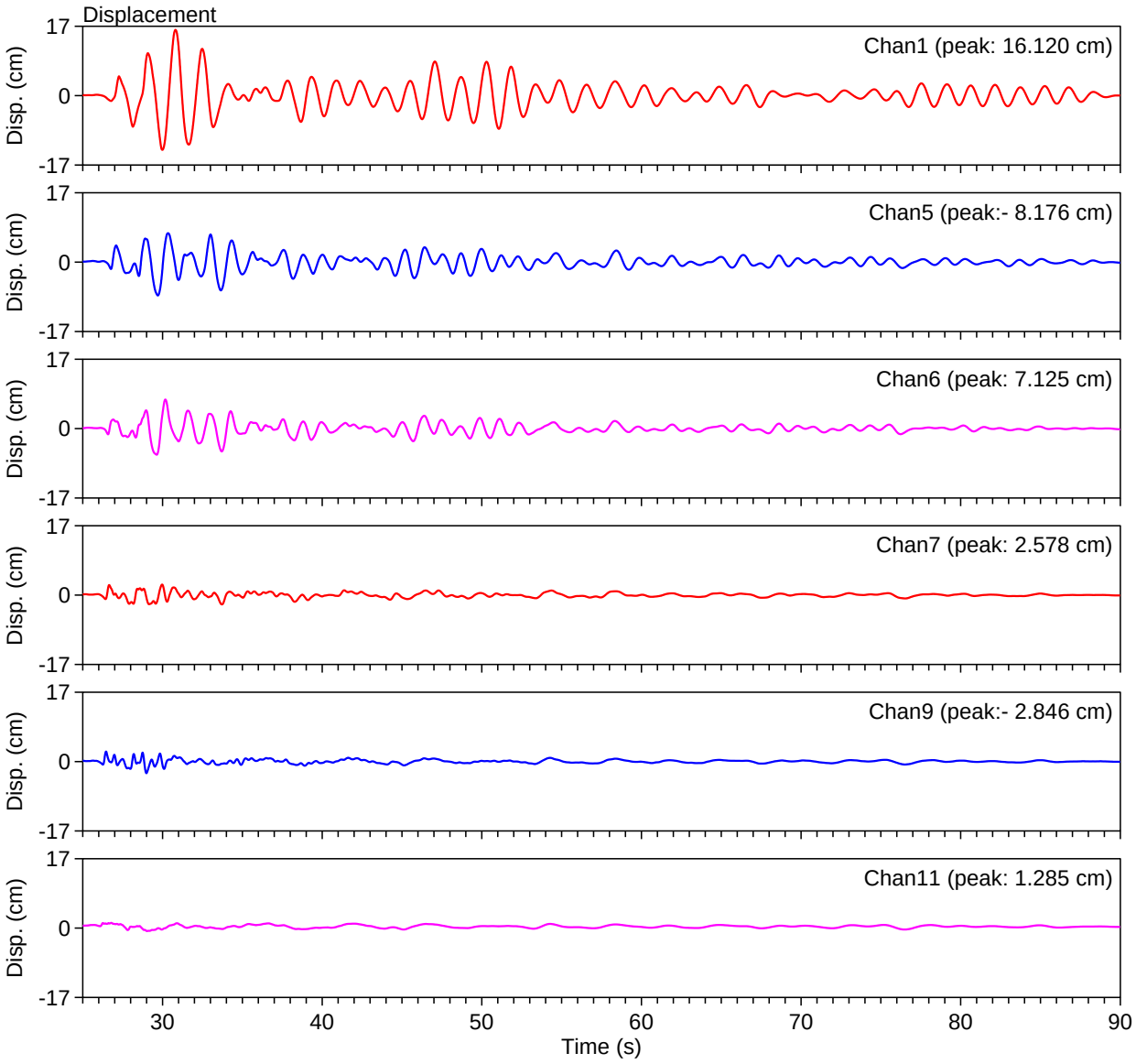
Displacement
Chan1 (peak: 16.120 cm)
Chan5 (peak:- 8.176 cm)
Chan6 (peak: 7.125 cm)
Chan7 (peak: 2.578 cm)
Chan9 (peak:- 2.846 cm)
Chan11 (peak: 1.285 cm)
Disp. (cm)
17
0
-17
30
40
50
60
70
80
90
Time (s)

(a)

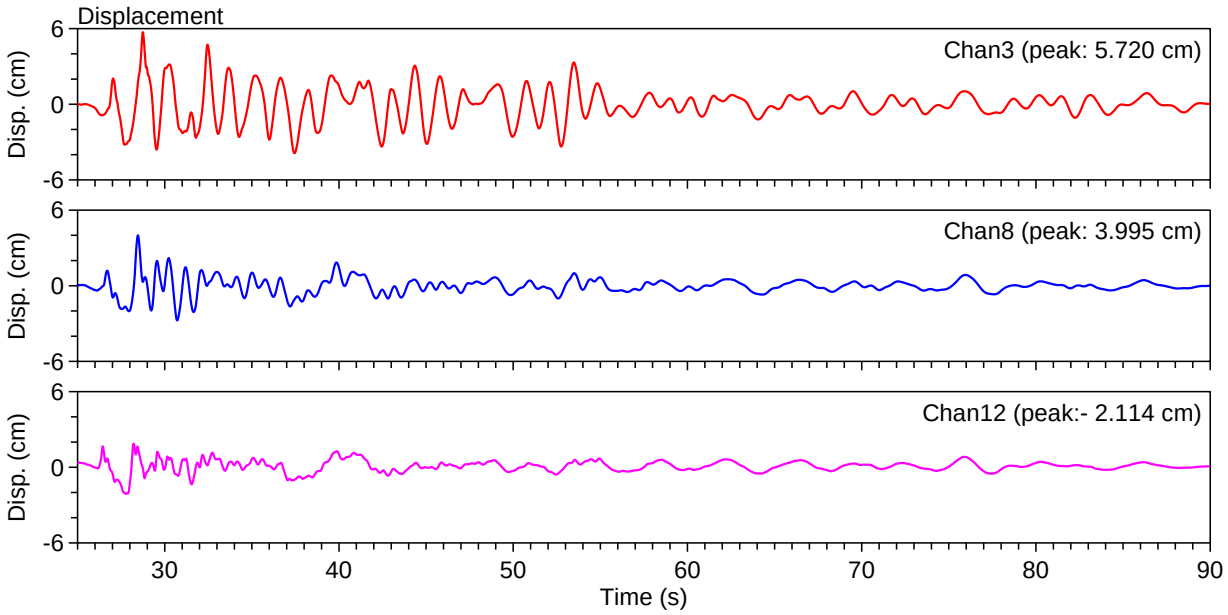

(b)

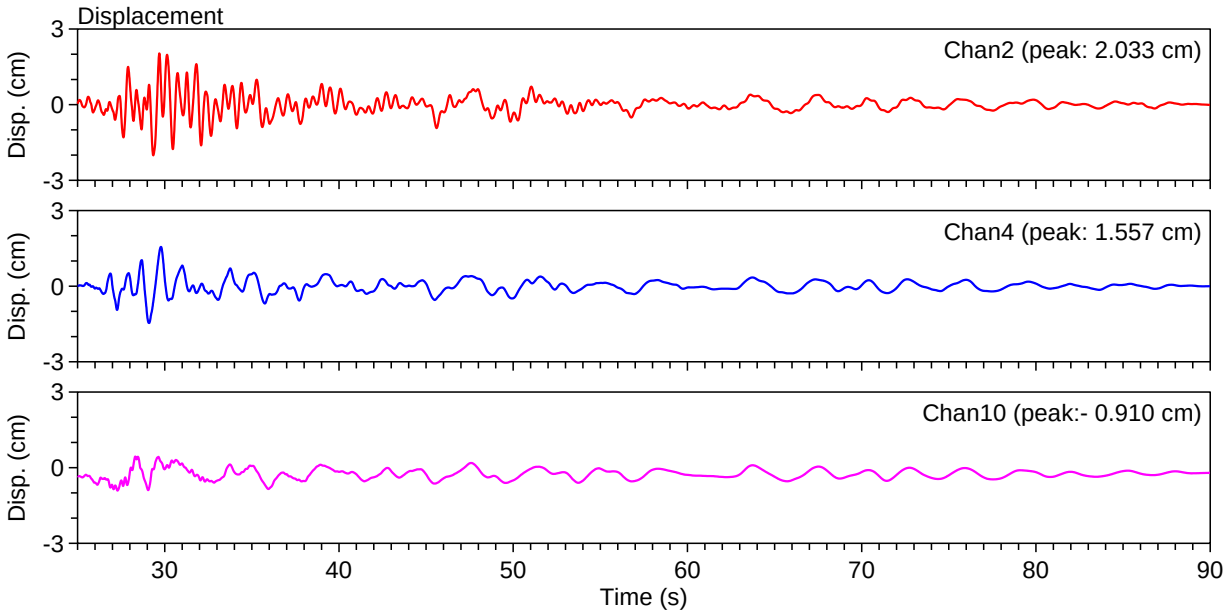

(c)

Figure 4.3 Displacement time history of the sensors located on the Napa River Bridge under the 2014 Napa earthquake (a) transverse direction (b) longitudinal direction (c) vertical direction

Table 4.1 Maximum acceleration, velocity and displacement recorded by the sensors

Chan No.	Peak Acceleration (cm/s/s)	Peak Velocity (cm/s)	Peak Displacement (cm)
1	-522.10	-60.81	16.12
2	-387.80	-19.58	2.03
3	-615.70	-24.20	5.72
4	-192.90	-9.12	1.55
5	463.10	45.82	-8.17
6	358.90	43.51	7.12
7	-369.70	26.06	2.58
8	-284.00	24.99	3.99
9	-643.50	-34.28	2.86
10	207.60	6.27	-0.91
11	-232.70	8.58	1.28
12	-430.00	21.73	-2.11

Moreover, free-field data was obtained during the earthquake by station CGS sta. 68310. The site consists of thin alluvial over rock (CSMIP). The array has three tri-axial accelerometers located at the surface, 18m and 44m deep. Figure 4.4 shows the p- and s-wave surveys conducted by Caltrans. It is observed that the s-wave at the surface is about 200m/s and increased to 600m/s at a depth of 19 meters.

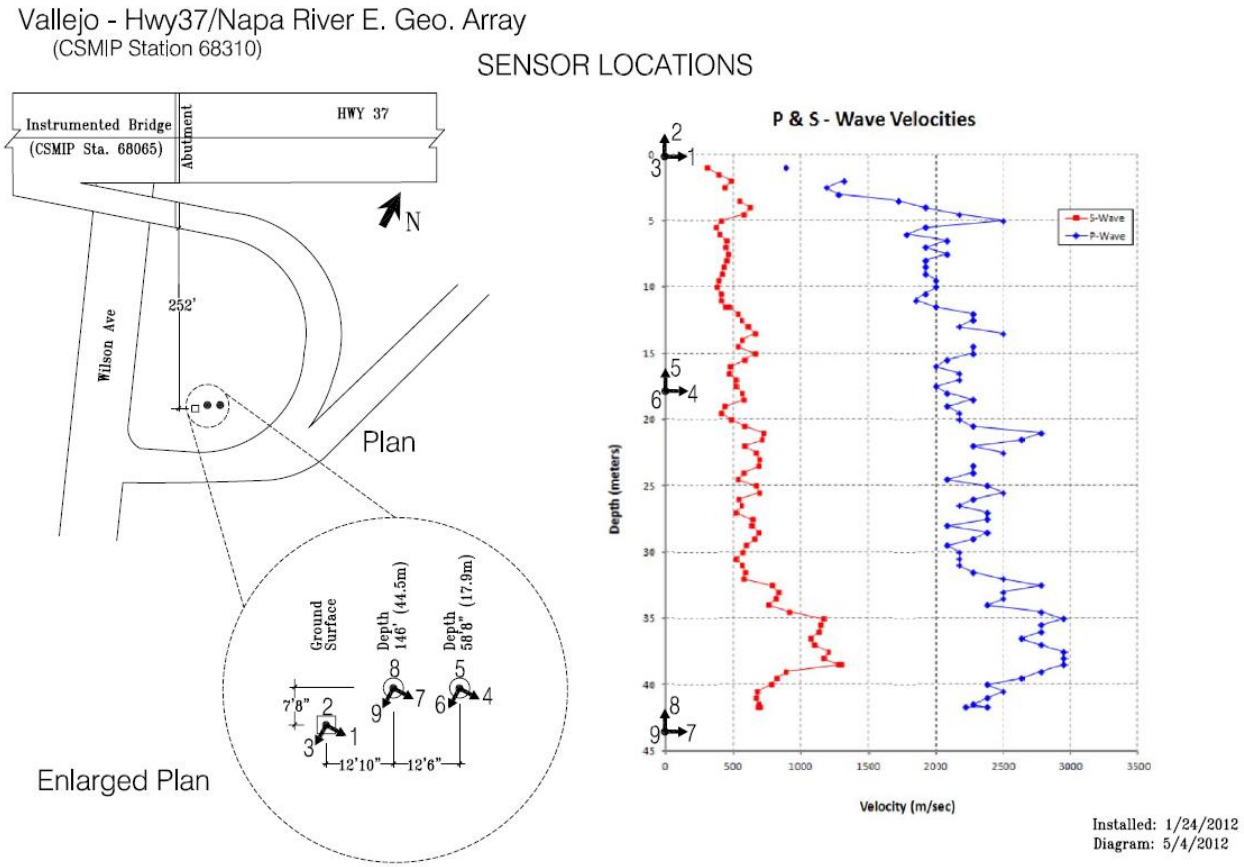

Figure 4.4 p- and s-wave profiles (CSMIP, 2012)

The recorded motion by the sensors 1 and 3 are used to simulate the peak displacement of the bridge during the earthquake by the developed FE model. This is discussed in Chapter 5.

4.1.2 Field Investigation of the Hw37 Napa River Bridge after the 2014 Napa Earthquake

After the 2014 Napa earthquake, a group of PEER (Kang and Mahin, 2014) inspectors conducted a survey of the infrastructure that was damaged during the earthquake. Minor damage was mainly observed near the approaches. The expansion joints showed cracks and the handrails separated themselves at the joints. Laser scanning of the piers showed that those near Mare

Island had some residual displacement. Figure 4.5 shows the tilt observed on one of the piers. Cracking was observed on the abutment wall from the Vallejo side and on the cap beam and the pile caps of a few piers on the Mare Island side. Figure 4.6 and Figure 4.7 show the cracking observed in some of the beam and pile caps, respectively.

These observations reflect the abrupt changes on the acceleration time history plots of the previous section. Even though the damage was minor, it was reflected on the recorded data. This is one of the big advantages of continuous monitoring of structures. A quick analysis of the recorded data can help to identify any possible damage that the structure has suffered. It can give engineers the advantage of deciding which structure to inspect based on analyzing the recorded data. Furthermore, with more refined signal processing and damage identification techniques damage can be located and quantified.

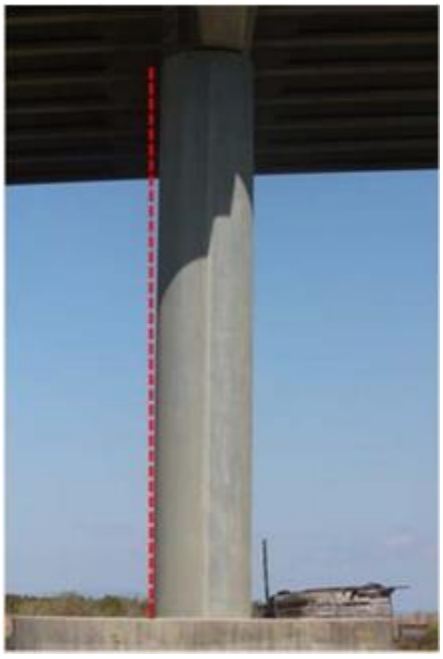

Figure 4.5 Pier tilted on the bridge approach from Mare Island (Kang and Mahin, 2014)

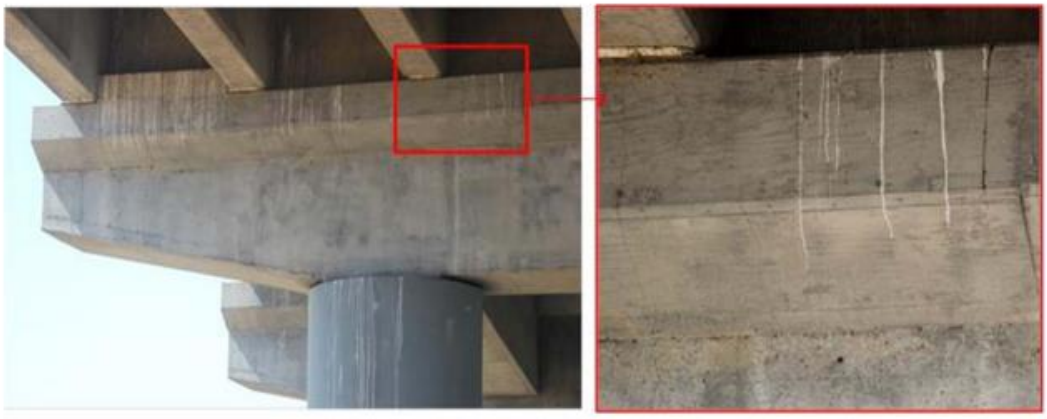

Figure 4.6 Cracks observed at the beam cap (Kang and Mahin, 2014)

Figure 4.7 Cracks observed on one of the pile caps of a pier (Kang and Mahin, 2014)

4.2 Fourier Analysis

Fourier analysis is one of the oldest and simplest techniques for identifying the modal properties of a structure. The Fourier spectrum of response signals under uniform or smooth input excitation is the common method used to identify the Frequency Response Function of a system. This is the theory behind the peak picking technique. However, this theoretical assumption of uniform excitation is not valid under strong motion excitation (Taciroglu, Shamsabadi et al., 2014), although it can be implemented as a preliminary analysis for system identification.

A Fourier analysis of the records was carried out to determine the dominant frequencies of each data channel. This was used to identify the dominant frequencies of the transverse and longitudinal directions. A single segment of the 90 seconds of data was used with a sampling rate of 0.01 seconds in the analysis. The data was not smoothed because it was just a preliminary analysis and the results of data without alteration were desired. Figure 4.8 and Figure 4.9 show the Fourier spectrum of recorded response signals for the longitudinal and transverse directions. As can be seen, the frequency range of interest is below 5Hz, because the dominant frequencies of the recorded data are 5Hz or below. It is important to mention that even though channels 11 and 12 are used in this preliminary analysis, they are not located on the bridge's main channel. They are part of the exit ramp, and for this reason they are not included in the system identification of the bridge. The summary of the peak frequencies is presented in

Table 4.2. This preliminary analysis produced some important conclusions, which are listed as follows:

- Based on the Fourier spectra of the sensors the first dominant mode in the transverse direction is 0.62Hz, with 0.76Hz for the longitudinal direction. For the longitudinal direction, on channel 3, two peaks are shown close together. This suggests that the dominant frequency may not be 0.76Hz.
- As expected, the first global mode of the system is in the transverse direction, because the bridge is more flexible in this direction.
- The system can be considered in two separate directions for system identification.

Table 4.2 First dominant peaks (Hz) from the sensors on the bridge

Event	**Longitudinal Direction**			**Transverse Direction**					
	3	8	12	1	5	6	7	9	11
Napa 2014	0.76	1.07	3.55	0.62	0.82	.082	1.21	3.46	5.23

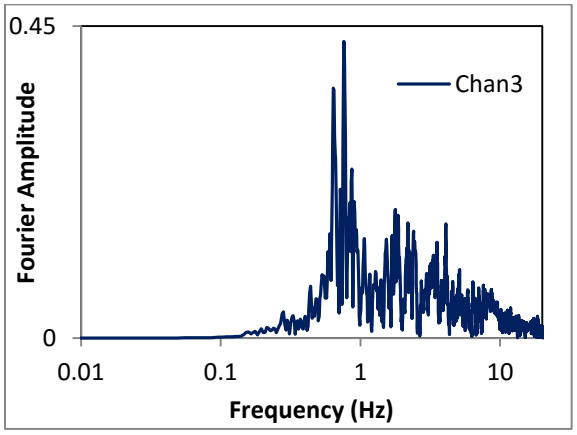

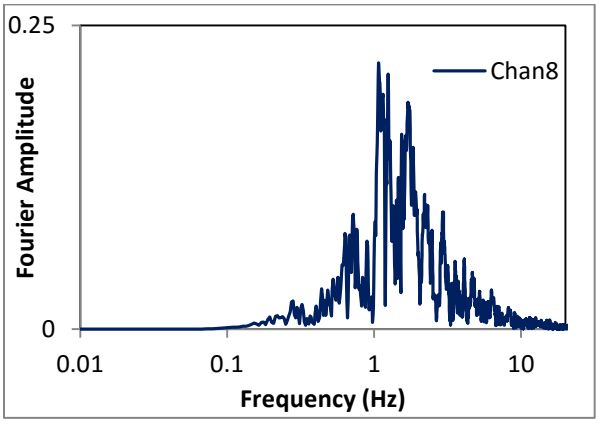

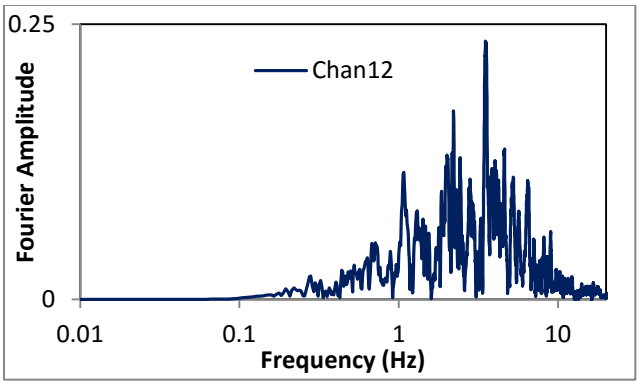

Figure 4.8 Fourier spectra of longitudinal response signals for the Napa earthquake, 2014

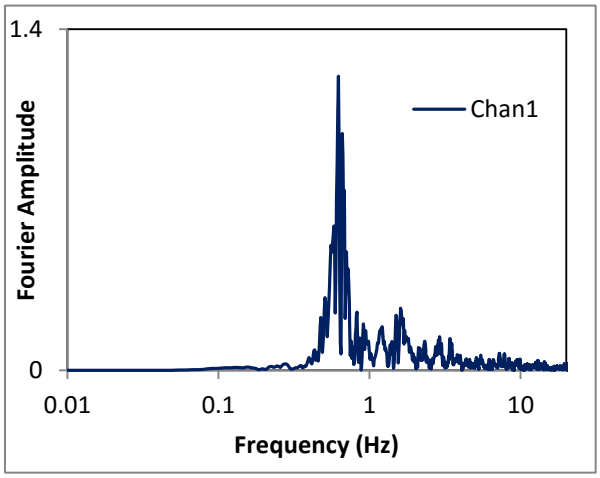

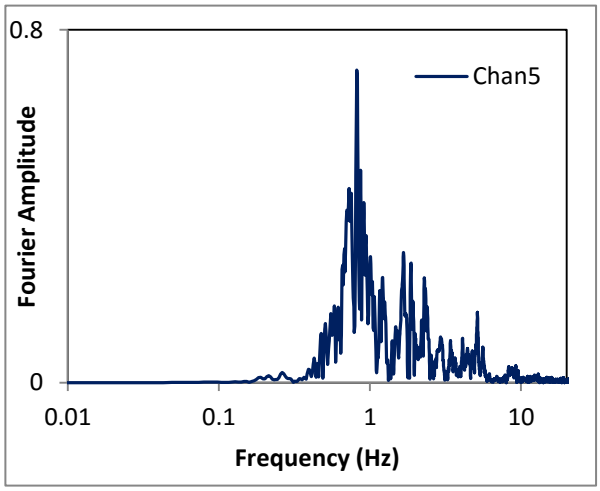

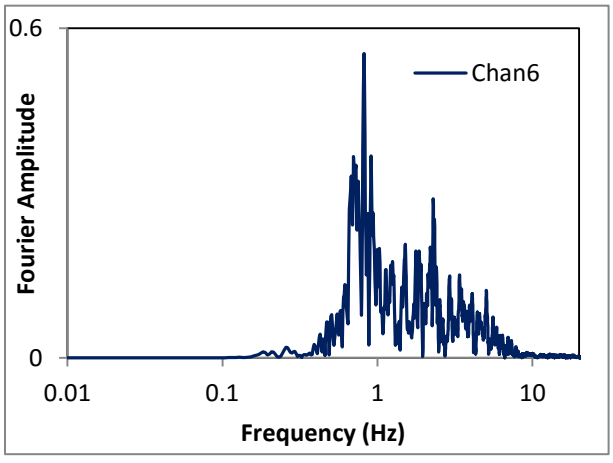

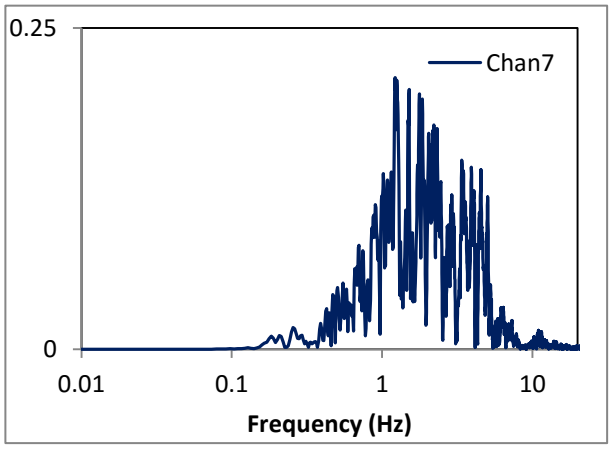

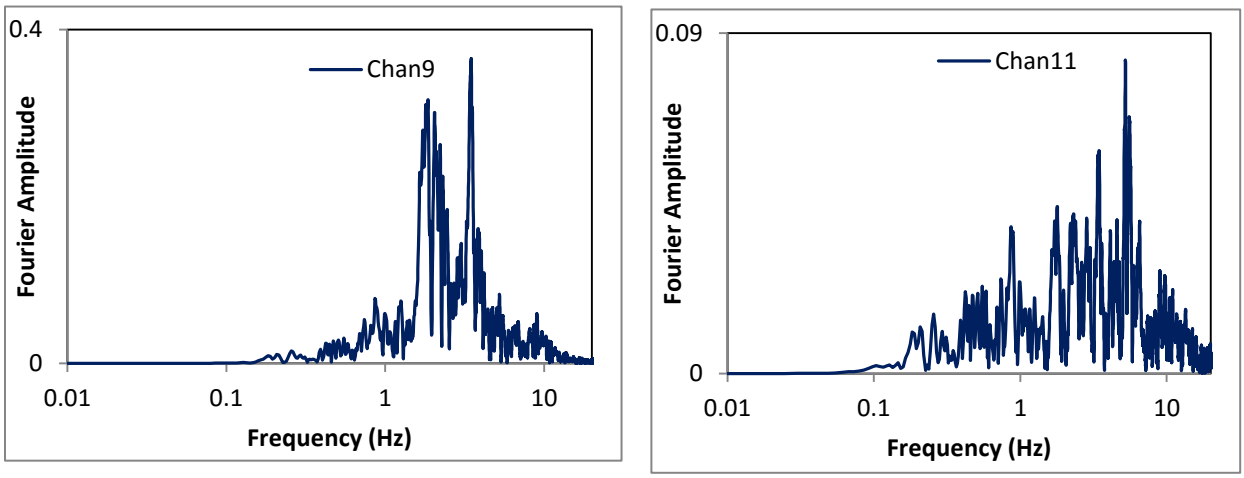

Figure 4.9 Fourier spectra of transverse response signals for the Napa earthquake, 2014

4.3 System Identification

In this section, an operational modal analysis is carried out on the recorded data to identify the dominant mode shapes and frequencies of the Hwy 37 Napa River Bridge. Two different techniques are used for comparison purposes; enhanced frequency domain decomposition (EFDD) and stochastic subspace identification (SSI).

Using the recorded data from the sensors on the bridge deck and ARTeMIS Modal Version 4.0 (Structural Vibration Solutions, Inc. 2015) software, a modal analysis was carried out. The bridge deck was modeled as a line with four nodes. Only the instrumented side of the bridge was modeled for identification purposes: from mid-span to the right, the Vallejo side. The sensors located at the ramps were not included, as they are not part of the bridge main channel. Moreover, the modal analysis for each direction is done independently to simplify the analysis and get dominant frequencies in each direction. Because of the limited instrumentation, only the first five modes in the transverse direction and the first mode in the longitudinal direction are

identified. Figure 4.10 and Figure 4.11 show the EFDD and SSI plots for the recorded data in the transverse direction. A summary of the identified modal frequencies and damping in the transverse direction is presented in Table 4.3. Figure 3.1 and Figure 4.13 show the EFDD and SSI plots of the longitudinal direction. Table 4.4 shows the frequencies and damping obtained for the longitudinal direction. A frequency range from 0.61Hz to 2.29Hz and the damping ranges from 2.07% to 3.93% for the transverse direction can be observed. For the longitudinal direction, only the first mode was of interest and it has a frequency of 0.66Hz and 3.5% damping.

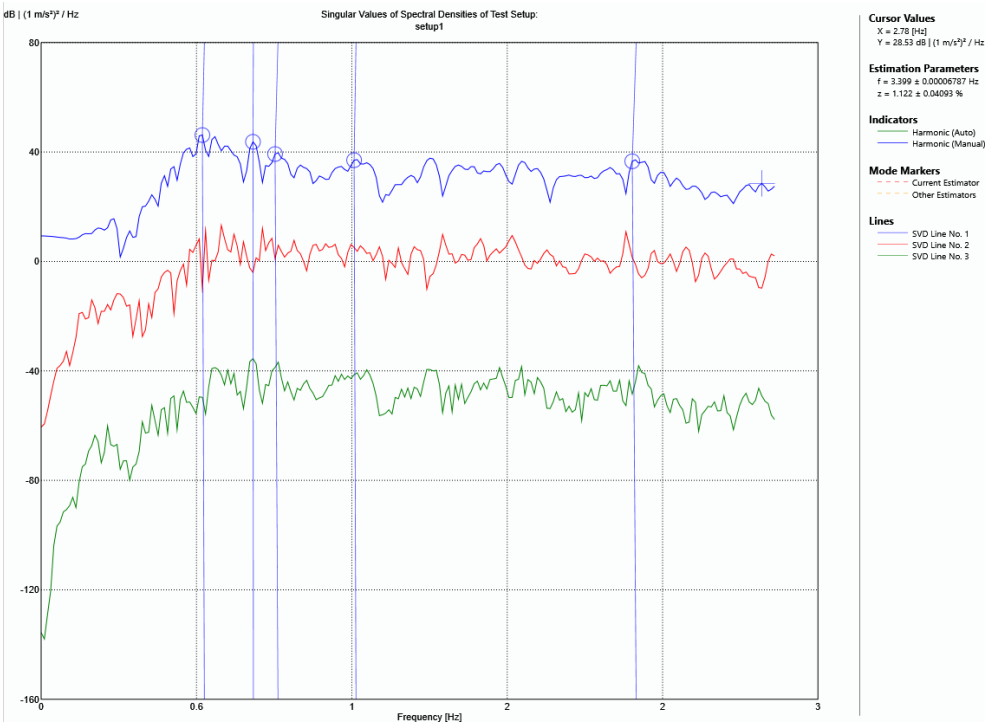

Figure 4.10 Singular value plot for recorded data of the transverse direction using EFDD method

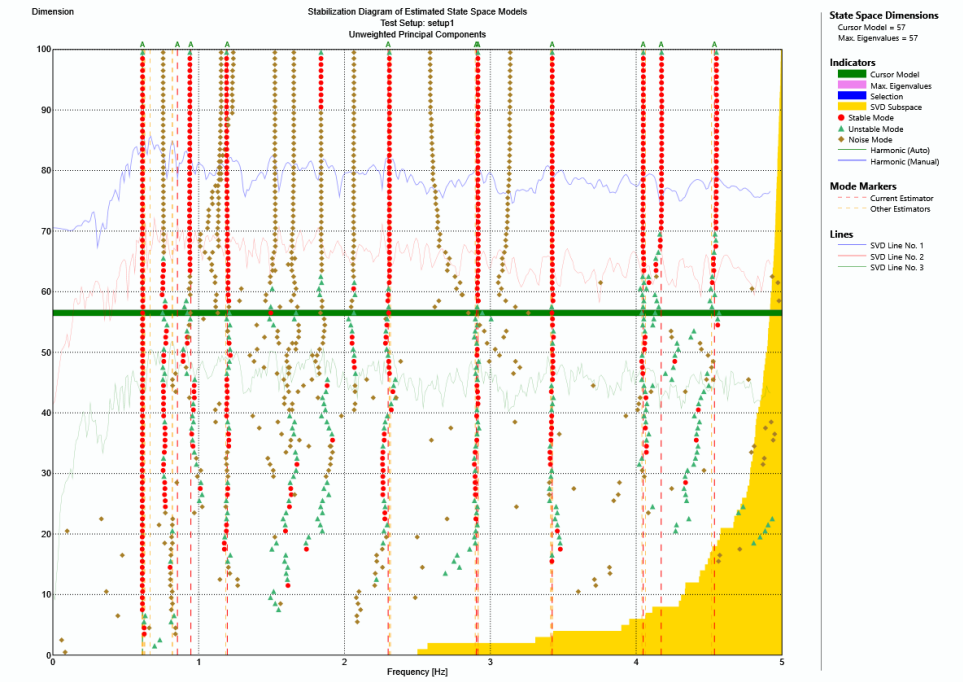

Figure 4.11 Stochastic subspace identification UPC plot for the recorded data of the transverse direction

Table 4.3 Modal frequencies and damping obtained through EFDD and SSI techniques, transverse direction

	EFDD		**SSI**	
Mode	Frequency (Hz)	Damping (%)	Frequency (Hz)	Damping (%)
1	0.61	3.60	0.61	3.71
2	0.86	3.79	0.85	3.93
3	0.94	2.32	0.94	2.38
4	1.19	3.71	1.19	3.75
5	2.22	2.12	2.29	2.07

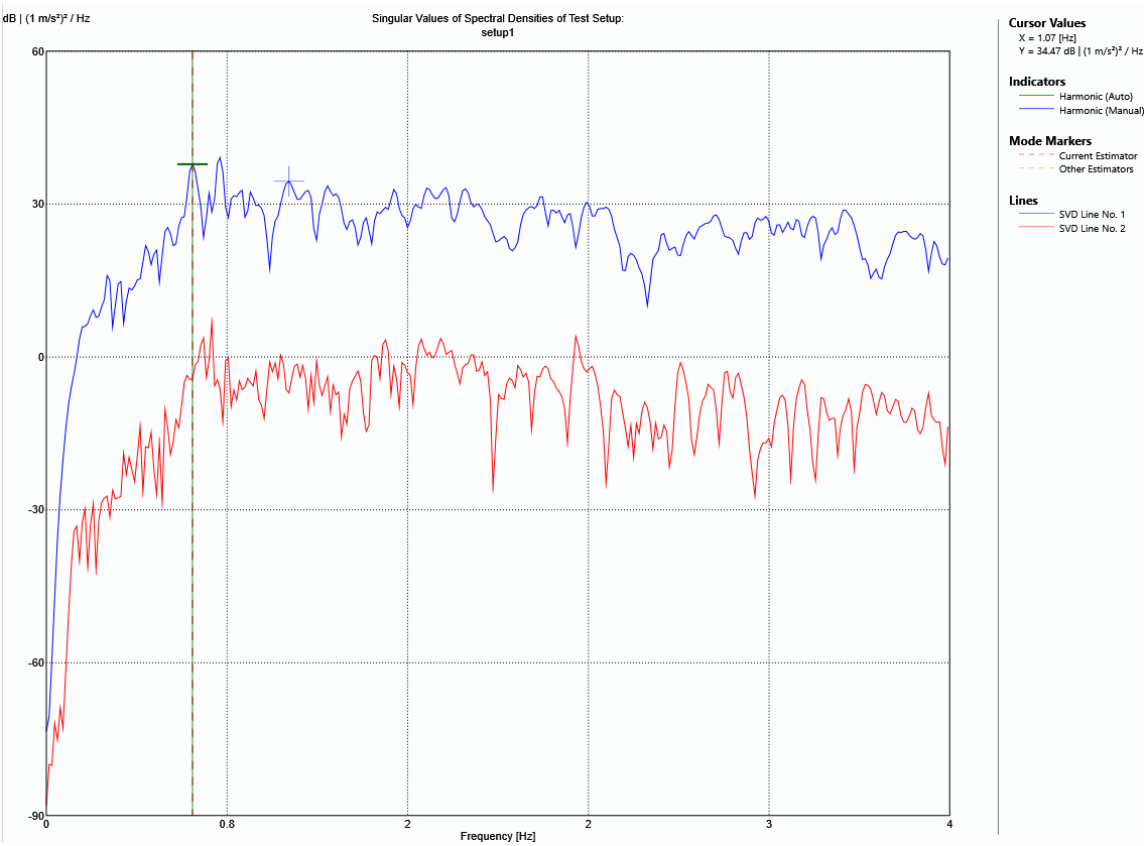

Figure 4.12 Singular value plot of the longitudinal direction using EFFD method

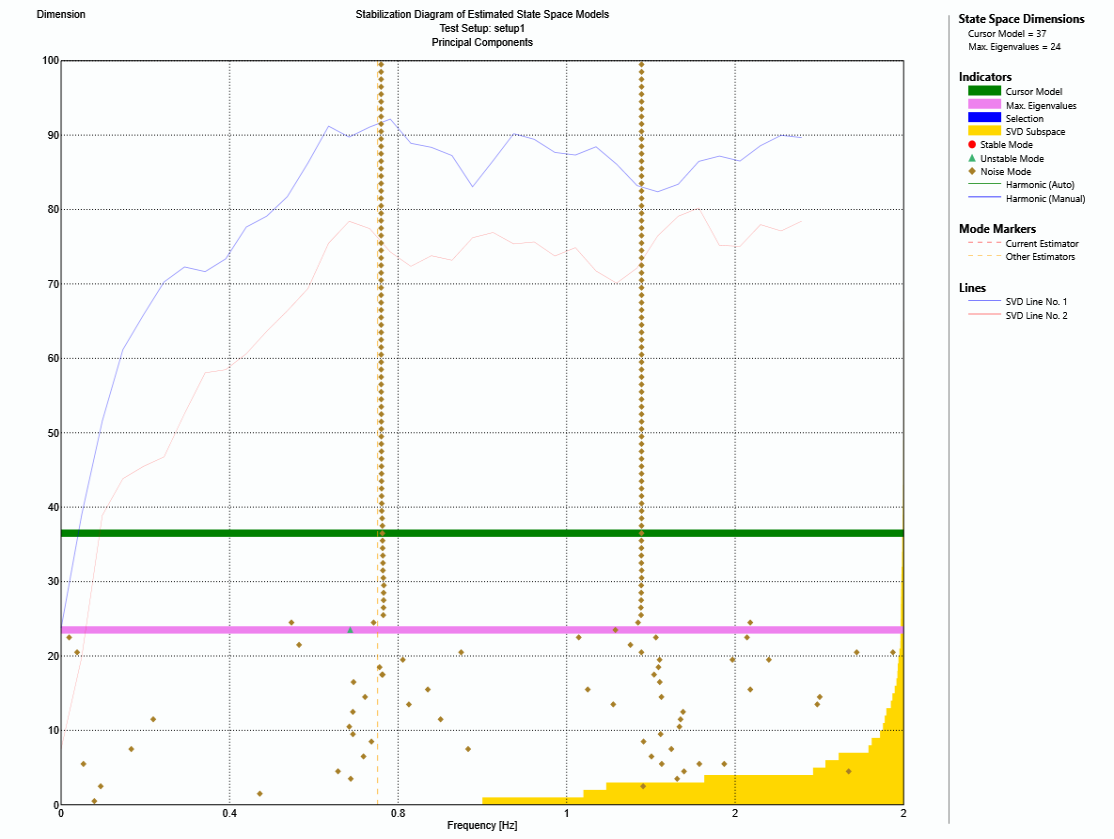

Figure 4.13 Stochastic subspace identification UPC plot of the longitudinal direction

Table 4.4 Modal frequencies and damping obtained using EFDD and SSI techniques, longitudinal direction

	EFDD		**SSI**	
Mode	Frequency (Hz)	Damping (%)	Frequency (Hz)	Damping
1	0.66	3.2	0.68	3.5

Based on the results obtained for the transverse and longitudinal direction's EFDD and SSI, it was decided to use the results of the EFDD technique for both the transverse direction and the longitudinal direction. The EFDD technique is robust and straightforward, while the SSI technique has many parameters to determine and no guidelines that exist in the literature (Svend

Gade, Nis B. Møller et al., 2005). Based on Figure 4.13, there is no stable modal frequency identified through the technique. This is due to the lack of sensors in the longitudinal direction. Figure 4.14 shows the section of the bridge that was used to identify the modal frequencies. The mode shapes obtained corresponded only to the right side of the bridge. Figure 4.15 and Figure 4.16 show the mode shapes obtained for the longitudinal and transverse direction, respectively.

The modal frequencies and identified damping can be improved if more sensors are added on the bridge deck. The lack of sensors on the left side of the bridge (Mare Island side) does not allow identification of a good range of modal shapes and corresponding frequencies. This in turn does not allow for more precise data for model updating and having a more accurate representation of the bridge through a finite element model. Moreover, if more sensors were located on the piles and pile caps, a more detailed investigation could have been done to study the effect that the foundation has on the structure. This more detailed study could have determined if the foundation rocked during the earthquake, allowing a correlation of the behavior of the foundation to the damage observed on the bridge.

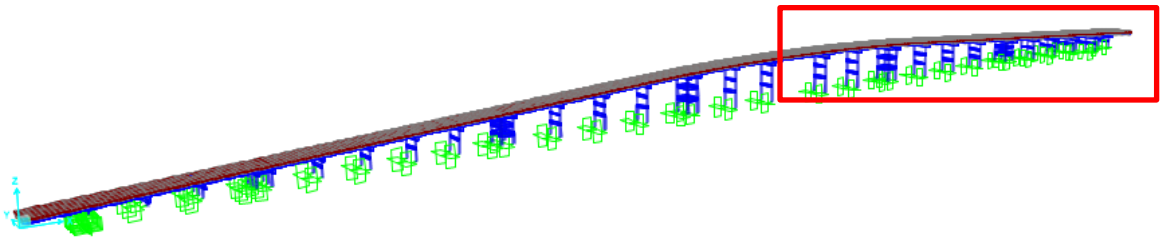

Figure 4.14 Section of the bridge used to identify mode shapes

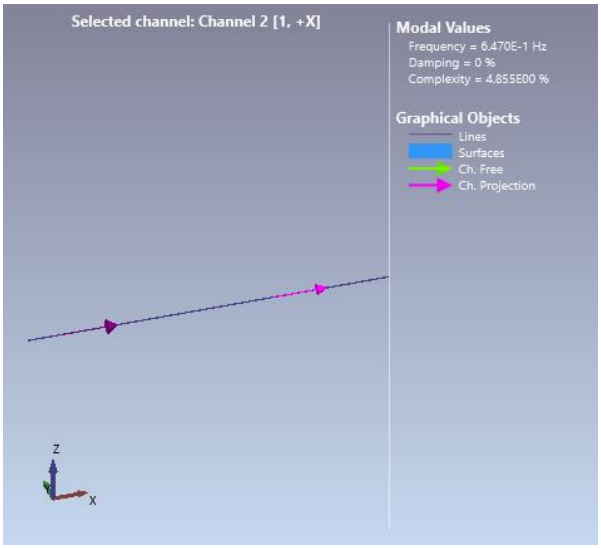

1st longitudinal (0.66 Hz)

Figure 4.15 First longitudinal mode shape of the Napa River Bridge

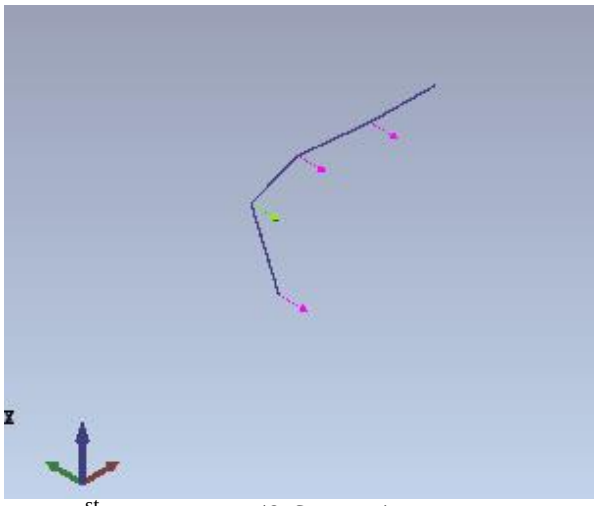

1st Transverse (0.614 Hz)

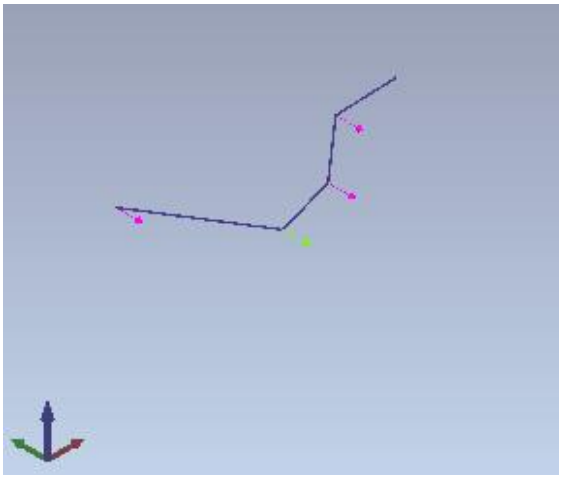

2nd Transverse (0.854 Hz)

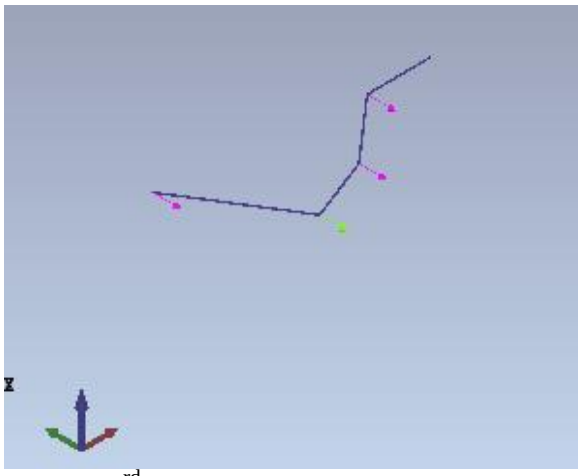

3rd Transverse (0.940 Hz)

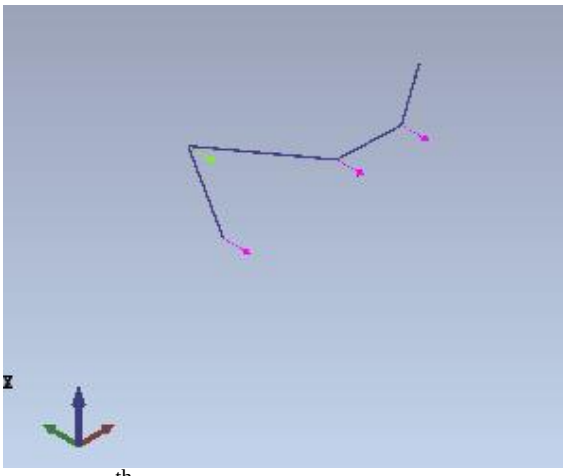

4th Transverse (1.196 Hz)

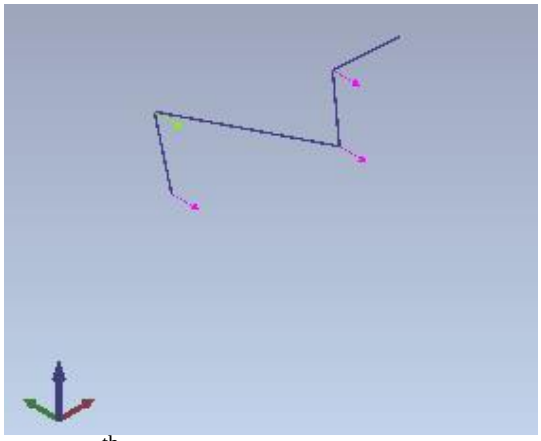

5th Transverse (2.290 Hz)

Figure 4.16 Mode shapes in the transverse direction of the Napa River Bridge

Chapter 5: Model Updating and Calibration of the Napa River Bridge to the 2014 Napa Earthquake

After performing a modal analysis and identifying the modal properties of the Hwy 37 Napa River Bridge during the 2014 earthquake, model updating was performed to the finite element model developed in CSI Bridge. In this chapter, first the finite element model developed is compared to the system identification results then a sensitivity analysis determines what elements and properties to update. Model updating is eventually carried out and compared to the modal shapes, frequencies and damping found in Chapter 4. Finally, a time history analysis is carried out using the ground motion time history record of the 2014 Napa earthquake, to simulate the response of the bridge to the recorded displacement of the sensors.

5.1 Base Finite Element Model Comparison

A comparison between the developed finite element model developed and the results obtained in the system identification section is conducted here. Table 5.1 is a comparison of the modal frequencies of the developed model and the identified frequencies. Figure 5.1 shows the first longitudinal mode shape and Figure 5.2 shows the five mode shapes in the transverse direction of the finite element model. The modal properties of the finite element model are based on un-cracking conditions of the bridge bents and columns.

Table 5.1 shows that the modal frequencies of the FE model are much larger than the identified modal frequencies. This is due to several reasons. First, the modal frequencies

identified are based on the recorded data of the 2014 Napa earthquake. From the bridge inspection, cracking on bent caps and columns were observed (see Chapter 4). This implies that the stiffness of the columns and bent caps needs to be updated and cracking stiffness should be applied. Moreover, the mass of the FE model might not be represented correctly, as the developed model only includes the mass of the structural elements and does not take into account the mass of non-structural components and vehicles that could have been on the bridge. It needs to be updated as well. Similarly, the equivalent stiffness used for the elastomeric bearings needs to be studied to determine if it needs updating.

Table 5.1 Comparison of modal frequencies of the base FE model and the identified frequencies

Mode No.	**Frequency (Hz)**		
	FE	Identified	Error (%)
Transverse Direction			
1	0.81	0.61	32
2	1.09	0.86	28
3	1.16	0.94	23
4	1.66	1.19	39
5	2.75	2.22	29
Longitudinal Direction			
1	0.92	0.66	39

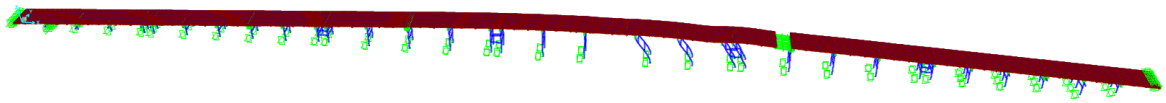

1st Longitudinal (0.918 Hz)

Figure 5.1 First longitudinal mode shape of the FE model

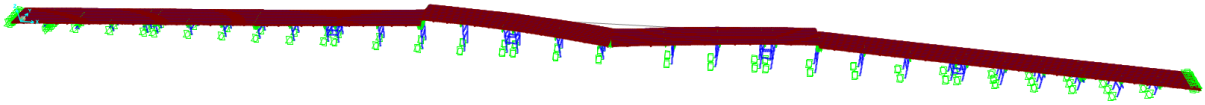

(a) 1st Transverse (0.813 Hz)

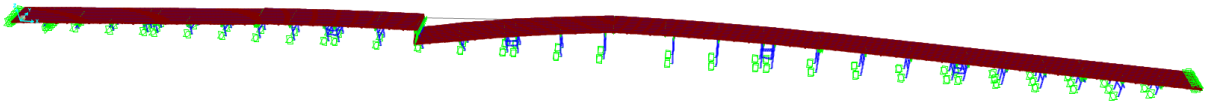

(b) 2nd Transverse (1.095 Hz)

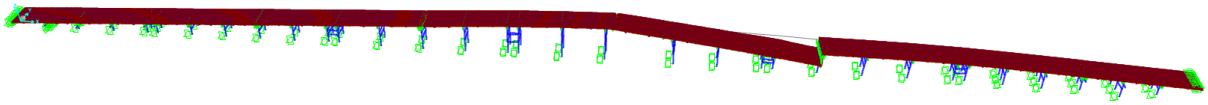

(c) 3rd Transverse (1.155 Hz)

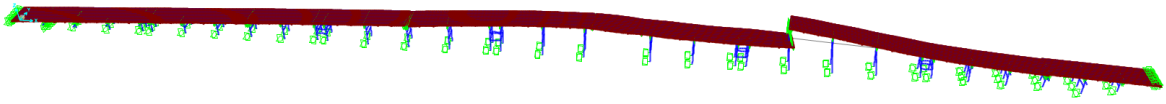

(d) 4th Transverse (1.658 Hz)

Figure 5.2 Transverse mode shapes of the FE model

5.2 Sensitivity Studies

A set of sensitivity studies of the stiffness of the columns, the mass of the bridge girders and the equivalent stiffness of the elastomeric bearings were carried out. This helped determine how sensitive the model was to changing its properties and if the model of the columns needed to be updated. To perform the sensitivity studies, a MATLAB code was developed to access the model through the OAPI interface of CSI Bridge. Figure 5.3 shows a screenshot of MATLAB accessing CSI Bridge. The MATLAB code is shown in Appendix B.1.

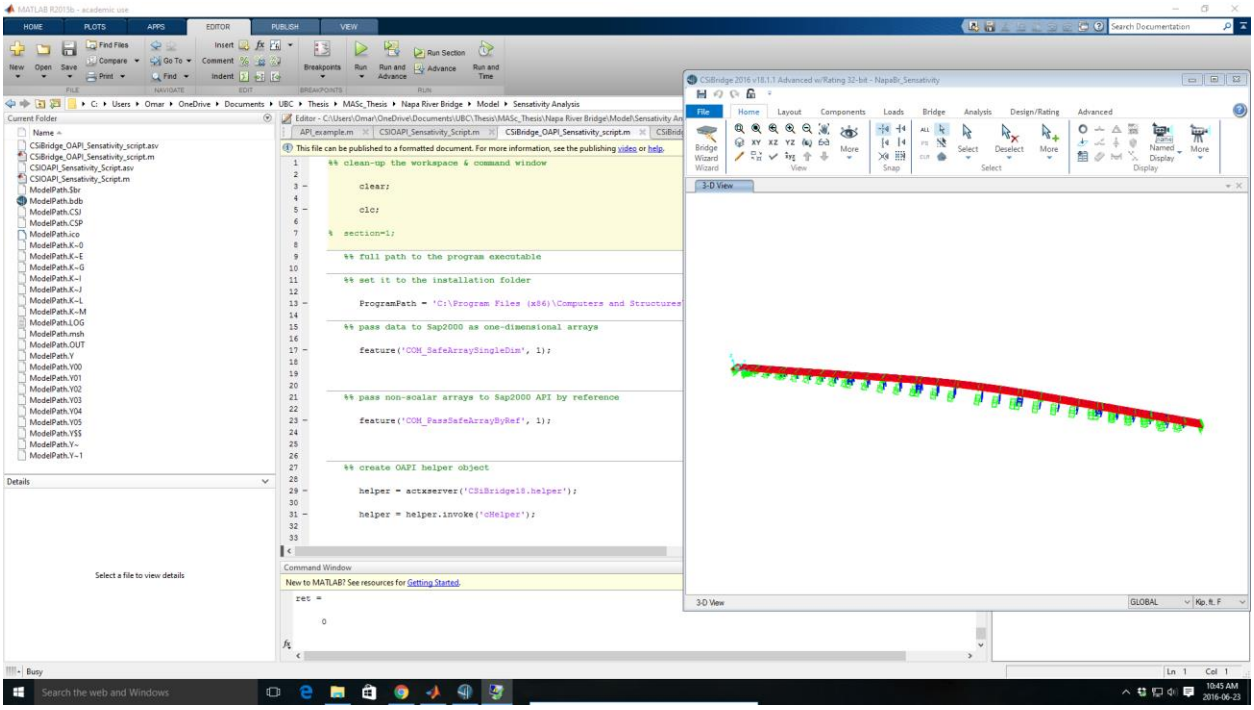

Figure 5.3 Screenshot of sensitivity procedure: MATLAB and CSI Bridge are connected through OAPI interface

Since the bridge has elastomeric bearing at its expansion joints, the column piers were grouped into sections. This helped to identify which columns or sections do not affect the modal frequencies identified. Figure 5.4 shows the location of the expansion joints divided into sections. It also shows which columns correspond to each section.

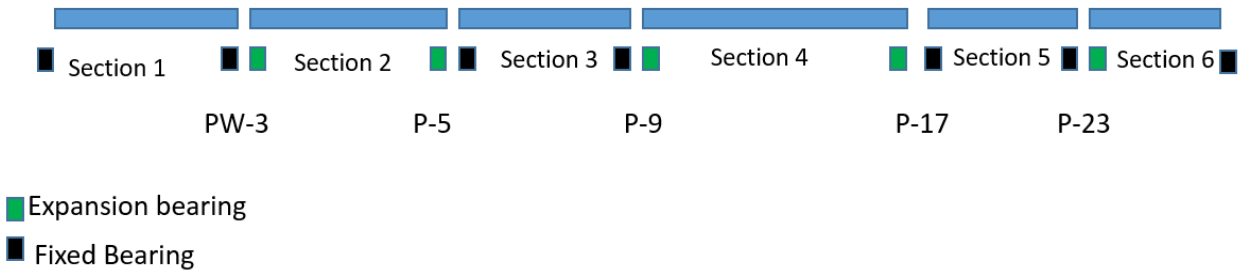

Figure 5.4 Location of the expansion bearings and sections with their corresponding columns

The stiffness of the columns from each section was modified from 50% to 150% of the value of the gross moment of inertia (Ig) individually. This was done in each direction, transverse and longitudinal independently, to identify if it had any influence on the modal frequencies and mode shapes.

After performing the sensitivity analysis, it was observed that only sections 3, 4 and 5 play an important role. The discussion of the sensitivity results, therefore, is based only on these three sections. For the sensitivity analysis of all the sections, see Appendix B.2. Figure 5.5, Figure 5.6 and Figure 5.7 show the plot frequency versus modification factor for the transverse direction for sections 3, 4 and 5 respectively. As can be seen in Figure 5.5, in which the stiffness factors of section 3 are modified from 1 to 0.5, only higher modes are affected. Modes 7, 8 and

10 seem to be the most affected by the change in stiffness and are more sensitive to lower stiffness. A similar observation is made in section 5, where higher modes are the only modes affected. Figure 5.7 shows that mode 6 becomes more sensitive as the stiffness is reduced. On the other hand, section 4 is more sensitive to the first transverse mode of the bridge, as shown in Figure 5.6. Similar observations are made for modes 4 and 5. At a stiffness of 0.5, it can be observed that a change in mode shape between mode 4 and 3 occurs. Modes 2 and 3 correspond to the first and second longitudinal direction of the bridge, and by reducing the stiffness in the transverse direction they become more flexible. For this reason, a change in mode shape occurs.

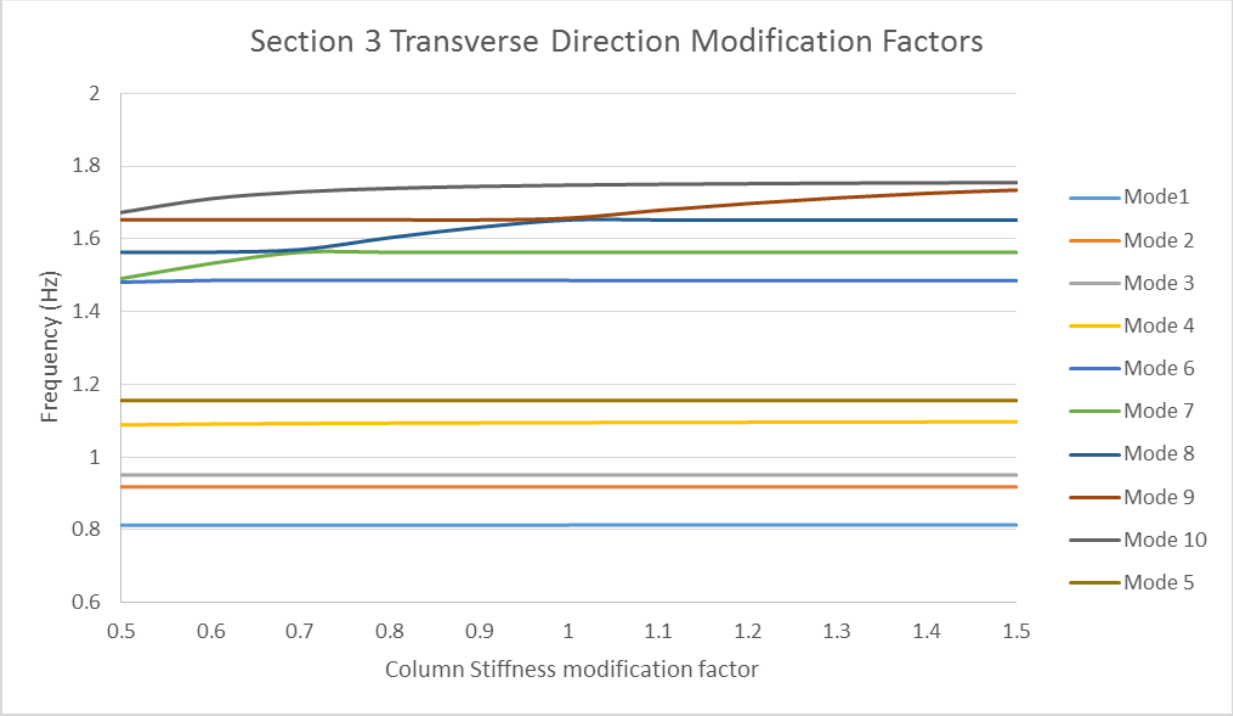

Figure 5.5 Sensitivity plot for section 3 in the transverse direction

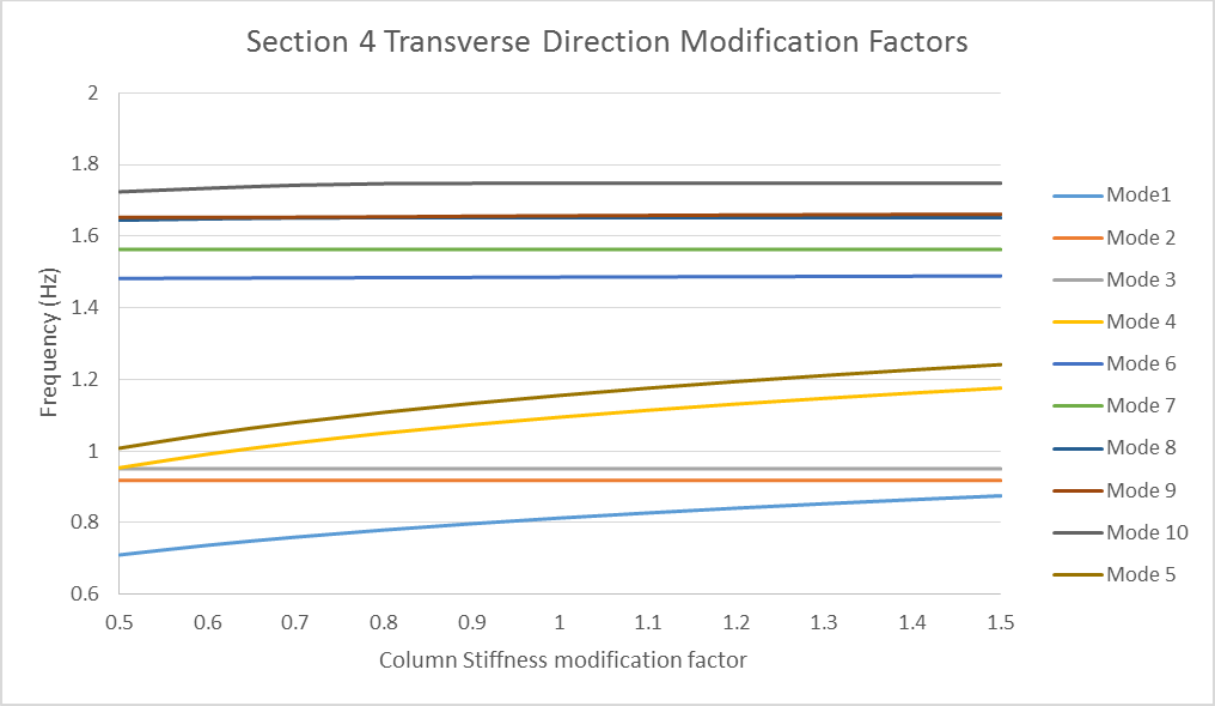

Figure 5.6 Sensitivity plot for section 4, transverse direction

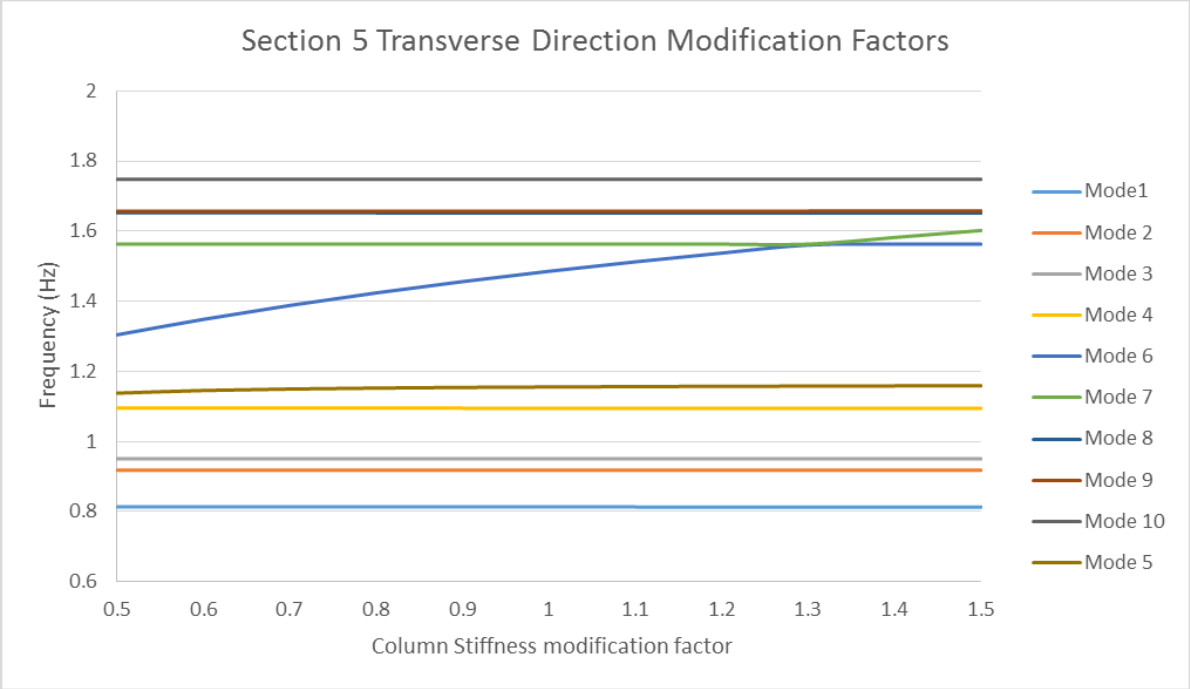

Figure 5.7 Sensitivity plot for section 5, transverse direction

The same sensitivity analysis was conducted in the longitudinal direction. The stiffnesses were modified from 50% to 150% of their gross value to see the effects in mode shapes and frequencies. Figure 5.8, Figure 5.9 and Figure 5.10 show the sensitivity plots in the longitudinal direction respectively. Based on Figure 5.8, it can be seen in section 3 that higher modes are affected in the longitudinal direction. There is a mode shape change between modes 7, 8 and 9. As the columns become more flexible in the longitudinal direction, a tendency of changing mode shapes occurs. Similar observations can be seen for modes 6 and 7 for section 3 in Figure 5.10. On the other hand, when section 4 is modified in the longitudinal direction, modes 2 and 3 – which correspond to the first and second longitudinal modes of the bridge – are highly sensitive. It can be seen that at a factor of 0.5 a mode change between modes 1 and 2 occurs.

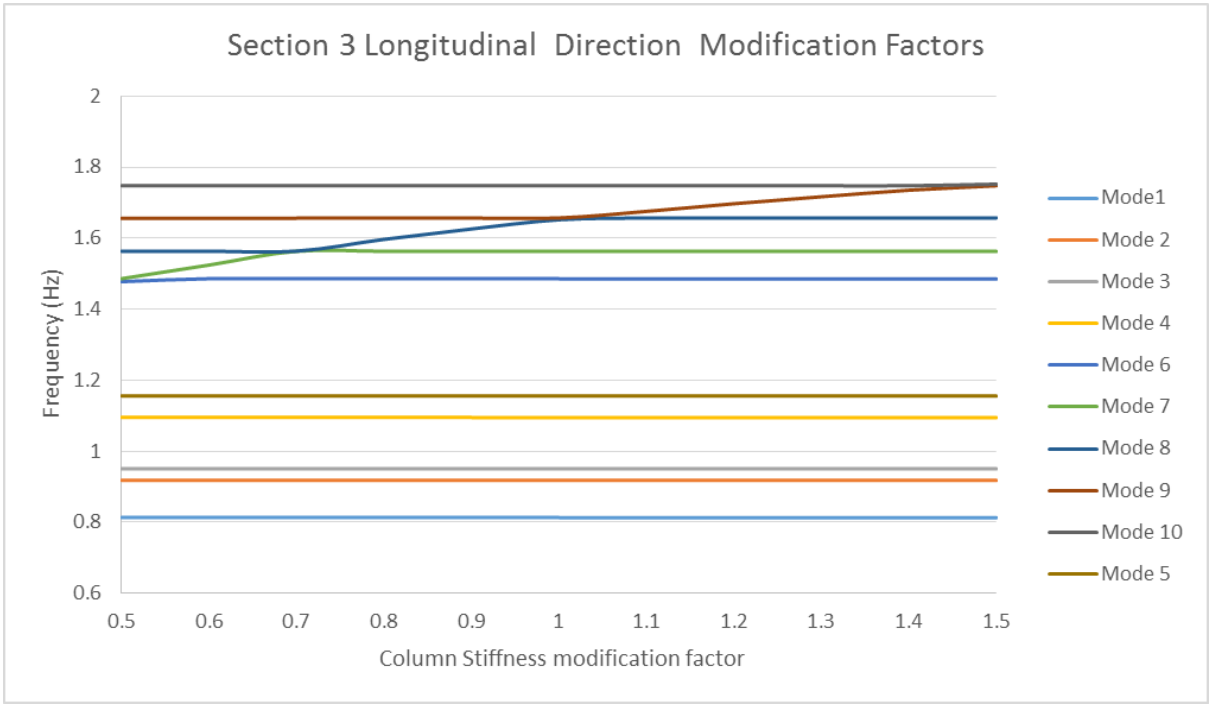

Figure 5.8 Sensitivity plot for section 3, longitudinal direction

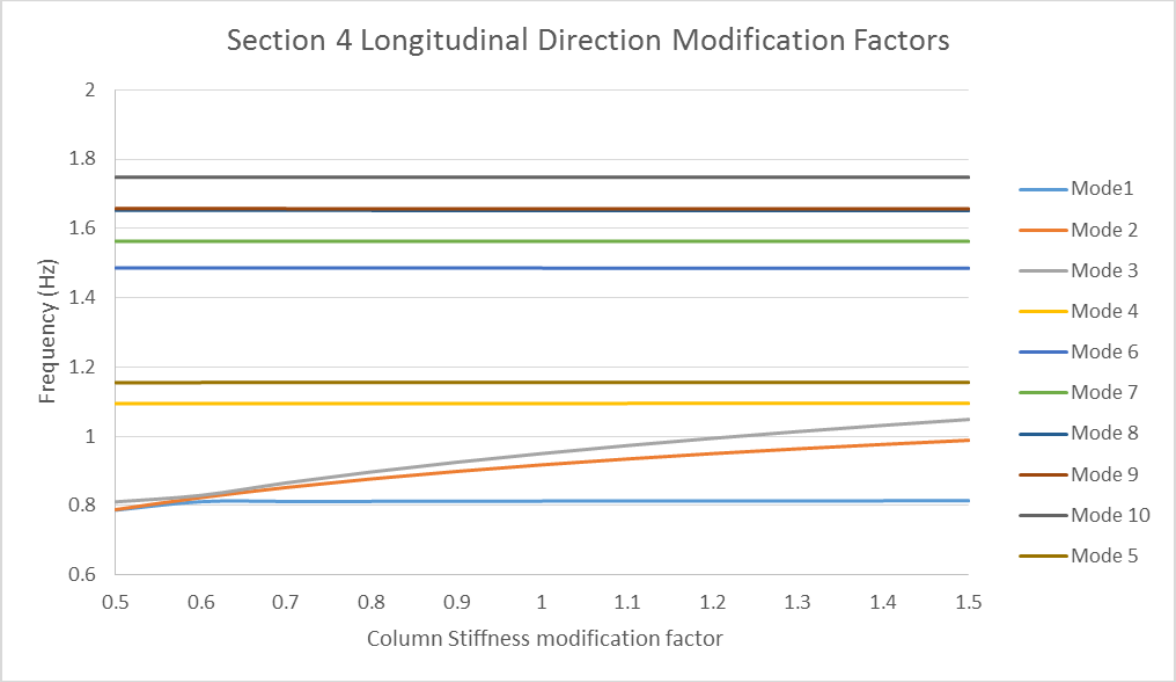

Figure 5.9 Sensitivity plot section 4, longitudinal direction

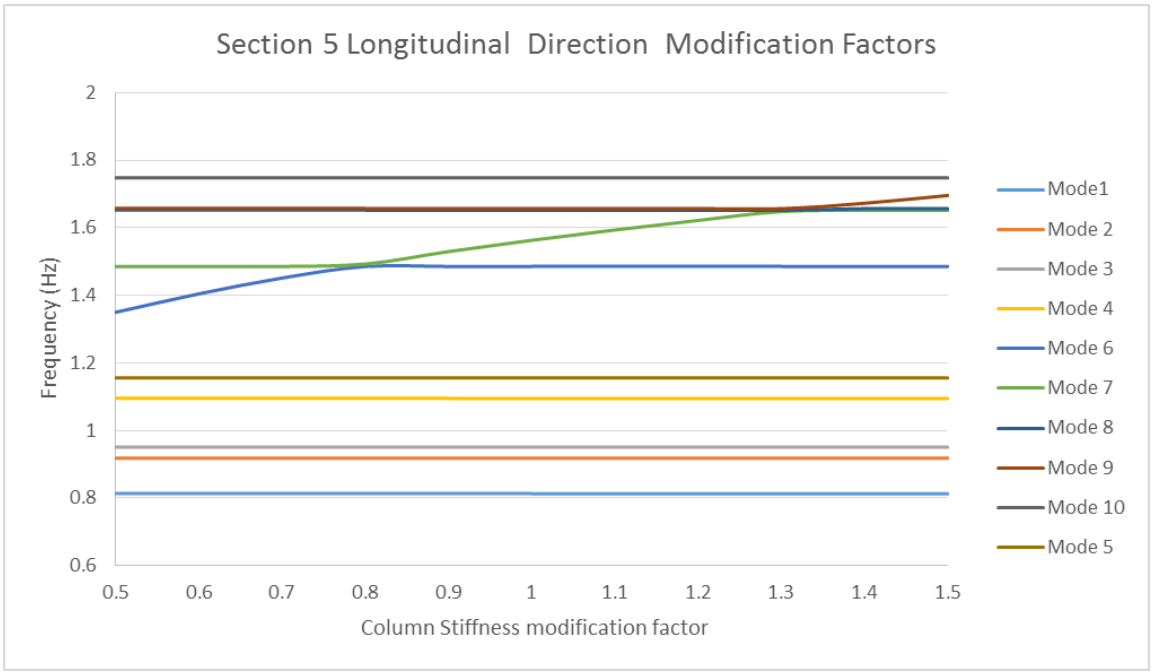

Figure 5.10 Sensitivity plot section 5, longitudinal direction

Based on the sensitivity study conducted on the column piers, it was decided that columns in section 3, 4 and 5 would be updated in the transverse and longitudinal directions. It is important to take into account that if the modification factors are below 0.8 and close to 0.5, the bridge becomes very sensitive and changes in mode shapes occur.

In addition, a sensitivity study of the mas of the bridge girders was conducted. This was done to understand how the mode shapes and frequencies change by adding or reducing mass to the girders. It helped to determine how much mass should be added to account for additional mass that could have been on the bridge during the earthquake. Figure 5.11 shows the results of the sensitivity analysis performed to the mass of the bridge girders. As seen in Figure 5.11, the first five modes are not too sensitive to a change in stiffness. However, for higher modes it is observed that they are highly sensitive when the mass is reduced from 0.9 to 0.5. It can also be inferred that there is a mode change between mode 9 and 10 if the mass is increased between 1 to 1.2 mass modification factors.

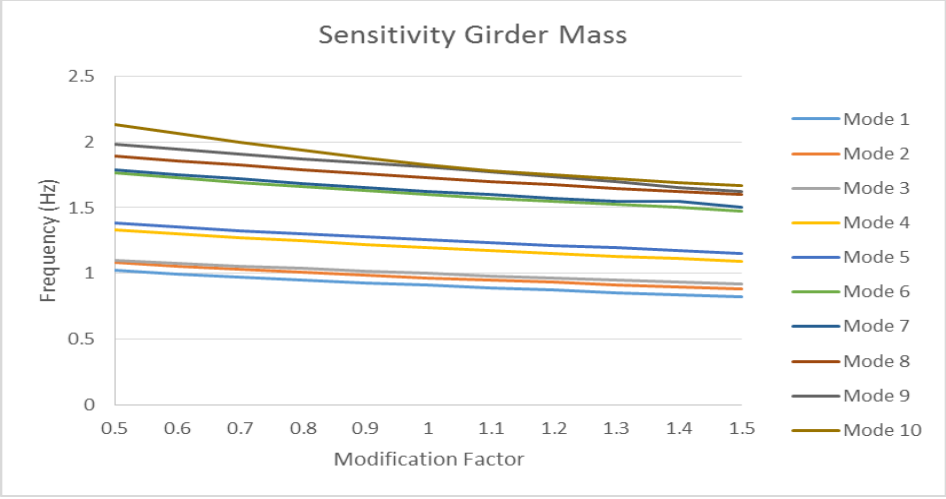

Figure 5.11 Sensitivity plot of girder mass

In order to have reasonable value for the equivalent stiffness of the elastomeric bearing of the bridge, a sensitivity study was performed. The initial values of the equivalent stiffness of the bearings were 1500 KN/m. This value was based on similar study conducted by C. Akogul and O.C. Celik (2008) of a bridge in California with similar properties and dimension as this case study. The values of the equivalent stiffness range from 1000 KN/m to 2000 KN/m. These values were selected to simulate the approximate values of the bearings, since there is no detailing available. Figure 5.12 shows a plot of the sensitivity of the elastomeric bearings equivalent stiffness. As seen, changing the equivalent stiffness between 1000 KN/m and 2000 KN/m does not have much effect on the first fundamental modes, up to mode 9. It only has some effect on mode 10, where the change is more visible below between 1000 KN/m and 1500 KN/m.

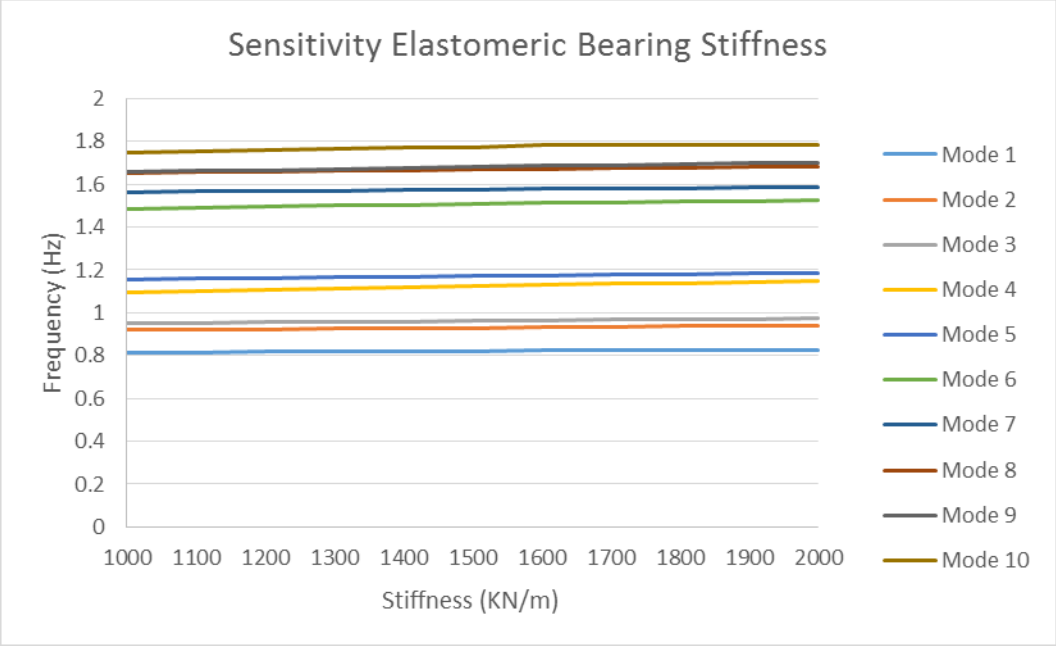

Figure 5.12 Sensitivity plot of the stiffness of the elastomeric bearing

5.3 Model Updating

In this section, the developed FE model is updated to match the modal frequencies found in section 4.3. Considering the available recorded data, the model is manually updated. The main properties to update are those identified in the sensitivity analysis.

There is a large degree of uncertainty in the modeling of bridge elements. There are many aspects of concrete elements that may not be captured through the FE model. For example, reinforcement in concrete is not modeled, nor is the interaction between concrete and steel. Also, the bridge deck has prestressing in the transverse direction at the bent cap, which is not modeled. The stiffness of the elastomeric bearings was modeled based on a previous study of a similar bridge since no details of the bearings were available. Similarly, the actual mass of extra elements on the bridge, those not taken into account, can contribute and modify the dynamic properties of the bridge.

Based on the sensitivity study conducted and knowing that the main properties of the bridge are the column stiffness, girder mass and elastomeric bearing stiffness, model updating was performed using two different steps. A summary of the model-updating task is presented in Table 5.2. The column piers were grouped into sections, as shown in section 5.2.

Table 5.2 List of updating steps

Step	Direction	Updating Parameter
1	Transverse	Sections 3-5, Girder Mass, Bearing Stiffness
2	Longitudinal	Sections 3-5, Girder Mass, Bearing Stiffness

5.3.1 Step 1: Updating the Initial Model to the Frequencies Obtained in the Transverse Direction

Using the developed FE model and knowing the frequencies obtained through system identification, model updating to sections 3 through 5 addressed girder mass and bearing stiffness. First, the girder mass was updated; it was increased by 10%. The modal frequency in the transverse direction was reduced but did not match the identified frequencies, having errors ranging from 15% to 21%. Then, the stiffness of the columns was updated to 0.4 Ig. This value is reasonable since it is not uncommon to have a reduction in stiffness ranging from 35 to 60% (Prestley, Seible and Calvin, 1996). Figure 5.13 shows the modification factors obtained through the model updating. After this updating, the modal frequencies were improved and the errors of the modal frequencies were reduced from 21% to 15%, and from 13% to 9%. In addition, the elastomeric bearing stiffness was updated; it was reduced from 1500 KN/m to 1100 KN/m. The frequencies were now closer to those identified. The error was reduced, and ranged from 10% to 7%. This error was reasonable but a smaller error was desired. Therefore, it was decided to update the stiffness of the cap beams. Based on the observations of the investigation team, the cap beams suffered cracking during the earthquake. For this reason, they were updated to 0.8 Ig. After this update, better matching was observed. Table 5.3 shows a comparison between the

modal frequencies of the initial FE model and after the update. The modal frequencies are very close to the values of the identified frequencies. Mode 5, which was identified from the Napa earthquake (2014), was observed to be mode 15 of the FE model. Other modes from the left-hand side of the bridge appear first and are not captured by the current instrumentation of the bridge. As result, only these first five modal frequencies are used for the updating and response prediction study.

Table 5.3 Comparison of modal frequencies of the initial FE model and the values of the updated FE model with the values identified from the Napa earthquake (2014) in the transverse direction

Mode No.	Identified Frequency (Hz)	Initial FE Frequency (Hz)	Updated FE Frequency (Hz)
1	0.62	0.81	0.66
2	0.86	1.09	0.89
3	0.95	1.16	0.93
4	1.19	1.66	1.23
5	2.29	2.75	2.15

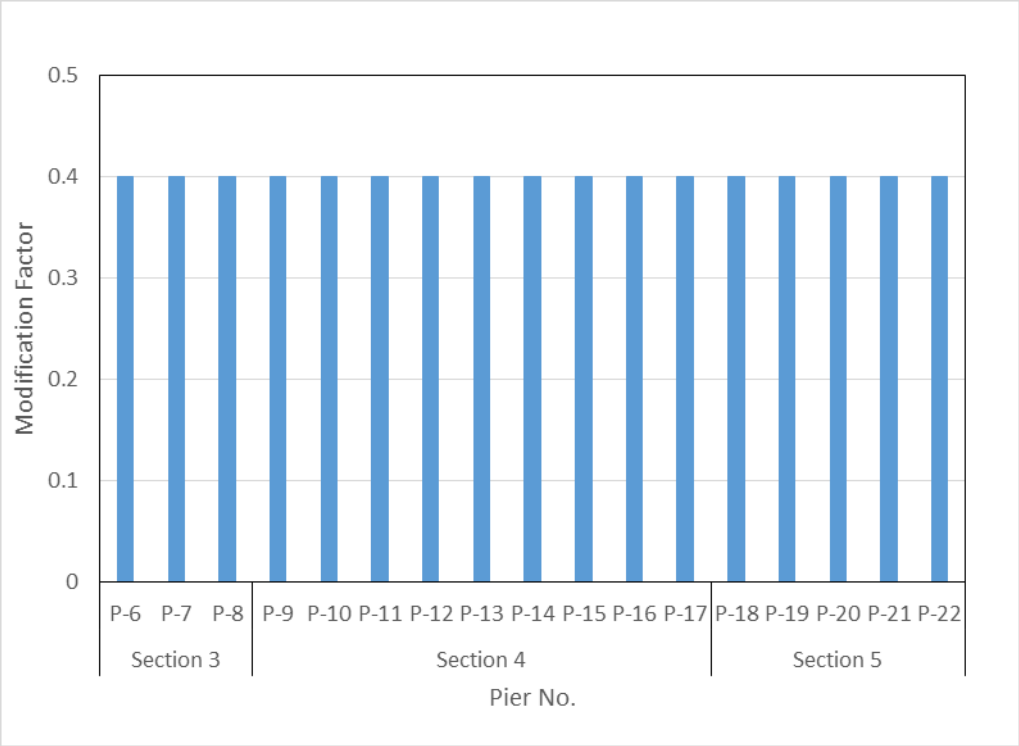

Figure 5.13 Modification factors applied to the stiffness of the piers of sections 3, 4 and 5 in the transverse direction

5.3.2 Step 2: Updating the First Mode Frequency Obtained in the Longitudinal Direction

After applying the model updating procedure to the transverse direction, the longitudinal direction was studied in the same way. Knowing that the girder mass was increase by 10% and a cracking stiffness was reduced for the cap beams, a new modal frequency was obtained for the longitudinal direction. It was reduced from 0.918Hz to 0.846Hz. This indicates that further updating of the column piers was needed in the longitudinal direction. The columns were updated manually and the modification factors were limited to the valued obtained in the transverse direction on 0.4 Ig. Figure 5.14 shows the modification factors obtained through the model updating of the column piers in the longitudinal direction. After updating the column piers

of sections 3, 4 and five5 the frequency was reduced to 0.74Hz. This value gives a 12% error between the identified and updated frequencies. For this reason, the elastomeric bearing stiffness was reduced to 1100 KN/m for the longitudinal direction. This gave a frequency of 0.713Hz, which corresponds to an 8% error between frequencies. Table 5.4 shows the values of the comparison between the frequencies of the FE model and the updated FE model with the identified values of the Napa earthquake (2014). As observed, the modal frequencies have a close match. It is important to mention that only the first mode was identified because it has limited sensors on the longitudinal direction.

Table 5.4 Comparison of modal frequencies of the initial FE model and the values of the updated FE model with the values identified from the Napa earthquake (2014) in the longitudinal direction

Mode No.	Identified Frequency (Hz)	Initial FE Frequency (Hz)	Updated FE Frequency (Hz)
1	0.66	0.92	0.71

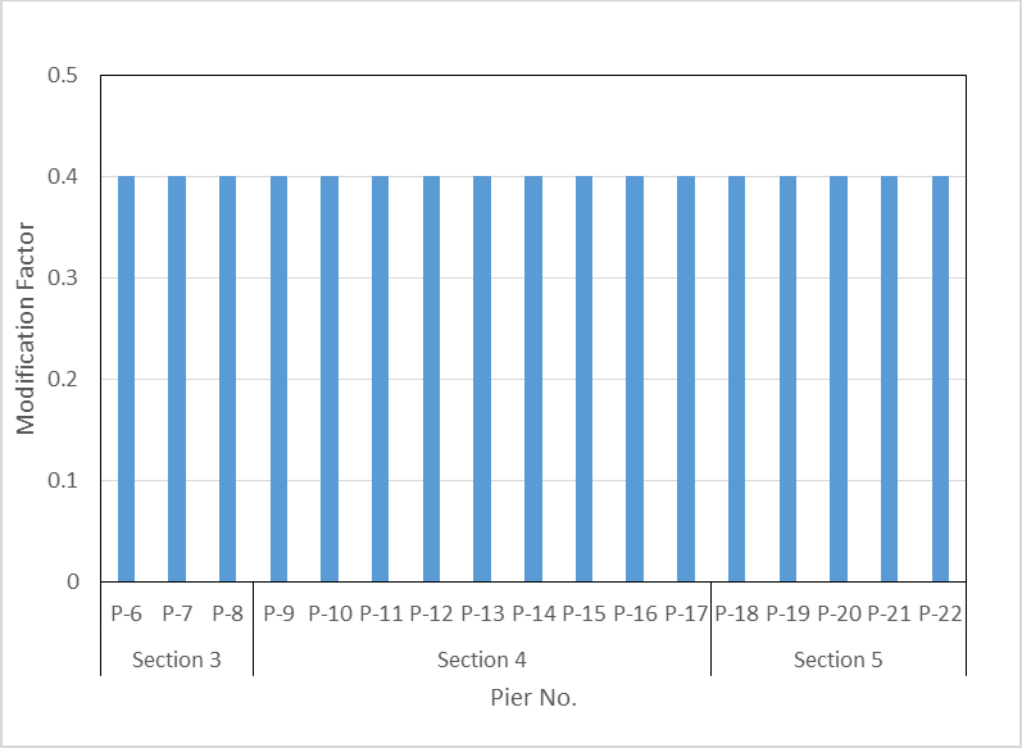

Figure 5.14 Modification factors applied to the stiffness of the piers of sections 3, 4 and 5 in the longitudinal direction

5.4 Summary of Model Updating

In order to understand how the parameters affect the dynamic properties of the bridge, a sensitivity analysis was carried out. The column stiffness (grouped in sections), girder mass and bearing stiffness were studied. The study reveals that not all of the columns have impact on the modal frequencies of the bridge. Only sections 3, 4 and 5 play an important role. The mass of the girders affect the modal frequencies, if there is big increase in mass and good judgment needs to be taken into account when adding mass. On the other hand, the stiffness of the elastomeric bearings seemed not to affect the mode shapes and frequencies of the FE model as much, when it

was increased or reduced. Based on these findings, and on careful consideration of the parameters, model updating to the FE model was performed. Table 5.5 shows a summary of the FE model results to the identified values of the Napa earthquake (2014).

Table 5.5 Summary of the FE model results and the identified frequencies

Mode No.	**Frequency (Hz)**		
	FE	Identified	Error (%)
Transverse Direction			
1	0.66	0.61	8.5
2	0.85	0.86	4.5
3	0.92	0.94	1.8
4	1.22	1.19	2.5
5	2.15	2.29	6.5
Longitudinal Direction			
1	0.71	0.66	8.0

As can be observed, the variation between the modal frequencies went from 8.5% to 1.8%. These are good values compared to the identified frequencies. These modes were limited to five, since the purpose of this study is to match the recorded peak displacement (section 5.5) of the 2014 Napa earthquake. Furthermore, if better representation of bridge behavior is desired, more instrumentation is required along the left side of the bridge.

5.5 Response prediction of the FE model to Response of the Hwy 37 Napa River Bridge to the 2014 Napa earthquake

The purpose of this study is to predict the response of the peak displacements at the sensor locations of the Hwy 37 Napa River Bridge during the 2104 Napa earthquake. In order to do so, and to have a good response prediction, the information required would be that of the motion recorded at the pile cap at the locations of interest. However, there is no data available at the location of the bridge mid-span, or other pile caps where the sensors are located. For this reason, a preliminary analysis was carried out using the free-field recorded data at the surface of the geotechnical array, located near abutment 26 of the bridge. It was observed that the time history results in the longitudinal direction for the peak displacement are very close to recorded data. On the other hand, the displacements resulting from the time history analysis in the transverse direction were very small compared to the recorded data. For this reason, the recorded data at the free-field in the transverse direction was studied and compared to the design spectrums given in the as-built drawings by Caltrans. Figure 5.15 (a) shows the Caltrans design spectrum near abutment 26 and the response spectrum of the Napa earthquake (2014), and Figure 5.15 (b) shows the Caltrans design spectrum at the bridge mid-span. As observed, the response spectrum of the free-field data in the transverse direction is different than the design spectrum at mid-span.

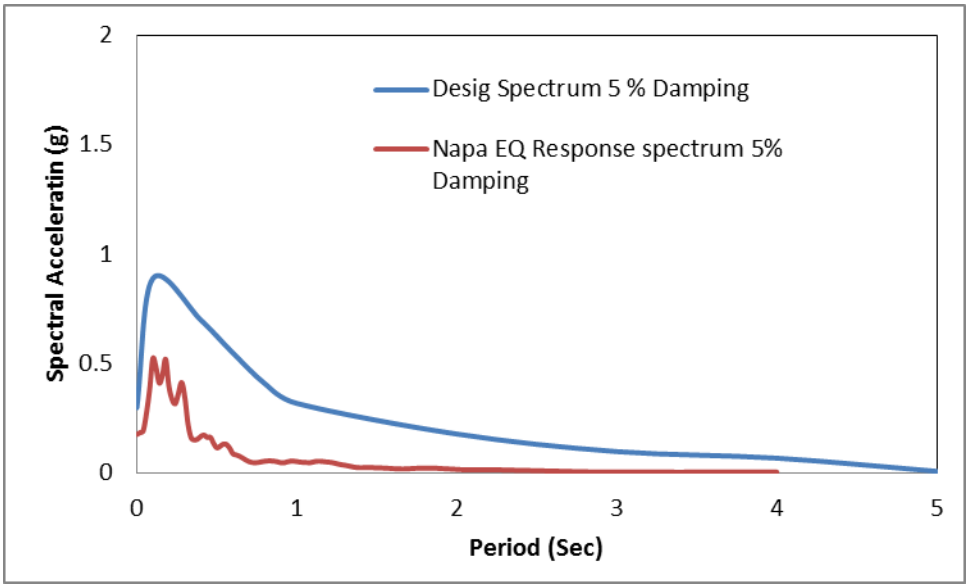

(a)

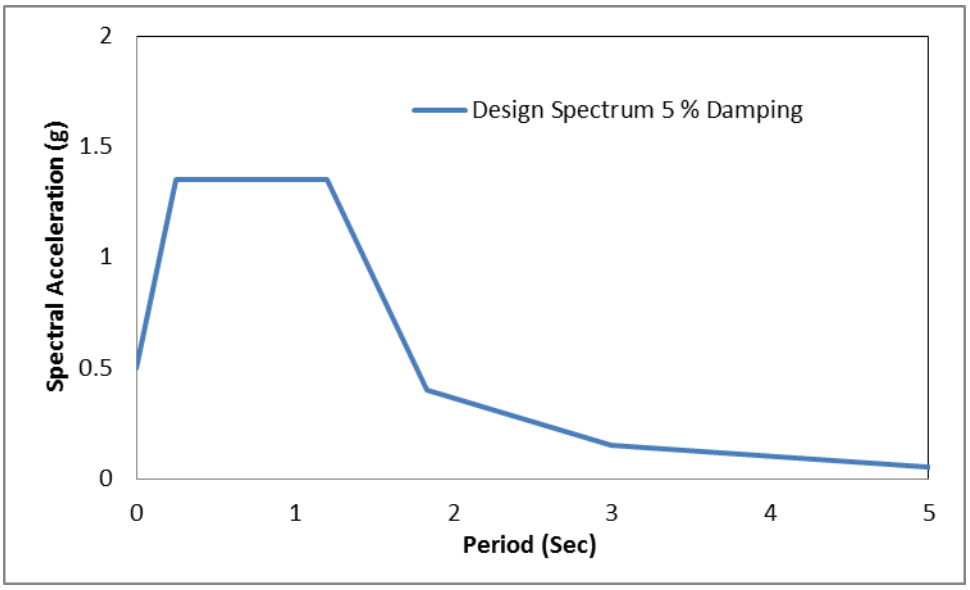

(b)

Figure 5.15 (a) Response spectrum near abutment 26 compared to the response spectrum of free-field (b) response spectrum at mid-span from the as-built drawing

Based on these reasons, the free-field motion in the transverse direction was scaled to match Caltrans' design spectrum at mid-span, see Figure 5.15 (b). Because the response spectrum of the 2014 Napa earthquake is about 50% of the Caltrans design spectrum at abutment 26 (Figure 5.15 (a)), the scaled motion at mid-span was reduced to 50% of its scale values. This was done to approximate the input motion, as the design spectrums were done for a probabilistic earthquake of 2% in 50 years. This was not the case for the 2014 Napa earthquake.

Figure 5.16 to Figure 5.21 show the acceleration time history comparison between the recorded data and results obtained from the FE model. As can be observed, the peak accelerations are underestimated for channels 1, 3 and 8, whereas the accelerations for channels 5, 6 and 7 are overestimated. The main reason for not getting better results for the peak values is because the input motion used in this study is a simulated (scaled) motion. For long-span bridges, multi-input motions are needed as the soil conditions change along the length of the bridge.

Figure 5.22 to Figure 5.27 show the velocity time history comparison between the recorded data and the results obtained from the simulated response. In this comparison it is observed that the peak velocities are within the values of the recorded data. Moreover, a beat effect appears in the histories after the big pulse of the earthquake. This appears when two frequencies are set close together, and it can be observed from the comparison that the model does not capture this phenomenon.

Figure 5.28 shows the displacement time history comparison between the recorded data of channel 3 and the FE model results for the longitudinal direction. As can be seen, the peak displacement is under-predicted. However, the response prediction is close to the recorded data. Similarly, Figure 5.29 shows the time history comparison between the FE model results and the recorded displacement at mid-span of channel 1. The peak displacements of the FE model are close to the values of the recorded data, however, the model is over-predicting them. This is because the input motion was a simulated (scaled) one. Moreover, the beat effect can be more clearly seen in these figures. Based on the Fourier analysis of channel1 (Figure 4.9), it can be seen two close frequencies. The first peak is around 0.62 Hz and the second is around 0.68 sec. The model was well updated to the first peak frequencies. For this reason, it is able to capture the peak displacement and frequency between 25- 40 sec of the recorded data (Figure 5.29). However, the model was not updated to the second frequency of 0.68 Hz and for that reason is not capturing the second peak (beat effect) in the time history plot. If better representation of the time history of the FE model is desired, the model needs to be updated to address these close frequencies and not only the five used in this study. In addition, sensors at the base of the column and in the foundation are needed. This would enable the gathering of more appropriate motions during earthquake events in the future.

Figure 5.30 shows the displacement comparison of the recorded and calculated response signal of channel 5 located above pier 16. As it is observed, the FE model overestimates the peak displacement, but it seems to capture the frequency content of the recorded data at the time of the earthquake pulse. The reasons for over-predicting displacement could be that frequencies not captured by the FE model are playing an important role, especially since a beat phenomenon is

observed on the recorded data. Moreover, a simulated ground motion was applied to the entire bridge. This is not necessarily correct, as the bridge is about 1 km long and the soil conditions vary along the length of the bridge. Multi-input motions are more desirable for such long bridges.

Figure 5.31 presents the displacement prediction to the calculated signal of channel 6 located on the bridge deck over pier 18. It is observed that the predictions have close values to the recorded data, in peak displacement and frequency content. The model is again over-predicting the peak values, and the beat phenomenon is again observed. But overall the peak displacement is close, given the assumptions taken when developing the FE model.

Figure 5.32 shows the displacement prediction of channel 7 located at the bridge deck over pier 20. The response over-predicts the peak displacements compare to the recorded data of channel 7. However, the response has a close match to the recorded data in displacement and frequency content. Again, a reason for over-predicting the displacement is that the model is using a single input motion for the entire length of the bridge.

Figure 5.33 shows the displacement prediction of channel 8, which is in the longitudinal direction. The sensor is located on the bridge deck above pier 20. This prediction is very close to the actual recorded data overall. The peak displacement is captured and the frequency content of the entire record is captured. The reason for this response being more accurate is that the input motion used for the longitudinal direction was the recorded data of the free-field. The input motion is in the range of the response spectrum of abutment 26, which corresponds to the free-

field data (Figure 5.15 (a)). Having a well-developed FE model and the exact input motion at the location of interest would yield good results and predictions. For these reasons, it is important to consider increasing the sensor instrumentation on the bridge.

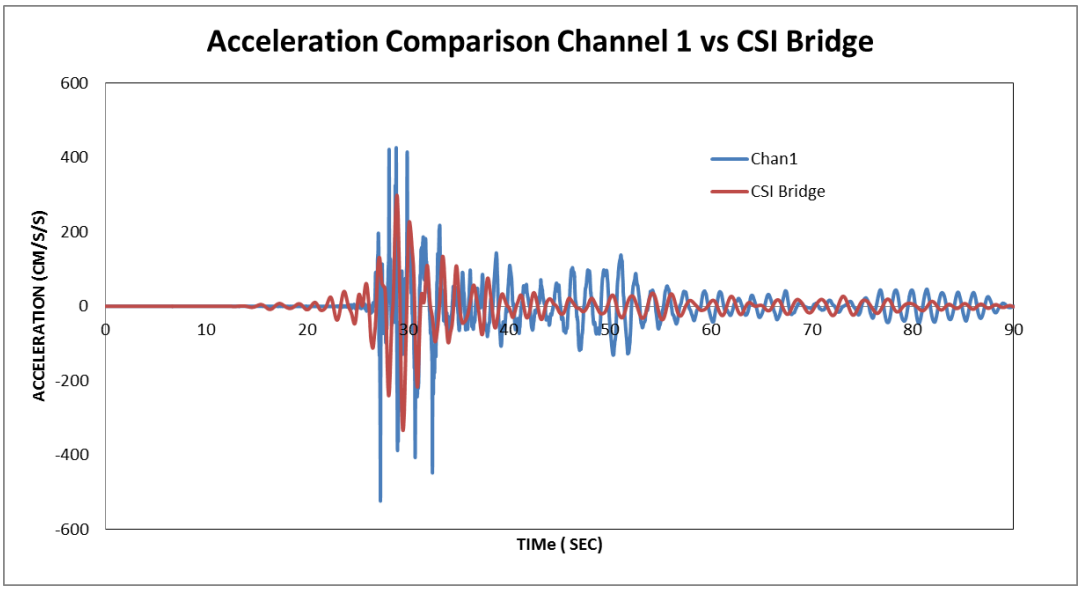

Figure 5.16 Acceleration comparison between the recorded data of channel 1 and the FE element model

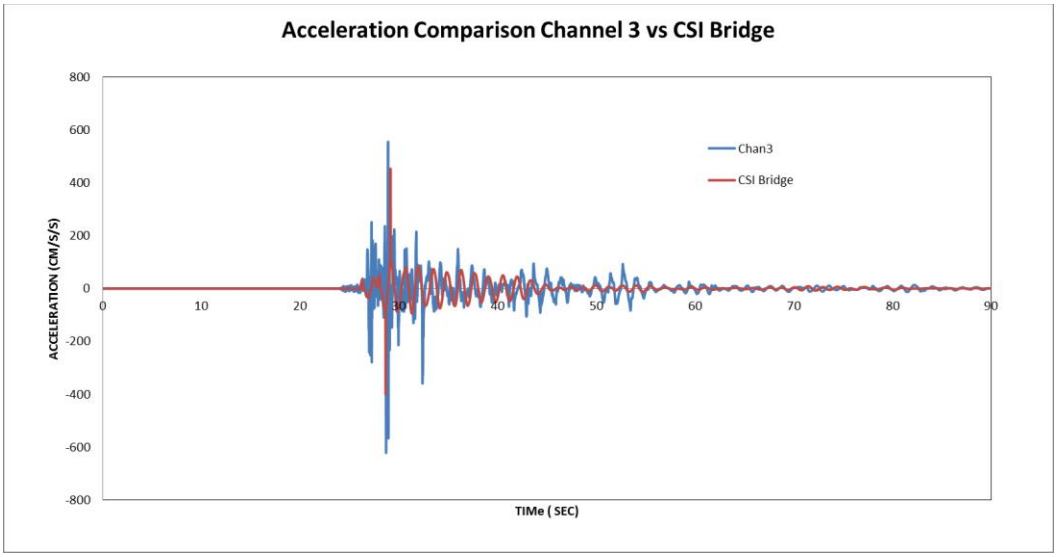

Figure 5.17 Acceleration comparison between the recorded data of channel 3 and the FE element model

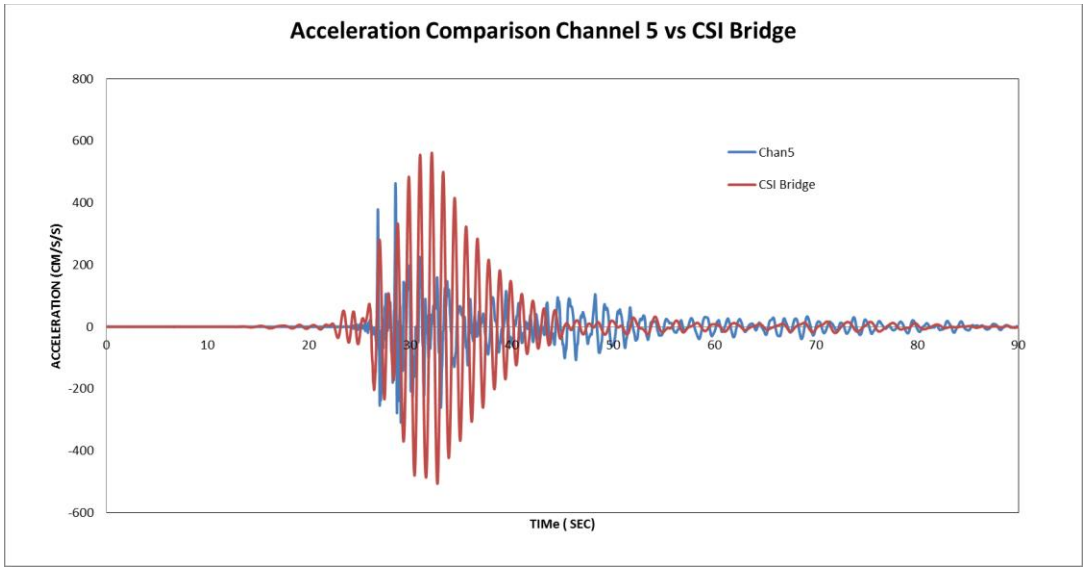

Figure 5.18 Acceleration comparison between the recorded data of channel 5 and the FE element model

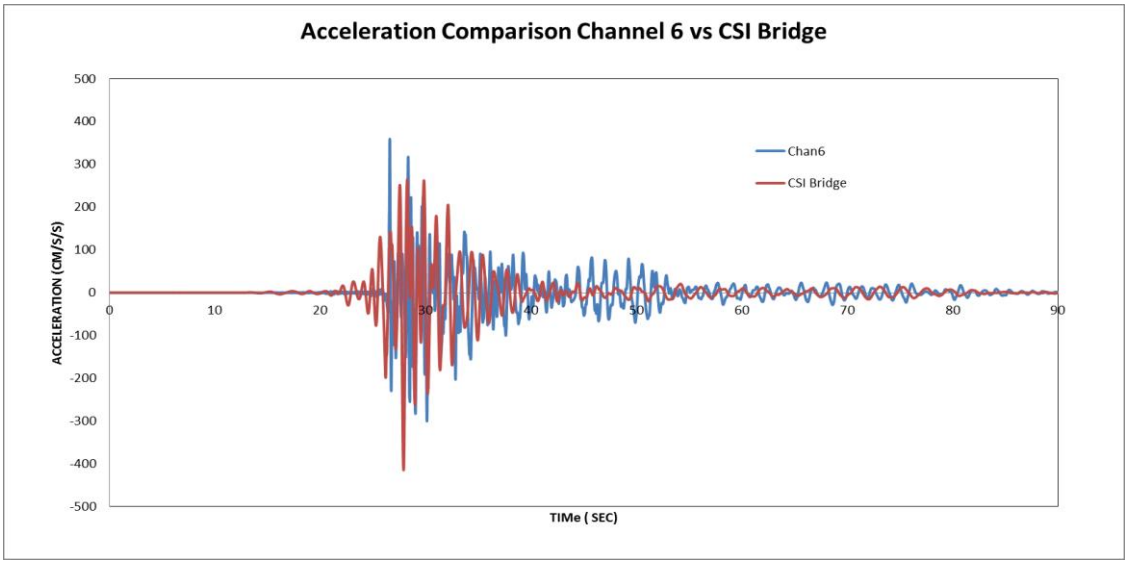

Figure 5.19 Acceleration comparison between the recorded data of channel 6 and the FE element model

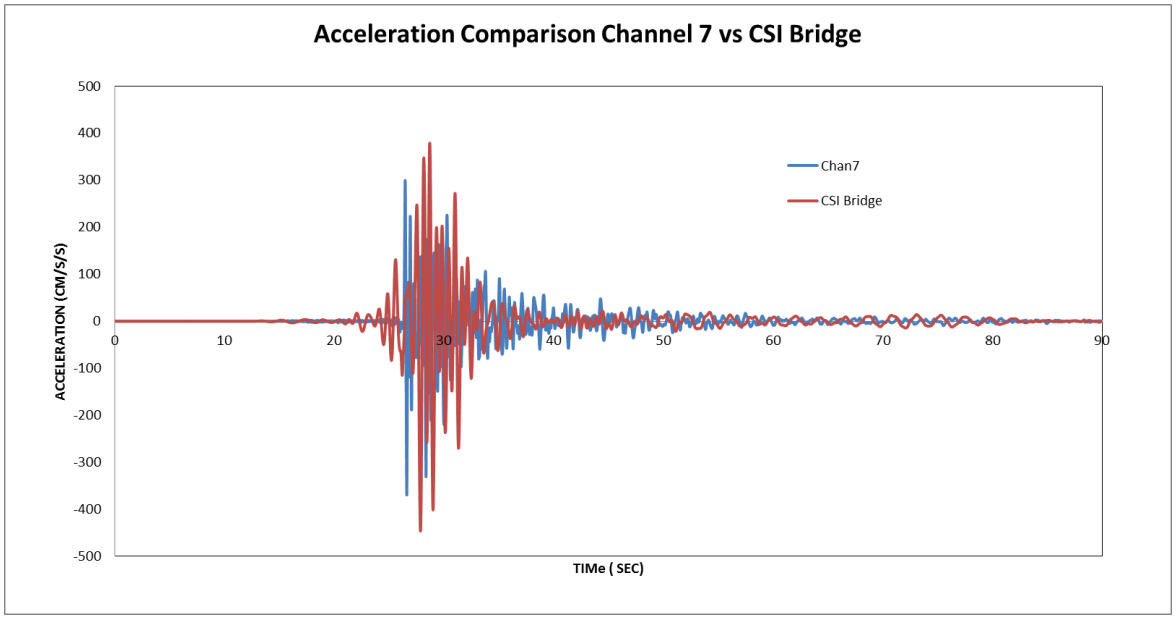

Figure 5.20 Acceleration comparison between the recorded data of channel 7 and the FE element model

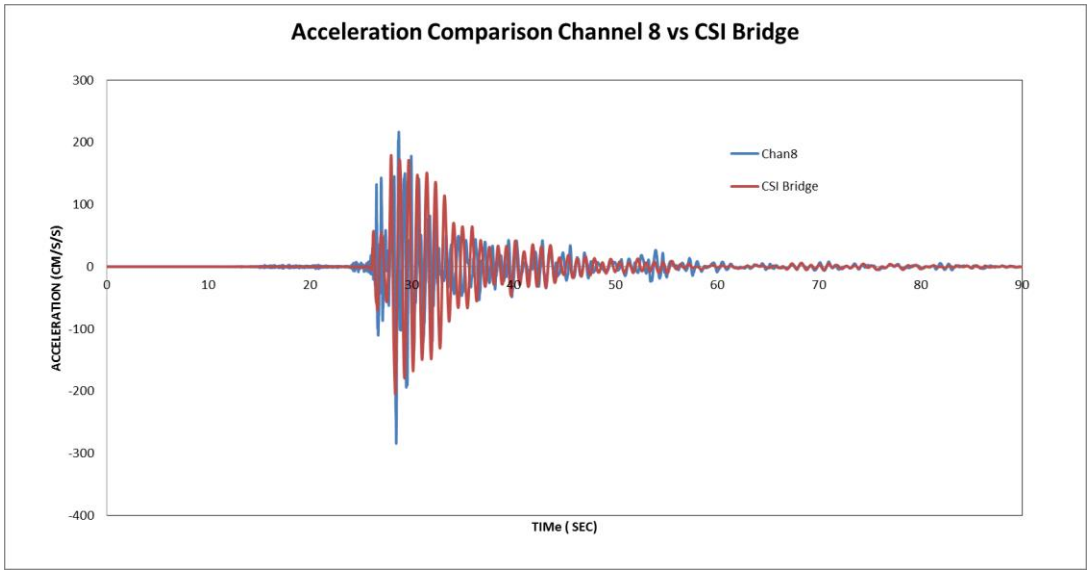

Figure 5.21 Acceleration comparison between the recorded data of channel 8 and the FE element model

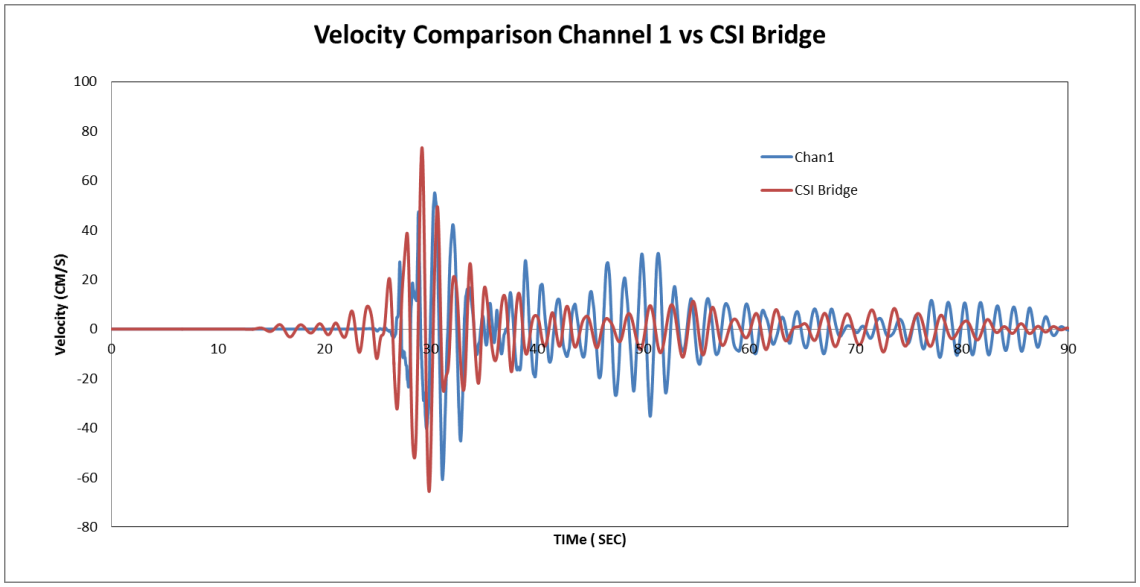

Figure 5.22 Velocity comparison between the recorded data of channel 1 and the FE element model

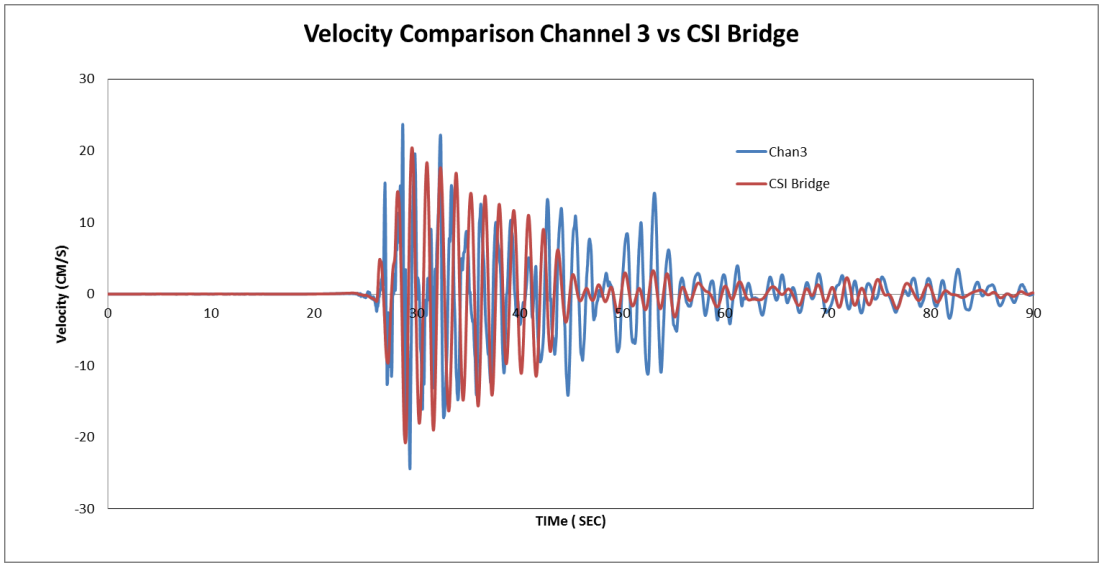

Figure 5.23 Velocity comparison between the recorded data of channel 3 and the FE element model

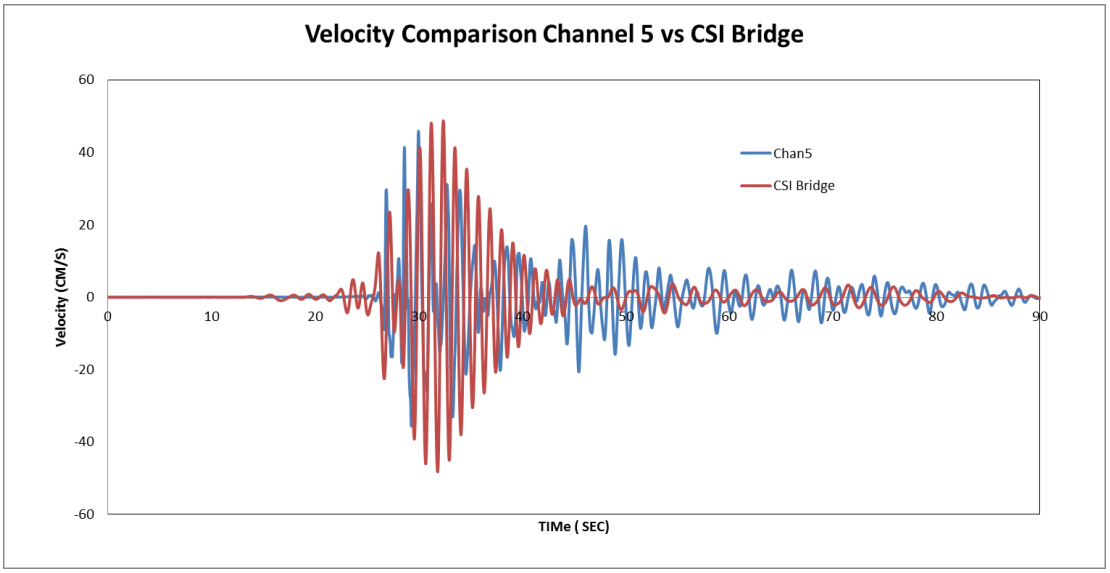

Figure 5.24 Velocity comparison between the recorded data of channel 5 and the FE element model

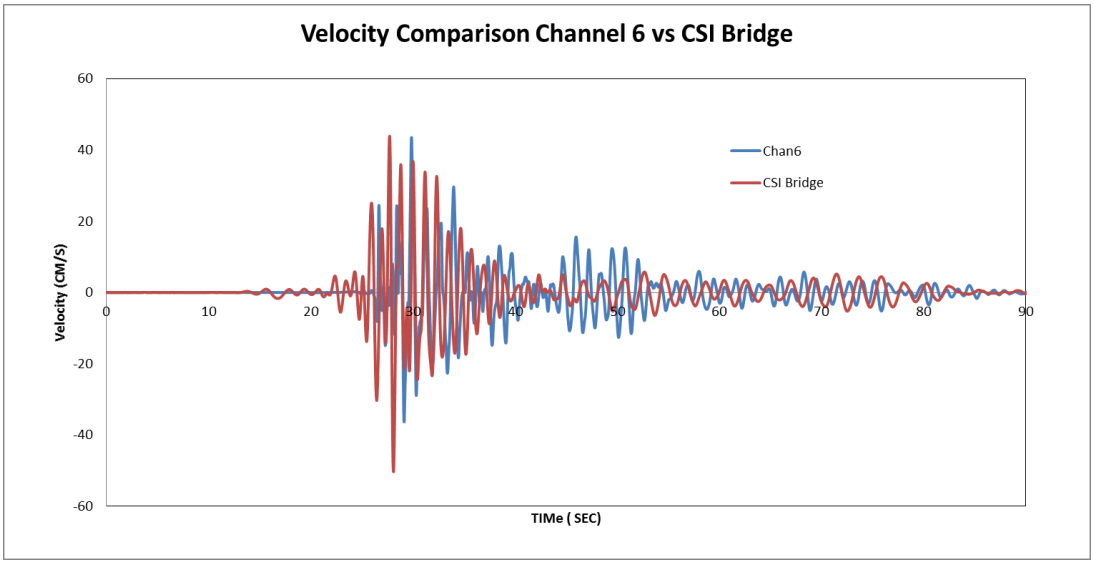

Figure 5.25 Velocity comparison between the recorded data of channel 6 and the FE element model

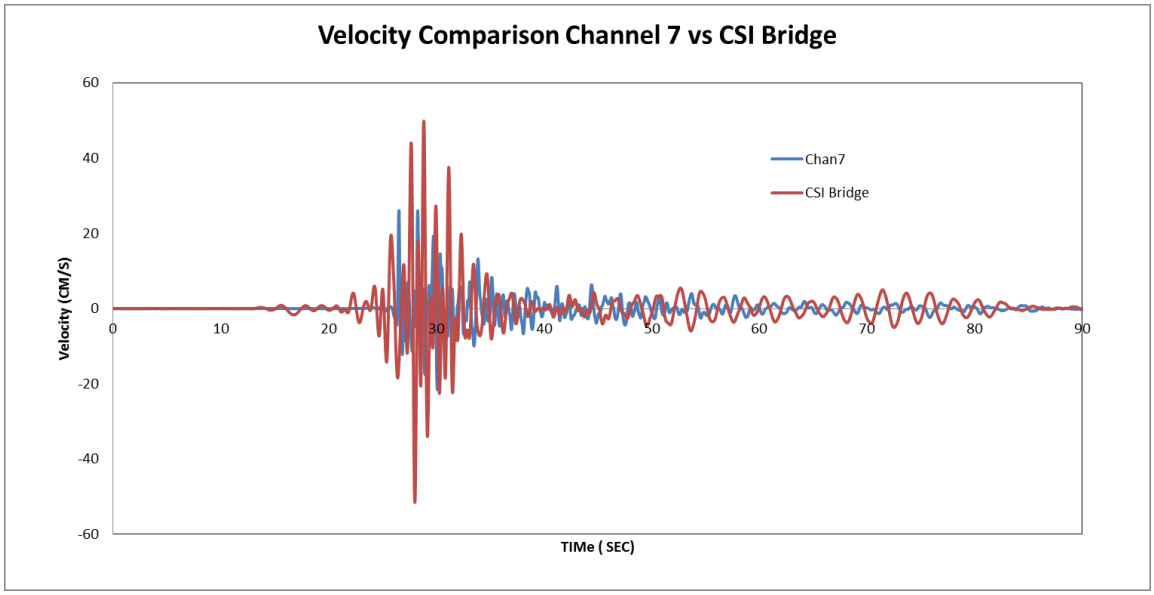

Figure 5.26 Velocity comparison between the recorded data of channel 7 and the FE element model

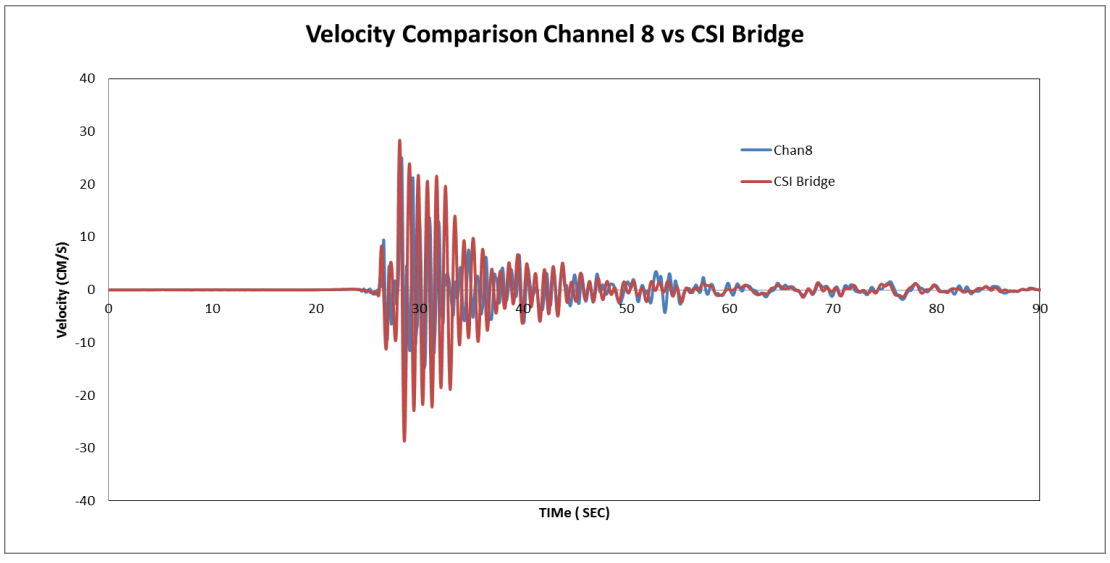

Figure 5.27 Velocity comparison between the recorded data of channel 8 and the FE element model

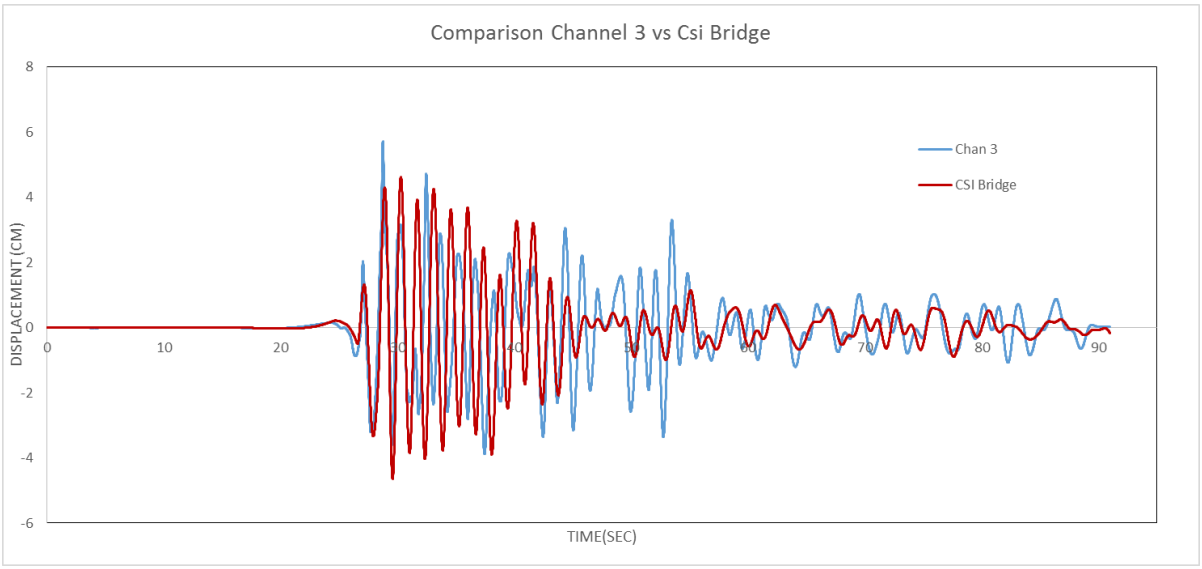

Figure 5.28 Displacement comparison between the recorded data of channel 3 and the FE element model

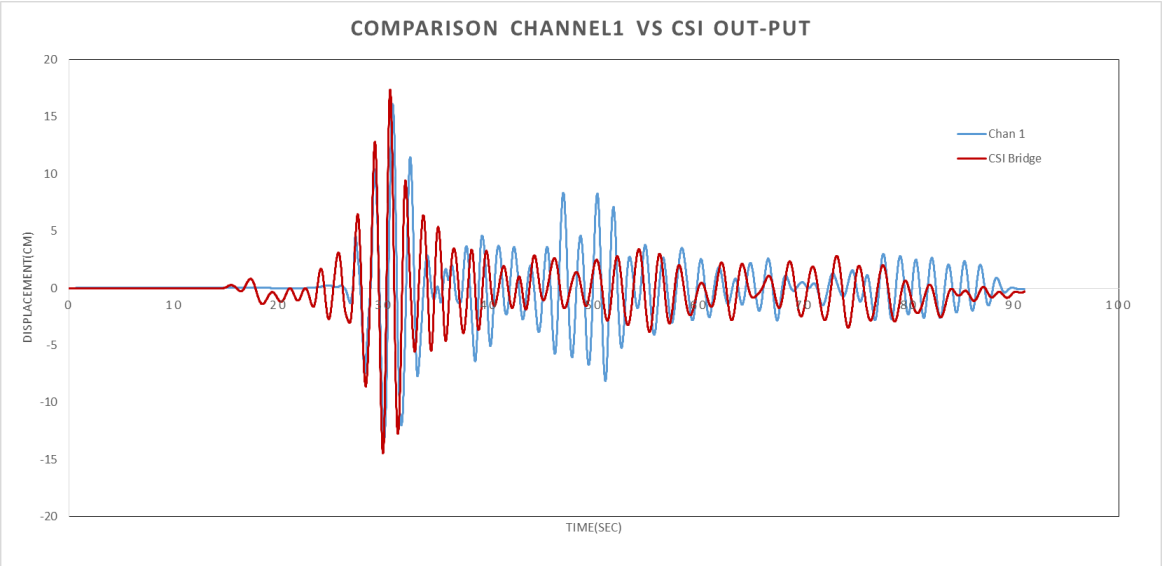

Figure 5.29 Displacement comparison between the recorded data of channel 1 and the FE element model

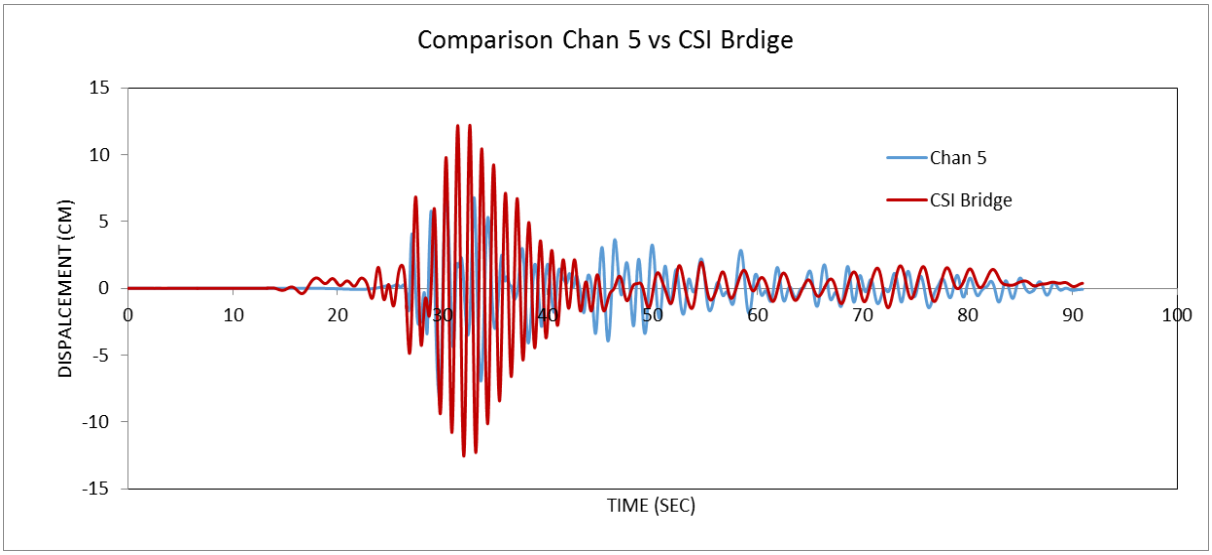

Figure 5.30 Displacement comparison between the recorded data of channel 5 and the FE element model

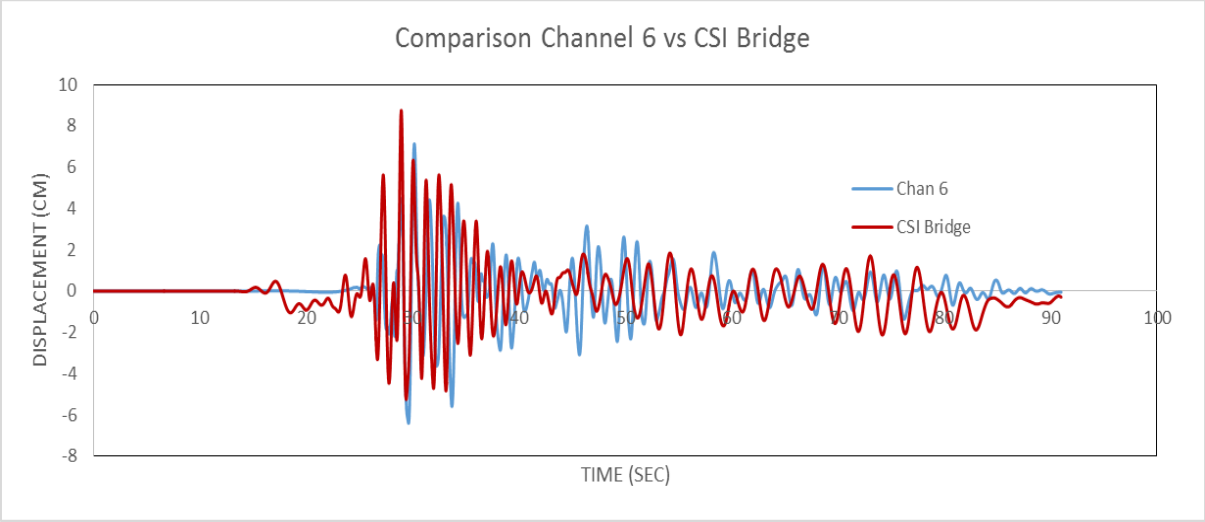

Figure 5.31 Displacement comparison between the recorded data of channel 6 and the FE element model

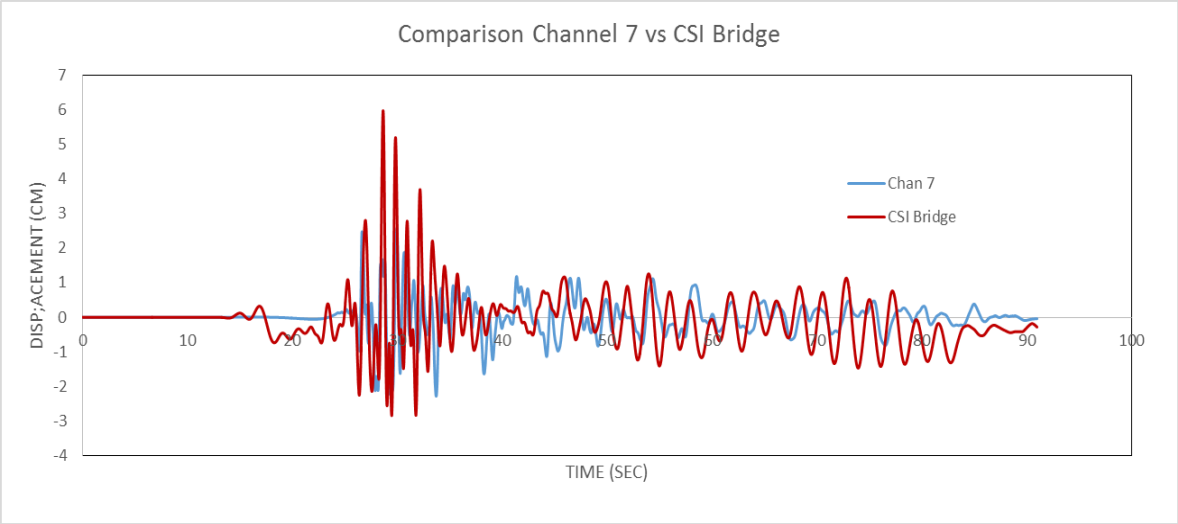

Figure 5.32 Displacement comparison between the recorded data of channel 7 and the FE element model

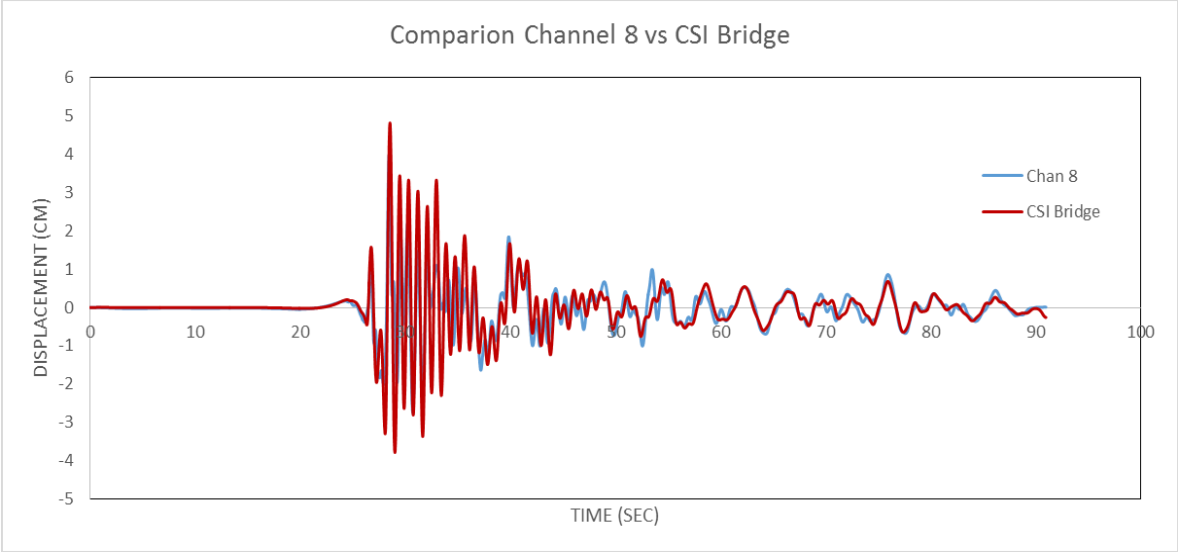

Figure 5.33 Displacement comparison between the recorded data of channel 8 and the FE element model

After performing the time history analysis to the FE model and comparing the results to the recorded data, it was observed that the FE model gives good predictions of the peak

displacement values of the Napa River Bridge to the 2014 Napa earthquake. The peak displacements at mid-span of the bridge for the longitudinal and transverse direction have a close match to the recorded data. The predicted response at mid-span does not correctly represent the entire response of the record because the free-field motions were scaled to the design spectrum at mid-span and a linear 50% reduction was done. This was done because no sensors were located at the base of the columns, pile caps or piles to use as an input motion. Moreover, a beat phenomenon is observed in channel 1, 2, 5 and 6. This shows that the model does not correctly capture the frequencies of the bridge, especially if the frequencies are close to each other. It is important to mention that updating a model to capture frequencies that are close is extremely difficult and is beyond the scope of this study.

Similarly, the peak acceleration and velocities for channels 1, 3, 5, 6 and 7 are not well predicted. The main reason is because a simulated motion is used for the entire length of the bridge, as there are no sensors located at the base of the column or in the pile.

On the other hand, the comparison in acceleration, velocity and displacement of channel 8, located near abutment 26, gives a better overall response prediction. At this location the ground motion that excited the bridge is closer to the recorded data at free-field. This proves that having a good FE model and input motions at the location of interest can give better results in a response prediction. Moreover, using the SDC guidelines from Caltrans allow to capture peak values of the response quantities of the bridge. However, it does not allow to capture the entire behavior of the bridge throughout the length of an earthquake, as seen in this study.

Chapter 6: Summary and Conclusions

The study of predicting the behavior of structures during earthquake loading has become of interest to engineers across many cities. Being able to understand and predict the dynamic behavior of bridges can give great insight for engineers about decision-making on the retrofitting of bridges that can potentially be damaged.

The Napa River Bridge located in Vallejo, California was subjected to the 2014 Napa earthquake (M 6.0). The bridge is part of the strong motion instrumentation network implemented by Caltrans to continuously monitor its infrastructure. The sensors located on the deck of the main channel of the bridge were used to identify the modal frequencies of the bridge during the earthquake. Five modal frequencies were identified from recorded data. It was concluded that more sensors are needed to properly identify all the mode shapes of the entire bridge, as the bridge only possesses sensors on the right side. Moreover, to better understand how the foundation behaves, more sensors are required at the base of the columns, pile caps and pile foundation. This would allow for more exact input motions for the response prediction.

A finite element model was developed in CSI Bridge 2016 using the available as-built drawing and retrofit drawings. The modal frequencies were compared to the identified frequencies; it was observed that model updating was necessary. Before any model updating was performed, sensitivity studies were carried out on the stiffness of the column piers, the girder mass and the elastomeric bearing stiffness. To simplify the analysis, the columns were combined into sections based on the location of the expansion joints. The sensitivity analysis of the

columns showed that only sections 3, 4 and 5 would be more impacted by the dynamic behavior of the bridge if they were modified. The sensitivity analysis of the girder mass showed that by increasing the mass above 20%, the model becomes more sensitive and a drastic change is observed. On the other hand, looking at the sensitivity analysis of the elastomeric bearings showed that there is a small change in frequencies when the stiffness is increase or reduced. Based on these observations, model updating was conducted to the FE model.

Model updating was performed on the bridge by modifying the column stiffness, girder mass and elastomeric bearing stiffness. The column stiffness of sections 3, 4 and 5 were reduced to 0.4 Ig for the longitudinal and transverse directions. The girder mass was increased to about 10% to take into account a mass of elements that were not modeled. This was the limit, as it was a reasonable value and based on the sensitivity study it would have a bigger impact if the value were increased more than 10%. Similarly, the elastomeric bearing stiffness was reduced from 1500 KN/m to 1100 Kn/m. After this update it was observed that the error between modal frequencies was about 10%. It was decided to update the stiffness of the cap beams of the columns, based on the findings of the investigation team that observed cracking of the cap beam. The stiffness was reduced to 0.8 Ig. After this update, the modal frequencies error ranged from 1.5% to 8.5%. These values were decided to be good results for updating purposes.

A time history analysis was performed on the updated FE model to predict the response of the bridge to the 2014 Napa earthquake at the location of the sensors of the strong motion instrumentation. First, time histories were analyzed by using the free-field data from the geotechnical array for the longitudinal direction. It was observed that the response in the

transverse direction was smaller than the recorded data. For this reason, a response spectrum was performed on the free-field data and it was observed that the response spectrum had the shape of the response spectrum near abutment 26. As a result, the ground motion was scaled to the response spectrum at the bridge mid-span, as provided in the as-built drawings. Then the time history was reduced linearly to 50% since the earthquake was not a '2% in 50 years' earthquake. This input motion was used for the transverse direction – for the longitudinal direction the original free-field record at the surface was used.

The response prediction was compared to the recorded data of each sensor located on the main channel of the bridge. It was observed that the acceleration comparison of the recorded data and the results of the FE model are not well predicted. This is because the input motion used was a simulated scaled motion and not the actual ground motion, as no sensors were located at the base of the column or foundation. Also, a beat phenomenon appears on the recorded data and the model does not capture it. This beat phenomenon is more clearly visible in the velocity and displacement time histories. The model does not capture this phenomenon, as it was not updated to those close frequencies that are causing the beat phenomenon. In addition it is extremely difficult to update a model to close frequencies, particularly in the time frame for this study; it was out of the scope of this research.

The result comparison of channel l shows good matching between FE model results and the recorded peak displacement and velocities. The peak displacements are over-predicted but have a close match to the recorded displacement. Similarly, channels 3, 5, 6 and 7 show good predictions for the peak values compared to the recorded data on the bridge. However, over-

predicting the peak displacement can be observed for channels 5, 6, and 7. This is because a single input motion was used for the entire length of the bridge, which is not the true motion of the earthquake at the desired location. If better results are wanted, more sensors need to be placed at the base of the column, pile caps and piles. This would allow for a more comprehensive understanding of the foundation behavior.

On the other hand, channel 8 comparisons show good agreement in peak displacement and frequency content throughout the time history. This is because the sensor is located closer to abutment 26 where the free-field motion was recorded. This shows that having a well-developed finite element model and input motion at the location of interest will ensure response prediction that can be more accurate, compared to the actual recorded data.

It has to be taken into consideration that there are some limitations in producing finite element models that can be compared to a physical, realistic structure. Therefore, engineering judgment into what components can be modeled and what assumptions are made during the modeling procedure is very important. Also, model updating needs to be carefully done since modifying parameters can yield unrealistic properties of a structure. It is important to have good judgment to decide up to what point the updating realistically represents the properties of the bridge.

Finally, the author of this study concludes that following the seismic design criteria provided by Caltrans allows capturing the peak response values of a bridge during an earthquake. These guidelines enable engineers to develop reasonable models of bridges that can give the

peak response values required for design. However, if better results are desired for instrumented bridges, more frequencies need to be identified and not just the peak frequencies from a Fourier analyses. This was observed in the results of this study. A beat phenomenon appeared in channels 1, 3 and 5 and was not captured by the FE model, as the model was not updated to frequencies that were close to each other.

The model developed can capture the peak responses required by Caltrans for design purposes dude to earthquake excitation, given the limitations in this study such as; the limited instrumentation on the bridge, the lack of information on the elastomeric bearing and not having multi-input motion for such a long bridge. In order to have a better representation of the bridge behavior following Caltrans guidelines, more instrumentation on the bridge and a more profound system identification is required. Model updating to the columns should be done individually. This allows having better dynamic properties, yielding better results than just the peak response values. These findings only apply to this study and cannot be generalized to other bridges. In order to have generalized conclusions that can apply to different type of bridges, more case studies are necessary for other instrumented bridges.

6.1 Recommendation for Future Work

A good match between the peak displacement prediction and the recorded data of the 2014 Napa earthquake were obtained. However, more insight is needed and a review of the assumptions should be made, based on the limitations that were found while developing the finite element model and analysis of the recorded data.

This research focuses on the main channel of the Hwy 37 Napa River Bridge. The ramps at the ends of the bridge are not modeled and only their mass was added to the bridge. Moreover, the bridge was modeled with fixed foundation. The contribution of the kinematic effect of the foundation can play an important role in bridge response. For this reason, future work will benefit by studying the contribution of the bridge foundation to the response of the bridge.

The bridge components are all modeled linearly or with equivalent stiffness. Currently, this simplified model gives good results in response prediction of the peak displacements to the 2014 Napa earthquake. However, applying nonlinearities to the model in the columns and expansion joints would give better response prediction and can be used for further studies trying to understand the behavior of the bridge in the nonlinear range.

The recorded data used to identify modal frequencies and use as input motion is limited. If more sensors were to be located on the left-hand side of the bridge, more accurate modal mode shapes can be identified. This would allow a more refined calibration for the developed finite element model. Moreover, in order to have a better understating of the foundation behavior more sensors need to be added at the bottom of the columns, pile caps and piles. This would also determine what input motion can be used if response predictions are desired for earthquake events. A full ambient vibration test is recommended to have a better understanding of the dynamic behavior of the bridge.

Finally, the finite element model was performed manually by adjusting specific parameters. During the updating, close frequencies were not calibrated properly and the beat phenomenon that appears on the recorded data is not captured. For future research a more profound updating procedure is required, possibly automated. This would allow for more parameters to be individually developed. In this research columns were grouped in sections to simplify the updating and the yielding of good results. However, if an optimization technique is used, improved results are possible.

In summary, future research would involve and focus on the following areas:

- conducting a full ambient vibration test of the bridge to obtained more modal frequencies and shapes;
- creating a nonlinear model to incorporate nonlinearities of the columns and foundation;
- increasing sensor instrumentation along the length of the bridge and at the base of the columns, pile caps and piles;
- performing model updating with automated procedures;
- conducting a multi-support excitation analysis of the bridge.

References

Akogul, C., & Celik, O. C. (2008). Effect of elastomeric bearing modeling parameters on the Seismis design of RC highway bridges with precast concrete girders. *In Proceedings of the 14th World Conference on Earthquake Engineering*.

Altunisik, A. C., & Bayraktar, A. (2014). Finite element model updating effect on the structural behavior of long span concrete highway bridges. *Computers and Concrete*, 14(6), 745-765.

Altunişik, A. C., Bayraktar, A., Sevim, B., & Ateş, Ş. (2011). Ambient vibration based seismic evaluation of isolated Gülburnu highway bridge. *Soil Dynamics and Earthquake Engineering*, 31(11), 1496-1510.

Altunisik, A. C., Bayraktar, A., Sevim, B., Kartal, M. E., & Adanur, S. (2010). Finite element model updating of an arch type steel laboratory bridge model using semi-rigid connection. *Steel and Composite* Structures, 10(6), 541-561.

Atamturktur, S., & Laman, J. A. (2012). Finite element model correlation and calibration of historic masonry monuments: review. *The Structural Design of Tall and Special Buildings*, 21(2), 96-113.

Alves, S. W., & Hall, J. F. (2006). System identification of a concrete arch dam and calibration of its finite element model. *Earthquake engineering & structural dynamics*, 35(11), 1321-1337.

Arslan, M. E., & Durmuş, A. (2013). Modal testing and finite element model calibration of in-filled reinforce concrete frames. *Journal of Vibration and Control*, 1946-1959

Bayraktar, A., Altunisik, A. C., Sevim, B., & Turker, T. (2010). Finite element model updating of Kömürhan Highway Bridge based on experimental measurements. *Smart Structures and Systems*, 6(4), 373-388.

Bayraktar, A., Altunişik, A. C., Sevim, B., & Türker, T. (2009). Modal testing, finite-element model updating, and dynamic analysis of an arch type steel footbridge. *Journal of Performance of Constructed Facilities*, 23(2), 81-89.

Bayraktar, A., Sevim, B., Altunışık, A. C., & Türker, T. (2010). Effect of the model updating on the earthquake behavior of steel storage tanks. *Journal of Constructional Steel Research*, 66(3), 462-469.

Bayraktar, A., Sevim, B., & Altunişik, A. C. (2011). Finite element model updating effects on nonlinear seismic response of arch dam–reservoir–foundation systems. *Finite Elements in Analysis and Design*, 47(2), 85-97.

Brincker, R., & Andersen, P. (2006). Understanding stochastic subspace identification. *Proceedings of the 24th IMAC, St. Louis, Missouri, 279-311*.

Brincker, R., Zhang, L., & Andersen, P. (2000). Modal identification from ambient responses using frequency domain decomposition. *In Proc. of the 18*'International Modal Analysis Conference (IMAC), San Antonio, Texas.*

Brocher, T. M., Baltay, A. S., Hardebeck, J. L., Pollitz, F. F., Murray, J. R., Llenos, A. L., & Langenheim, V. E. (2015). The Mw 6.0 24 August 2014 South Napa Earthquake. *Seismological Research Letters*, 86(2A), 309-326.

Brownjohn, J. and Xia, P. (2000). Dynamic Assessment of Curved Cable-Stayed Bridge by Model Updating. Journal Structural Engineering, 10.1061/(ASCE)0733-9445(2000)126:2(252), 252-260.

Caltrans (1967), As-Built Drawings, Hwy 37 Napa River Bridge. California Dept. of Transportation, Sacramento, CA

Caltrans (1998), As-Built Drawings, Seismic Retrofit of the Hwy Napa River Bridge. California Dept. of Transportation, Sacramento, CA.

Caltrans SDC (2015) Seismic Design Criteria, v 1.7. California Department of Transportation, Sacramento, CA.

Chen, W. F., & Duan, L. (2014). Bridge Engineering Handbook: Construction and Maintenance. CRC press.

Chen, Y. (1996). Modeling and analysis methods of bridges and their effects on seismic responses: I—*Theory. Computers & structures*, 59(1), 81-98.

Chopra, A.(2001) "Dynamics of Structures, Theory & Applications to Earthquake Engineering", *Second edition, Prentice Hall*

CESMD (2014) Center of Engineering Strong Motion Data, Retrived March 16, 2016 http://www.strongmotioncenter.org/.

CSMIP (2012) California Strong Motion Instrumentation Program. Retrived March 15, 2016, *http://www.conservation.ca.gov/cgs/smip*.

Chung, Fu C., and Wang Shuqing (2015). Computational Analysis and Design of Bridge Structures. CRC Press.

Computers and Structures, Inc., CSIBridge, Version 18.1.1, 2016.

El-Borgi, S., Neifar, M., Cherif, F., Choura, S., & Smaoui, H. (2008). Modal identification, model updating and nonlinear analysis of a reinforced concrete bridge. *Journal of Vibration and Control*, 14(4), 511-530.

Friswell, M.I., Mottershead, J.E. (1995). Finite element model updating in structural dynamics. *Kluwer Academic Publishers Group, Norwell.*

Garcia-Palencia, Javier Antonio.(2008). A Frequency Response Functions-Based Model Updating Algorithm for Condition Assessment of In-Service Bridges, a Doctoral Dissertation. Ann Arbor: ProQuest LLC 2014.

García-Palencia, A. J., & Santini-Bell, E. (2013). A Two-Step Model Updating Algorithm for Parameter Identification of Linear Elastic Damped Structures. *Computer-Aided Civil and Infrastructure Engineering*, 28(7), 509-521.

Ghahari, S. F., Abazarsa, F., Ghannad, M. A., Taciroglu, E. (2013b). Response-only modal identification of structures using strong motion data, *Earthquake Engineering and Structural Dynamics*, 42, 1221–1242.

Ghahari, S.F., Abazarsa, F., Ghannad, M.A., Celebi, M., Taciroglu, E. (2013c). Blind modal identification of structures from spatially sparse seismic response signals, *Structural Control and Health Monitoring*, 21, 649-674.

Gade, S., Møller, N., Herlufsen, H., & Konstantin-Hansen, H. (2005). Frequency domain techniques for operational modal analysis. *In 1st IOMAC Conference.*

Hemez, F. M., & Stull, C. J. (2012). On the legitimacy of model calibration in structural dynamics. *In Topics in Model Validation and Uncertainty Quantification*, Volume 4 (pp. 95-108). Springer New York.

He, X., Moaveni, B., Conte, J. P., Elgamal, A., Masri, S. F. (2009). System identification of Alfred Zampa Memorial Bridge using dynamic field test data. *Journal of Structural Engineering*, 135(1), 54-66.

Hipley, P. and Huang, M. (1997): Caltrans/CSMIP bridge strong motion instrumentation. 2nd National Seismic Conference on Bridge and Highway, Sacramento, CA.

Ivanovic, S. S., Trifunac, M. D., & Todorovska, M. I. (2000). Ambient vibration tests of structures-a review. *ISET Journal of Earthquake Technology*, 37(4), 165-197.

Jacobsen, N. J., Andersen, P., & Brincker, R. (2006). Using enhanced frequency domain decomposition as a robust technique to harmonic excitation in operational modal analysis. *In International Conference on Noise and Vibration Engineering (ISMA), Leuven, Belgium (p. 12).*

Jaishi, Bijaya, Hyo-Jin Kim, Moon Kyum Kim, Wei-Xin Ren, and Sang-Ho Lee. (2007). "Finite element model updating of concrete-filled steel tubular arch bridge under operational condition using modal flexibility." *Mechanical Systems and Signal Processing*, 2406-2426.

Jang, Shinae, Jian Li, and Billie F. Spencer. (2013). Corrosion Estimation of a Historic Truss Bridge Using Model Updating. *Journal of Bridge Engineering*, 678-689.

Jangid, R.S., (2002). Seismic Response of Bridges, *Journal of Engineering*, 9(2), 156-166.

Kang, G. S., Mahin, S. A. (2014). Preliminary Notes and Observations on the August 24, 2014 South Napa Earthquake. Pacific Earthquake Engineering Research Center, Report No. 2014/12, UC Berkely.

Kaviani, P., Zareian, F., Taciroglu, E. (2014). Performance-based Seismic Assessment of Skewed Bridges," PEER Report No. 2014/1, Pacific Earthquake Engineering Research Center, Berkeley, CA.

Kharrazi, Mehdi H.K., Carlos E. Ventura, Rune Brincker, and Eddy Dascotte. (2002). A Study on Damage Detection using Output-Only Modal Data. *Proceedings of IMAC-XX: Conference and Exposition on Structural Dynamics*. Los Angeles: Society for Experimental Mechanics.

Kudu, F. N., Bayraktar, A., Bakir2b, P. G., Türker1c, T., & Altunişik1d, A. C. (2014). Ambient vibration testing of Berta Highway Bridge with post-tension tendons. *Steel and Composite Structures*, 16(1), 21-44.

Li, Y., Zhang, W., & Liu, Y. (2012). A Method Based on Meta-Model for Updating the Finite Element Model of Bridges Using the Measured Static and Dynamic Data. *In CICTP 2012*: *Multimodal Transportation Systems—Convenient, Safe, Cost-Effective, Efficient* (pp. 3175-3186). ASCE.

Liu, Y., & Duan, Z. (2012). Fuzzy finite element model updating of bridges by considering the uncertainty of the measured modal parameters. *Science China Technological Sciences*, 55(11), 3109-3117.

MATLAB. The language of technical computing. Version Rb2016, Mathworks, 2016.

McDonald, S. (2016). Operational modal analysis, model updating, and seismic analysis of a cable-stayed bridge (Master Thesis, University of British Columbia).

Minshui, H., & Hongping, Z. (2008). Finite element model updating of bridge structures based on sensitivity analysis and optimization algorithm. *Wuhan University Journal of Natural Sciences*, 13(1), 87-92.

Mirzabozorg, H., Hariri-Ardebili, M. A., Heshmati, M., & Seyed-Kolbadi, S. M. (2014). Structural safety evaluation of Karun III Dam and calibration of its finite element model using instrumentation and site observation. *Case Studies in Structural Engineering*, 1, 6-12.

Mottershead, J. E., and M. I. Friswell. (1993) Model Updating in Structural Dynamics: A Survey. Journal of Sound and Vibration, 347-375.

Niu, J., Zong, Z., & Chu, F. (2015). Damage identification method of girder bridges based on finite element model updating and modal strain energy. *Science China Technological Sciences*, 58(4), 701-711.

Park, Hyun-Sung, Young-Soo Park, Jong-Jae Lee, Jung-Sik Kong, and Chang-Geun Lee.(2011) Evaluation of Load Carrying Capacity of a PC Girder Bridge using Model Updating Techniques. *2011 International Conference on Multimedia Technology. Hangzhou: IEEE*. 6349-6352.

Priestley, M. N., Seible, F., & Calvi, G. M. (1996). Seismic design and retrofit of bridges. *John Wiley & Sons.*

Priestley, M. N., Seible, F., & Xiao, Y. (1994). Steel jacket retrofitting of reinforced concrete bridge columns for enhanced shear strength--Part 2: Test results and comparison with theory. *Structural Journal*, 91(5), 537-551.

Ribeiro, D., R. Calcada, R. Delgado, M. Brehm, and V. Zabel. (2012) Finite element model updating of a bowstring-arch railway bridge based on experimental modal parameters. *Engineering Structures*, 413-435.

Sevim, Baris, Alemdar Bayraktar, Ahmet Can Altunisik, Sezer Atamturktur, and Fatma Birinci. (2011). Finite element model calibration effects on the earthquake response of masonry arch bridges. *Finite Elements in Analysis and Design*, 2011: 621-634

Sevim, Baris, Alemdar Bayraktar, and Ahmet Can Altunisik.(2009). Finite element model calibration of berke arch dam using operational modal testing. *Journal of Vibration and Control*, 1065-1079.

Shunlong Li, Hui Li, Jinping Ou.(2007) Model updating for Binzhou Yellow River Highway Bridge considering uncertainties. *Health Monitoring of Structural and Biological Systems*. San Diego: SPIE.

Sipple, Jesse D., and Masoud Sanayei.(2015). Full-Scale Bridge Finite-Element Model Calibration Using Measured Frequency-Response Functions. *Journal of Bridge Engineering*.

Structural Vibration Solutions, Inc. (2016) ARTeMIS Modal Software. http://www.svibs.com/.

Taciroglu, E., Shamsabadi, A., Abazarsa, F., Nigbor, R. L., & Ghahari, S. F. (2014). Comparative Study of Model Predictions and Data from the Caltrans-CGS Bridge

Instrumentation Program: A Case study on the Eureka-Samoa Channel Bridge.*TECHNICAL REPORT*.

Taylor Sepúlveda, D. P. (2007). Calibración del modelo del puente Marga Marga considerando variación espacial del movimiento sísmico a nivel de cepa y estribo.

Teughels, A., and G. De Roeck.(2004) Structural damage identification of the highway bridge Z24 by FE model updating. *Journal of Sound and Vibration*, 589-610.

The Napa River Bridge is the Highway 37 crossover. Between Mare Island and "mainland Vallejo," the river is known as the Mare Island Strait, Retrived, July, 25 2016, http://solanoopenspace.org/OtherOutdoor_VallejoWaterfront.asp

Teughels, Anne, and Guido De Roeck.(2003) Damage Assessment of the Z24 bridge by FE Model Updating. *Key Engineering Materials*, 2003: 19-26.

Turek, Martin, Carlos E. Ventura, and Eddy Dascotte. (2010).Model Updating of the Ironworkers Memorial Second Narrows Bridge, Vancouver, Canada. *Proceedings of the IMACXXVIII. Jacksonville: Society for Experimental Mechanics.*

Turek, Martin, Yavuz Kaya, Carlos Ventura, and Sharlie Huffman.(2013). Structural Monitoring and Analysis of Bridges for Emergency Response. Topics in Dynamics of Bridges, Volume 94 3: Proceedings of the 31st IMAC. Orange County: Society for Experimental Mechanics.

Türker, Temel, and Alemdar Bayraktar.(2013). Finite element model calibration of steel frame buildings with and without brace. *Journal of Construction Steel Research*, 164- 173.

Turker, Temel, and Alemdar Bayraktar.(2014). Structural safety assessment of bowstring type RC arch bridges using ambient vibration testing and finite element model calibration. *Measurement*, 33-45.

Türker, Temel, and Alemdar Bayraktar. (2014). Vibration based damage detection in a scaled reinforced concrete building by FE model updating. *Computers and Concrete*, 73- 90.

Venegas Bravo, B. M. (2013). Análisis del comportamiento dinámico del puente Marga Marga sometido al terremoto del 27 de Febrero de 2010.

Ventura, Carlos E., Rune Brincker, Eddy Dascotte, and Palle Andersen.(2001). FEM Updating of the Heritage Court Building Structure. *Proceedings of IMAC XIX: 19th International Modal Analysis Conference. Orlando: Society for Experimental Mechanics*.

ViewWave Software©, http://iisee.kenken.go.jp/staff/kashima/viewwave.html.

Wang, H., Li, A. Q., & Li, J. (2010). Progressive finite element model calibration of a long-span suspension bridge based on ambient vibration and static measurements. *Engineering Structures*, 32(9), 2546-2556.

Yashinsky, M., Mahan, M., Lee, D., Bromenschenkel R., Zezoff, R. (2014) Bridge Investigation Team Report for the August 24, 2014 South Napa Earthquake, Caltrans.

Zhao, Qing. (2011). Dynamic Model Updating of Long-span Bridge Based on Optimization Design Principle under Environment Excitation. *International Conference on Consumer Electronics, Communications and Networks. Xianning: IEEE*, 1178-1181.

Zhu, D., Fang, C. H., Cho, C., Guo, J., Wang, Y., & Lee, K. M. (2012). Finite element model updating of a space frame bridge with mobile sensing data. *In SPIE Smart Structures and Materials+ Nondestructive Evaluation and Health Monitoring* (pp. 834513-834513). International Society for Optics and Photonics.

Appendices

Appendix A

It shows the line weight calculate for the extras mass use at the cap beams of the piers that are supporting the exit ramp.

Span 1						
Weight of extra griders				Weight of the deck		
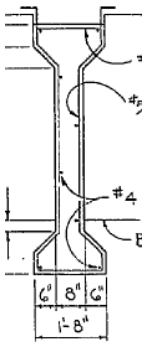				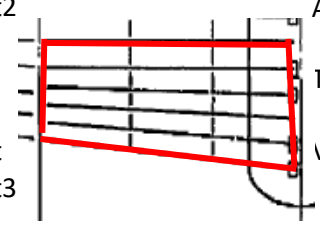		
Agir=	9	ft2		Adeck=	4529	ft2
No. extra girders=	7			Thickness=	7	in
Girder length=	98.92	ft		Volume=	2642	ft3
Volume=	6232	ft3				
γc=	150	lb/ft3		γc=	150	lb/ft3
Weight=	934794	lb		Weight=	396312	lb
Total Weight at abutment=			665553	lb		
Line Weight **AbutmentW-1=**			**8954**	**lb/ft**		

Span 2

Weight of extra griders

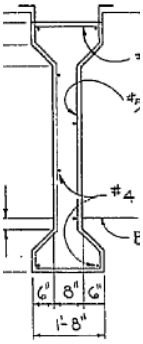

Agir=	9	ft2
No. extra girders=	6	
Girder length=	100	ft
Volume=	5400	ft3
γc=	150	lb/ft3
Weight=	810000	lb

Weight of the deck

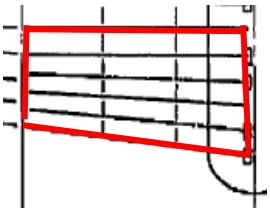

Adeck=	3192	ft2
Thickness=	7	in
Volume=	1862	ft3
γc=	150	lb/ft3
Weight=	279300	lb

Total Weight=	1210203	lb
Line Weight		
PW-2=	**15128**	**lb/ft**

Span 3

Weight of extra griders

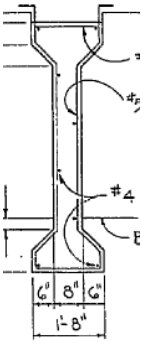

Agir=	9	ft2
No. extra girders=	4	
Girder length=	100	ft
Volume=	3600	ft3
γc=	150	lb/ft3
Weight=	540000	lb

Weight of the deck

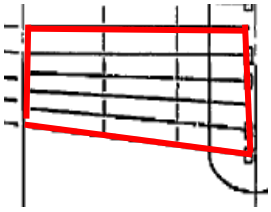

Adeck=	1942	ft2
Thickness=	7	in
Volume=	1133	ft3
γc=	150	lb/ft3
Weight=	169925	lb

Total Weight=	899613	lb
Line Weight		
PW-3=	**8996**	**lb/ft**

Span 4

Weight of extra griders

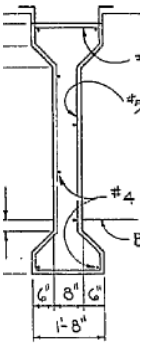

Agir=	9	ft2			
No. extra girders=	3				
Girder length=	100	ft			
Volume=	2700	ft3			
γc=	150	lb/ft3			
Weight=	405000	lb			

Weight of the deck

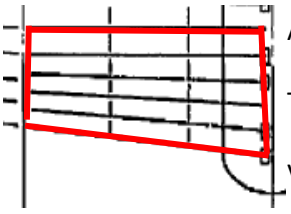

Adeck=	957	ft2
Thickness=	7	in
Volume=	558	ft3
γc=	150	lb/ft3
Weight=	83738	lb

Total Weight=	599331	lb
Line Weight		
P-1=	**6830**	**lb/ft**

Span 5

Weight of extra griders

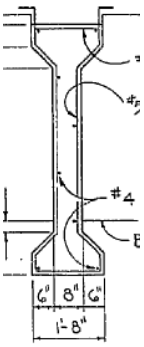

Agir=	9	ft2			
No. extra girders=	1				
Girder length=	30	ft			
Volume=	270	ft3			
γc=	150	lb/ft3			
Weight=	40500	lb			

Weight of the deck

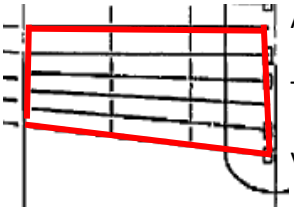

Adeck=	160	ft2
Thickness=	7	in
Volume=	93	ft3
γc=	150	lb/ft3
Weight=	13965	lb

Total Weight=	271601	lb
Line Weight		
P-2a=	**3440**	**lb/ft**

Span 6

Weight of extra griders

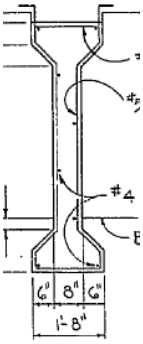

Agir=	9	ft2			Adeck=	267	ft2
No. extra girders=	1				Thickness=	7	in
Girder length=	100	ft			Volume=	156	ft3
Volume=	900	ft3					
γc=	150	lb/ft3			γc=	150	lb/ft3
Weight=	135000	lb			Weight=	23363	lb
	Total Weight=		106414	lb			
	Line Weight						
	P-2b=		**1348**	**lb/ft**			

Weight of the deck

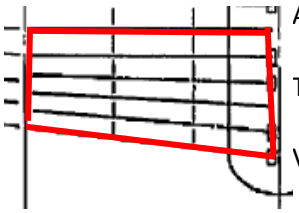

Span 7

Weight of extra griders

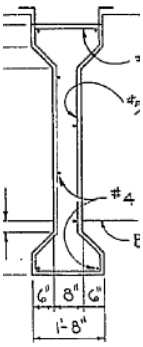

Agir=	9	ft2			Adeck=	34	ft2
No. extra girders=	1				Thickness=	7	in
Girder length=	100	ft			Volume=	20	ft3
Volume=	900	ft3					
γc=	150	lb/ft3			γc=	150	lb/ft3
Weight=	135000	lb			Weight=	2931	lb
	Total Weight=		148147	lb			
	Line Weight						
P-3=	**1976**	**lb/ft**	**P-4=**	**965**	**lb/ft**		

Weight of the deck

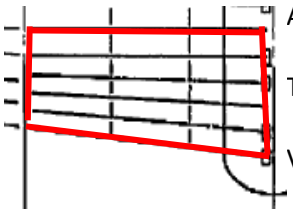

Span 28

Weight of extra griders

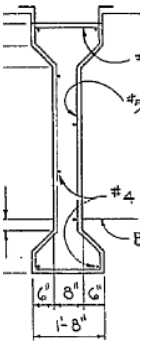

Agir=	9	ft2
No. extra girders=	1	
Girder length=	100	ft
Volume=	900	ft3
γc=	150	lb/ft3
Weight=	135000	lb

Weight of the deck

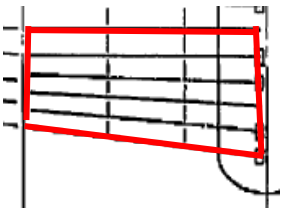

Adeck=	159	ft2
Thickness=	7	in
Volume=	92	ft3
γc=	150	lb/ft3
Weight=	13869	lb

Total Weight= 74434 lb

Line Weight

P-20b= 1041 lb/ft

Span 29

Weight of extra griders

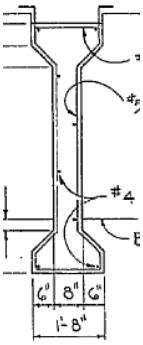

Agir=	9	ft2
No. extra girders=	2	
Girder length=	100	ft
Volume=	1800	ft3
γc=	150	lb/ft3
Weight=	270000	lb

Weight of the deck

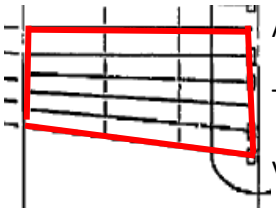

Adeck=	717	ft2
Thickness=	7	in
Volume=	418	ft3
γc=	150	lb/ft3
Weight=	62738	lb

Total Weight= 240803 lb

Line Weight

P-21= 3107 lb/ft

Span 30

Weight of extra griders

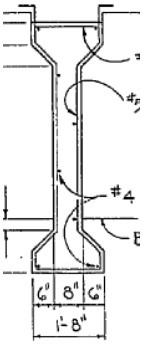

Agir=	9	ft2		Adeck=	1577	ft2
No. extra girders=	3	f		Thickness=	7	in
Girder length=	100	ft		Volume=	920	ft3
Volume=	2700	ft3				
γc=	150	lb/ft3		γc=	150	lb/ft3
Weight=	405000	lb		Weight=	137988	lb

Weight of the deck

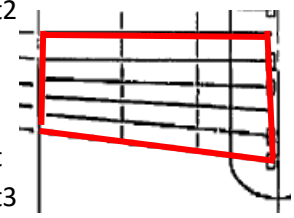

Total Weight= 437863 lb

Line Weight

P-22= 5091 lb/ft

Span 31

Weight of extra griders

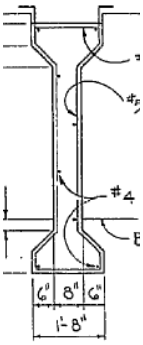

Agir=	9	ft2		Adeck=	2402	ft2
No. extra girders=	4			Thickness=	7	in
Girder length=	100	ft		Volume=	1401	ft3
Volume=	3600	ft3				
γc=	150	lb/ft3		γc=	150	lb/ft3
Weight=	540000	lb		Weight=	210175	lb

Weight of the deck

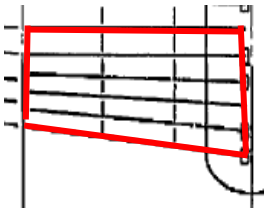

Total Weight= 646581 lb

Line Weight

P-23= 6866 lb/ft

Span 32

Weight of extra griders

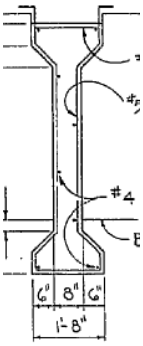

Agir=	9	ft2
No. extra girders=	2	
Girder length=	100	ft
Volume=	1800	ft3
γc=	150	lb/ft3
Weight=	270000	lb

Weight of the deck

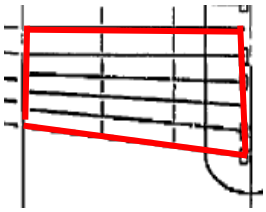

Adeck=	3233	ft2
Thickness=	7	in
Volume=	1886	ft3
γc=	150	lb/ft3
Weight=	282888	lb

Total Weight= 651531 lb

Line Weight

P-24= 6356 lb/ft

Appendix B

B.1 MATLAB code

This code allows to modify the column stiffness and gives the modal frequencies for different modification factors.

```
%% clean-up the workspace & command window

      clear;

      clc;

%  section=1;

   %% full path to the program executable

   %% set it to the installation folder

      ProgramPath     =     'C:\Program     Files     (x86)\Computers     and
Structures\CSiBridge 2016\CSiBridge.exe';

   %% pass data to Sap2000 as one-dimensional arrays

      feature('COM_SafeArraySingleDim', 1);


   %% pass non-scalar arrays to Sap2000 API by reference

      feature('COM_PassSafeArrayByRef', 1);


   %% create OAPI helper object

      helper = actxserver('CSiBridge18.helper');

      helper = helper.invoke('cHelper');


   %% create Sap2000 object

        sapObject = helper.CreateObject(ProgramPath);
          %% start Sap2000 application
```

```
   sapObject.ApplicationStart;



%% create SapModel object

   SapModel = sapObject.sapModel;
%% initialize model

   ret = SapModel.InitializeNewModel;

 %opens an existing file
   FileName = 'C:\File location'
   ret = SapModel.File.OpenFile(FileName)

 % UnLocks model
   ret = SapModel.SetModelIsLocked(false())

 %sets the modification factors for all columns to 1
    for i=1:8;
      Value(i,:) = 1;

    end
   ret = SapModel.PropFrame.SetModifiers('Column PW3)', Value);
   ret = SapModel.PropFrame.SetModifiers('Column P1', Value);
   ret = SapModel.PropFrame.SetModifiers('Column P2', Value);
   ret = SapModel.PropFrame.SetModifiers('Column P3', Value);
   ret = SapModel.PropFrame.SetModifiers('Column P4)', Value);
   ret = SapModel.PropFrame.SetModifiers('Column P5', Value);
   ret = SapModel.PropFrame.SetModifiers('Column P6', Value);
   ret = SapModel.PropFrame.SetModifiers('Column P8(1)', Value);
   ret = SapModel.PropFrame.SetModifiers('Column P8(2)', Value);
   ret = SapModel.PropFrame.SetModifiers('Column P7(1)', Value);
   ret = SapModel.PropFrame.SetModifiers('Column P7(2)', Value);
   ret = SapModel.PropFrame.SetModifiers('P9(1)', Value);
   ret = SapModel.PropFrame.SetModifiers('P9(2)', Value);
    ret = SapModel.PropFrame.SetModifiers('Column P13(1)', Value);
   ret = SapModel.PropFrame.SetModifiers('Column P13(2)', Value);
   ret = SapModel.PropFrame.SetModifiers('Column P14(1)', Value);
   ret = SapModel.PropFrame.SetModifiers('Column P13(2)', Value);
   ret = SapModel.PropFrame.SetModifiers('Column P11(1)', Value);
   ret = SapModel.PropFrame.SetModifiers('Column P11(2)', Value);
   ret = SapModel.PropFrame.SetModifiers('Column P16(1)', Value);
   ret = SapModel.PropFrame.SetModifiers('Column P16(2)', Value);
   ret = SapModel.PropFrame.SetModifiers('P10(1)', Value);
   ret = SapModel.PropFrame.SetModifiers('P10(2)', Value);
   ret = SapModel.PropFrame.SetModifiers('P12(1)', Value);
   ret = SapModel.PropFrame.SetModifiers('P12(2)', Value);
   ret = SapModel.PropFrame.SetModifiers('P17(1)', Value);
   ret = SapModel.PropFrame.SetModifiers('P17(2)', Value);
   ret = SapModel.PropFrame.SetModifiers('P18(1)', Value);
   ret = SapModel.PropFrame.SetModifiers('P18(2)', Value);
```

```
   ret = SapModel.PropFrame.SetModifiers('P19(1)', Value);
   ret = SapModel.PropFrame.SetModifiers('P19(2)', Value);
   ret = SapModel.PropFrame.SetModifiers('Column P20(1)', Value);
   ret = SapModel.PropFrame.SetModifiers('Column P20(2)', Value);
   ret = SapModel.PropFrame.SetModifiers('Column P21', Value);
   ret = SapModel.PropFrame.SetModifiers('Column P22', Value);
   ret = SapModel.PropFrame.SetModifiers('Column P23', Value);
   ret = SapModel.PropFrame.SetModifiers('Column P25', Value);
   ret = SapModel.PropFrame.SetModifiers('Column P24', Value);

   ret = SapModel.File.Save('ModelPath');

 %assign modification factors
  %redim Value(7)
  %runs different modification factors
  if section==1;
     for j=1:2;

  % UnLocks model
   ret = SapModel.SetModelIsLocked(false())
    for i=1:8;
      Value(i,:) = 1;

    end
    Value(5,:) = .4+.1*j;

   ret = SapModel.PropFrame.SetModifiers('Column PW3)', Value);

   %% save model

   ret = SapModel.File.Save('ModelPath');

   Valuenew(j,:)=Value(5,:);

%% run model (this will create the analysis model)

   ret = SapModel.Analyze.RunAnalysis();

 %% clear all case and combo output selections
  % ret = SapModel.Results.Setup.DeselectAllCasesAndCombosForOutput

 %% set case and combo output selections
   ret = SapModel.Results.Setup.SetCaseSelectedForOutput('MODAL')



 %% get modal period


       NumberResults = 1;
```

```
        LoadCase = cellstr(' ');

        Period = reshape(0:1,2,1);

        Frequency = reshape(0:1,2,1);

        StepType = cellstr(' ');

        StepNum = reshape(0:1,2,1);

        CircFreq = reshape(0:1,2,1);

        EigenValue = reshape(0:1,2,1);

      [ret, ~, LoadCases, StepType, CircFreq, StepNum, Frequency, Period,
EingenValue]    =    SapModel.Results.ModalPeriod(NumberResults,    LoadCase,
StepType, StepNum, Period, Frequency, CircFreq, EigenValue);

%stores the frequecies for desire mode
       Frequencynew1(j,:)=Frequency(1,1);
       Frequencynew2(j,:)=Frequency(1,2);
       Frequencynew3(j,:)=Frequency(1,3);
       Frequencynew4(j,:)=Frequency(1,4);
       Frequencynew5(j,:)=Frequency(1,5);
       Frequencynew6(j,:)=Frequency(1,6);
       Frequencynew7(j,:)=Frequency(1,7);
       Frequencynew8(j,:)=Frequency(1,8);
       Frequencynew9(j,:)=Frequency(1,9);
       Frequencynew10(j,:)=Frequency(1,10);
        end

end

    %Plots Modification factor vs Frequency
    plot(Valuenew,Frequencynew1);

% close Sap2000

      ret = sapObject.ApplicationExit(false());

      SapModel = 0;

      SapObject = 0;
```

B.2 Column Sensitivity Plots

Sensitivity plots for columns stiffness in the longitudinal and transverse direction.

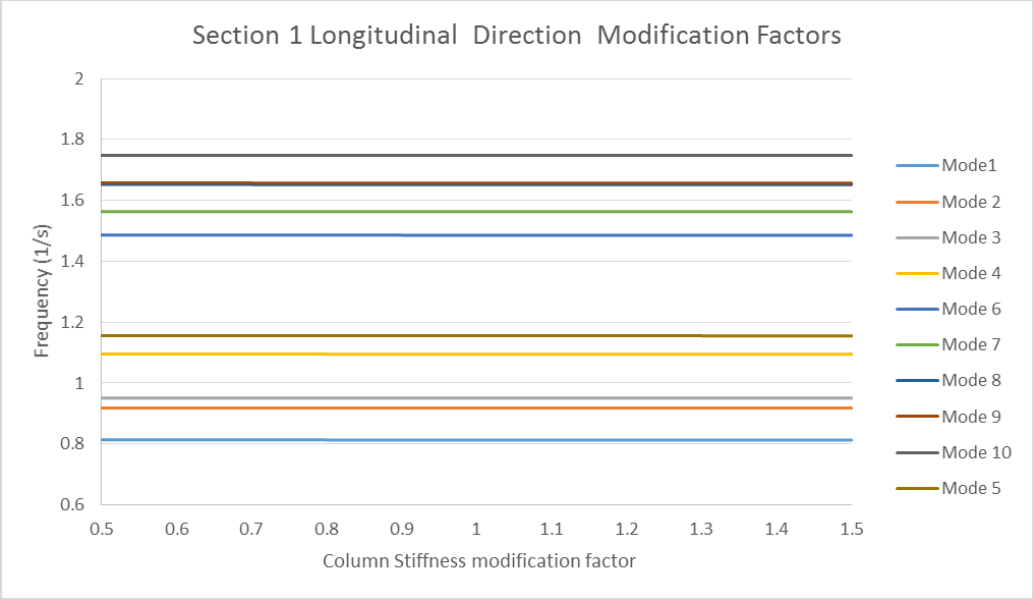

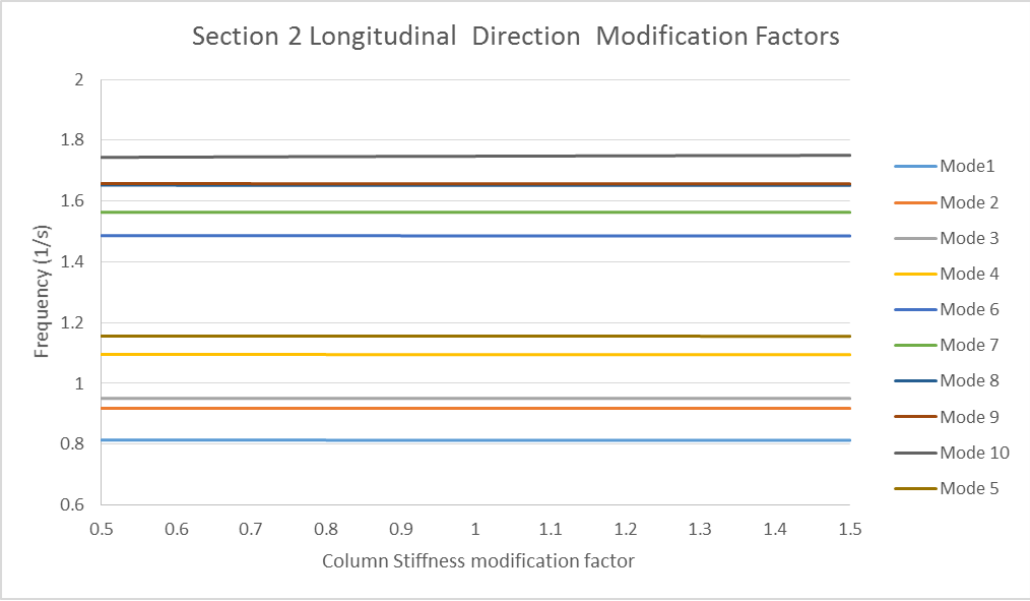

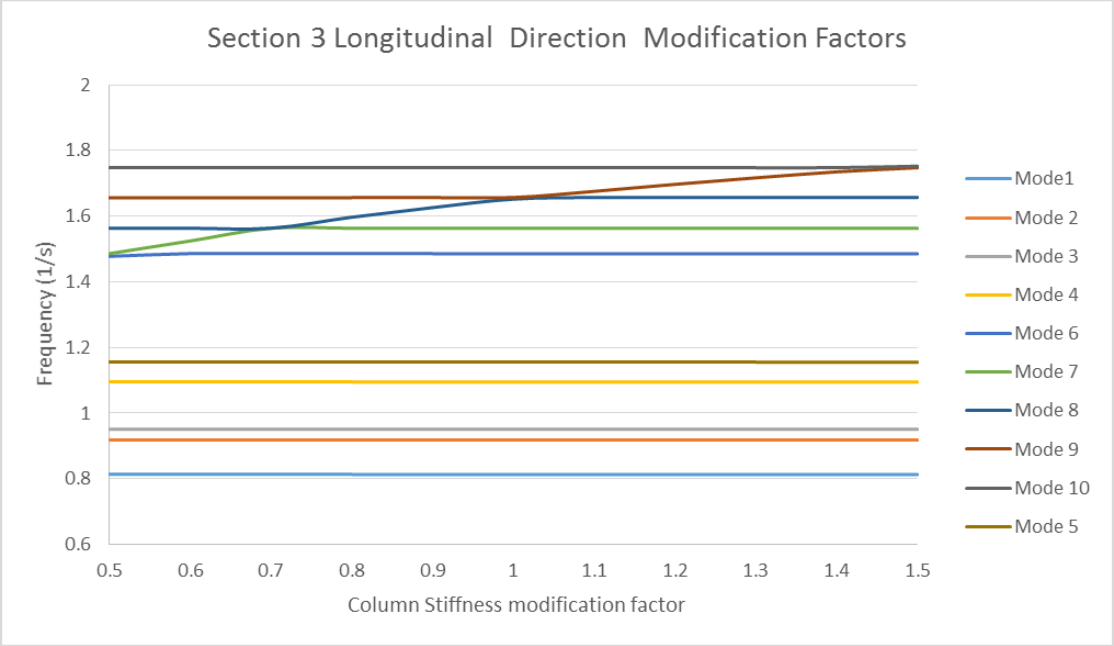
Section 3 Longitudinal Direction Modification Factors
Frequency (1/s)
2
1.8
1.6
1.4
1.2
1
0.8
0.6
0.5 0.6 0.7 0.8 0.9 1 1.1 1.2 1.3 1.4 1.5
Column Stiffness modification factor
Mode1
Mode 2
Mode 3
Mode 4
Mode 6
Mode 7
Mode 8
Mode 9
Mode 10
Mode 5

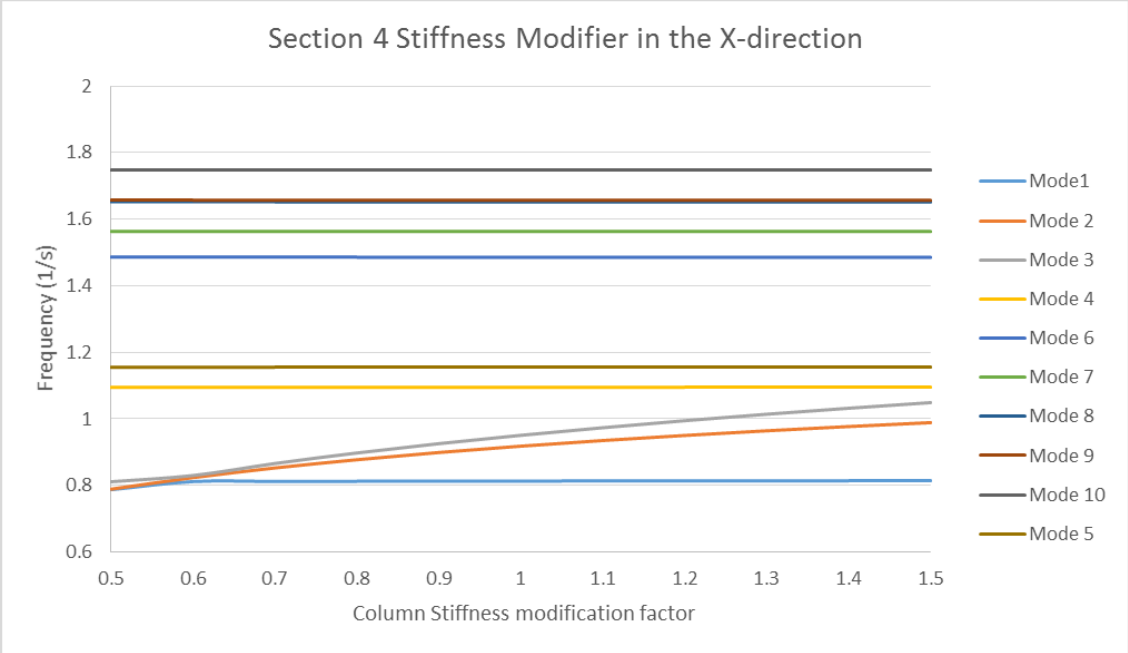
Section 4 Stiffness Modifier in the X-direction
Frequency (1/s)
2
1.8
1.6
1.4
1.2
1
0.8
0.6
0.5 0.6 0.7 0.8 0.9 1 1.1 1.2 1.3 1.4 1.5
Column Stiffness modification factor
Mode1
Mode 2
Mode 3
Mode 4
Mode 6
Mode 7
Mode 8
Mode 9
Mode 10
Mode 5

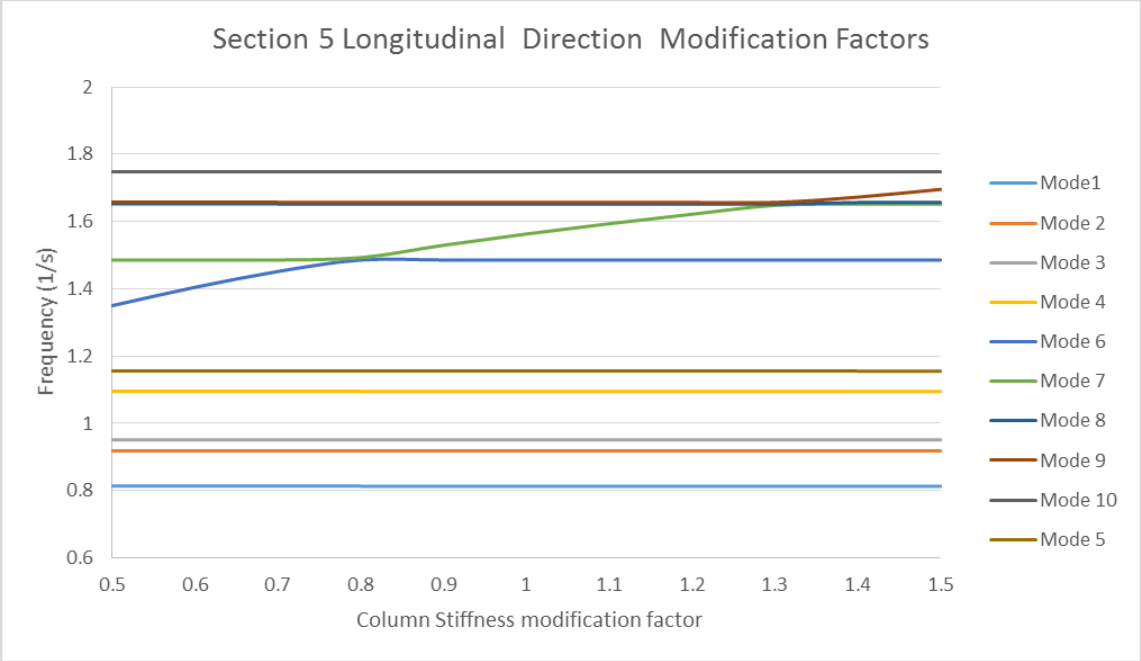
Section 5 Longitudinal Direction Modification Factors
Frequency (1/s)
2
1.8
1.6
1.4
1.2
1
0.8
0.6
0.5 0.6 0.7 0.8 0.9 1 1.1 1.2 1.3 1.4 1.5
Column Stiffness modification factor
Mode1
Mode 2
Mode 3
Mode 4
Mode 6
Mode 7
Mode 8
Mode 9
Mode 10
Mode 5

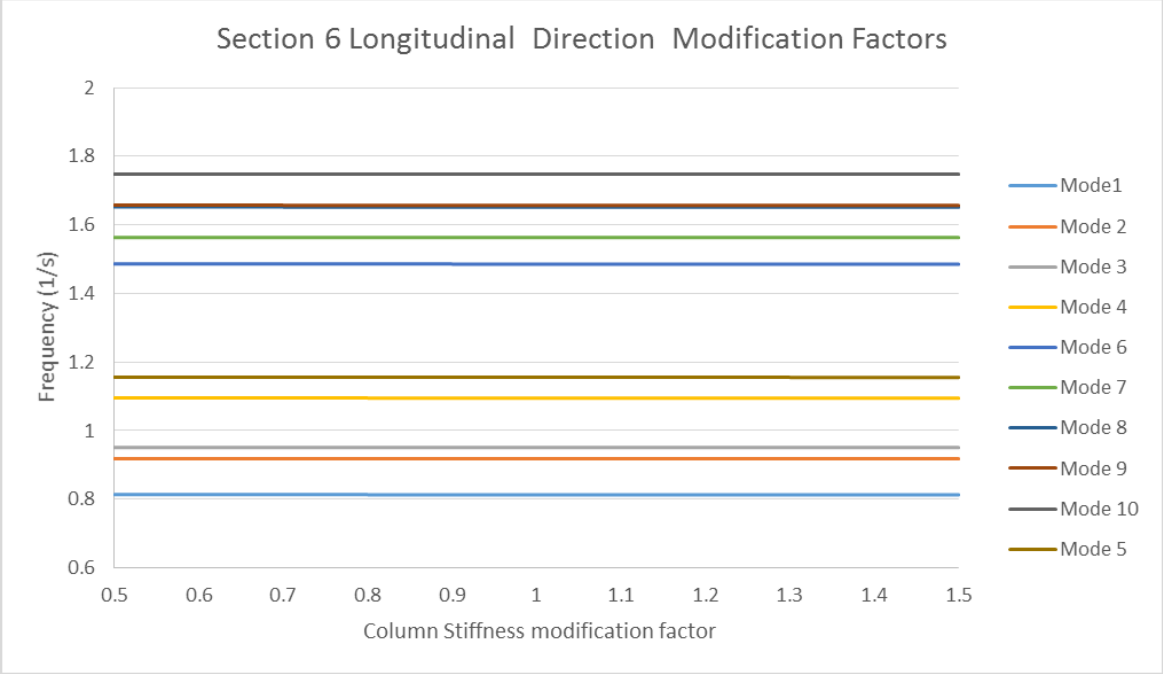
Section 6 Longitudinal Direction Modification Factors
Frequency (1/s)
2
1.8
1.6
1.4
1.2
1
0.8
0.6
0.5 0.6 0.7 0.8 0.9 1 1.1 1.2 1.3 1.4 1.5
Column Stiffness modification factor
Mode1
Mode 2
Mode 3
Mode 4
Mode 6
Mode 7
Mode 8
Mode 9
Mode 10
Mode 5

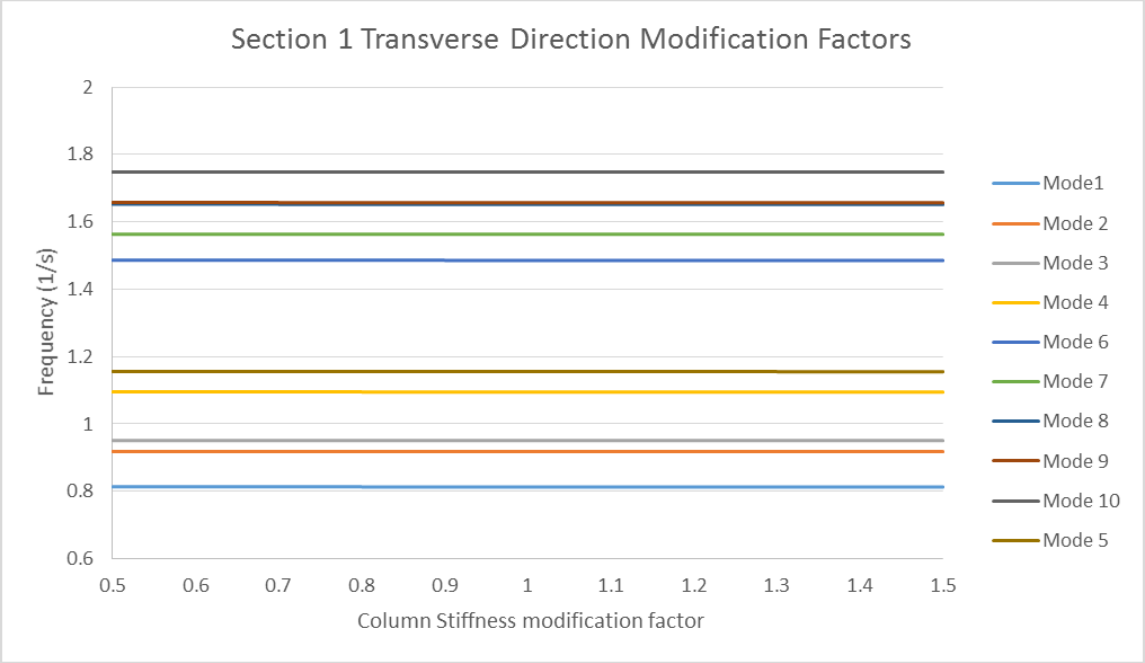
Section 1 Transverse Direction Modification Factors
Frequency (1/s)
2
1.8
1.6
1.4
1.2
1
0.8
0.6
0.5 0.6 0.7 0.8 0.9 1 1.1 1.2 1.3 1.4 1.5
Column Stiffness modification factor
Mode1
Mode 2
Mode 3
Mode 4
Mode 6
Mode 7
Mode 8
Mode 9
Mode 10
Mode 5

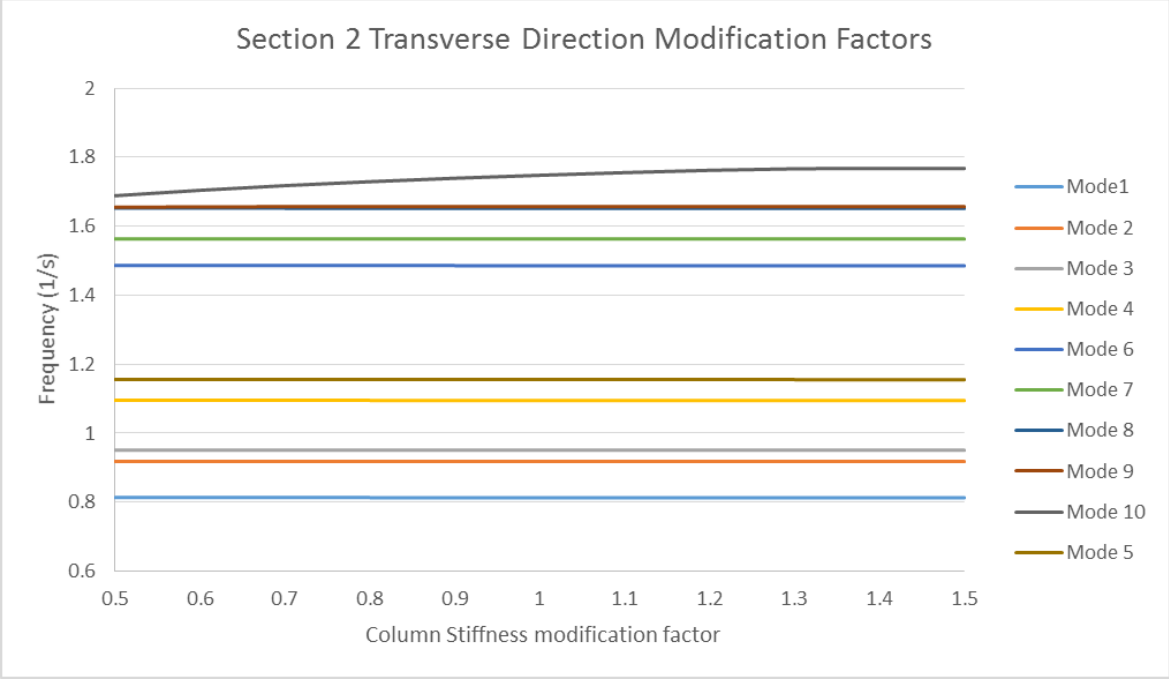
Section 2 Transverse Direction Modification Factors
Frequency (1/s)
2
1.8
1.6
1.4
1.2
1
0.8
0.6
0.5 0.6 0.7 0.8 0.9 1 1.1 1.2 1.3 1.4 1.5
Column Stiffness modification factor
Mode1
Mode 2
Mode 3
Mode 4
Mode 6
Mode 7
Mode 8
Mode 9
Mode 10
Mode 5

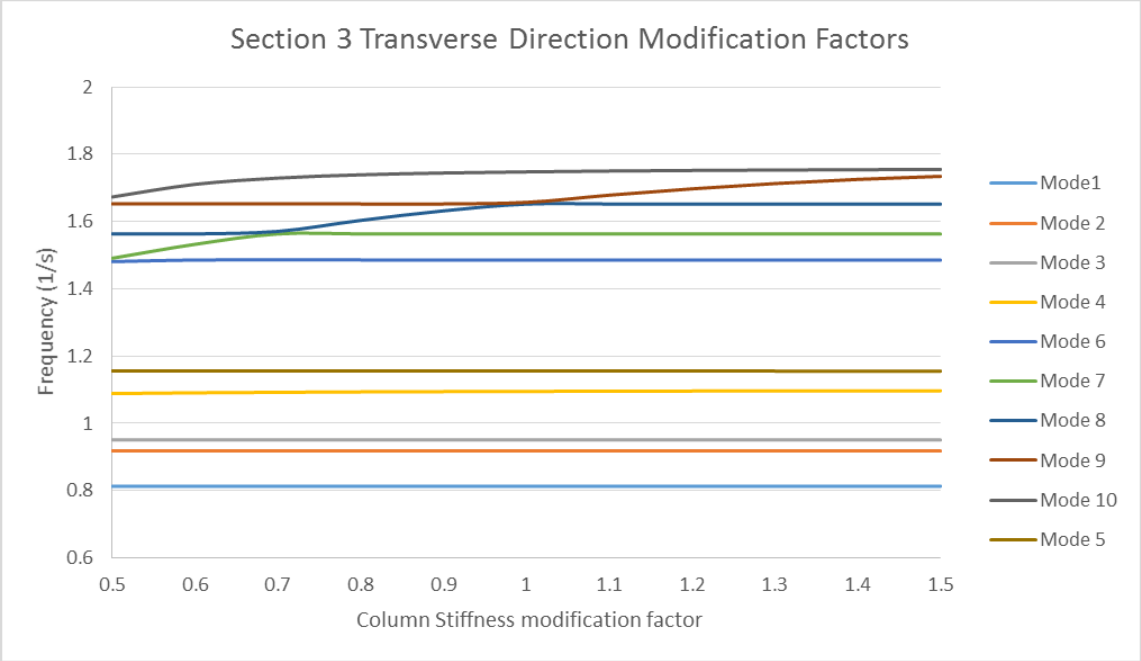
Section 3 Transverse Direction Modification Factors
Frequency (1/s)
2
1.8
1.6
1.4
1.2
1
0.8
0.6
0.5
0.6
0.7
0.8
0.9
1
1.1
1.2
1.3
1.4
1.5
Column Stiffness modification factor
Mode1
Mode 2
Mode 3
Mode 4
Mode 6
Mode 7
Mode 8
Mode 9
Mode 10
Mode 5

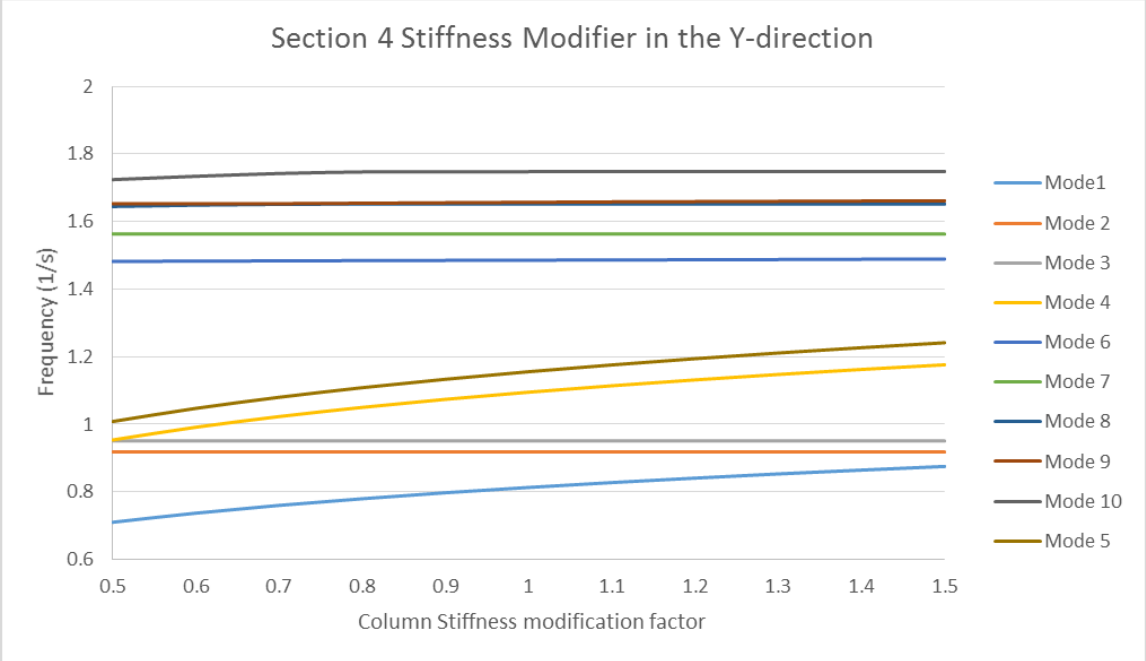
Section 4 Stiffness Modifier in the Y-direction
Frequency (1/s)
2
1.8
1.6
1.4
1.2
1
0.8
0.6
0.5
0.6
0.7
0.8
0.9
1
1.1
1.2
1.3
1.4
1.5
Column Stiffness modification factor
Mode1
Mode 2
Mode 3
Mode 4
Mode 6
Mode 7
Mode 8
Mode 9
Mode 10
Mode 5

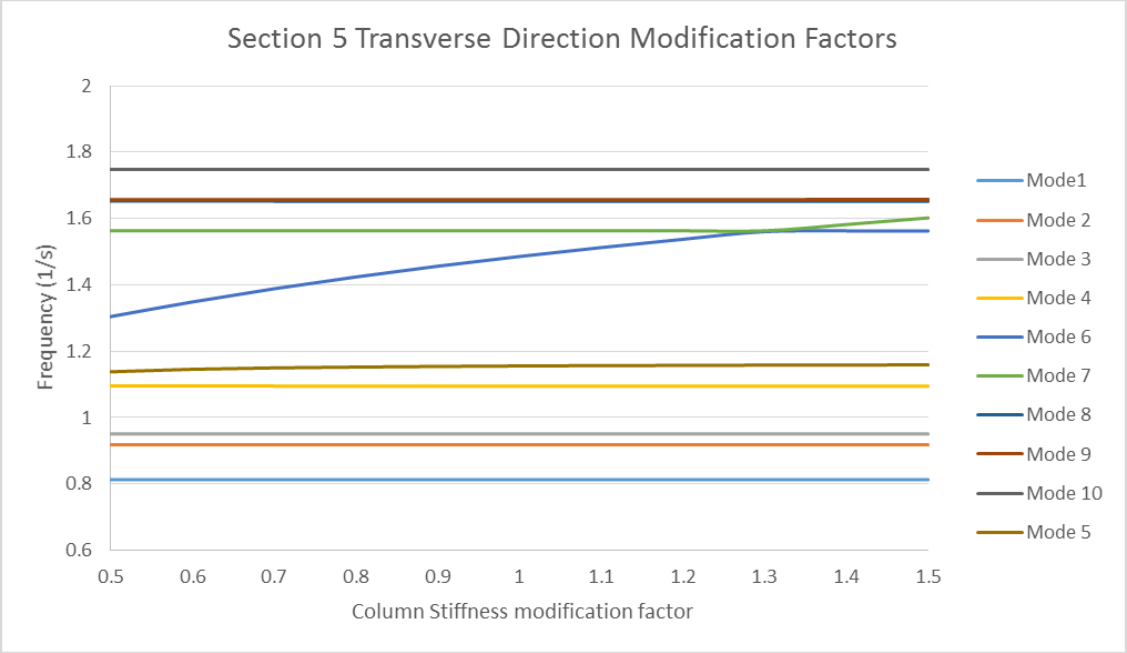
Section 5 Transverse Direction Modification Factors
Frequency (1/s)
2
1.8
1.6
1.4
1.2
1
0.8
0.6
0.5 0.6 0.7 0.8 0.9 1 1.1 1.2 1.3 1.4 1.5
Column Stiffness modification factor
Mode1
Mode 2
Mode 3
Mode 4
Mode 6
Mode 7
Mode 8
Mode 9
Mode 10
Mode 5

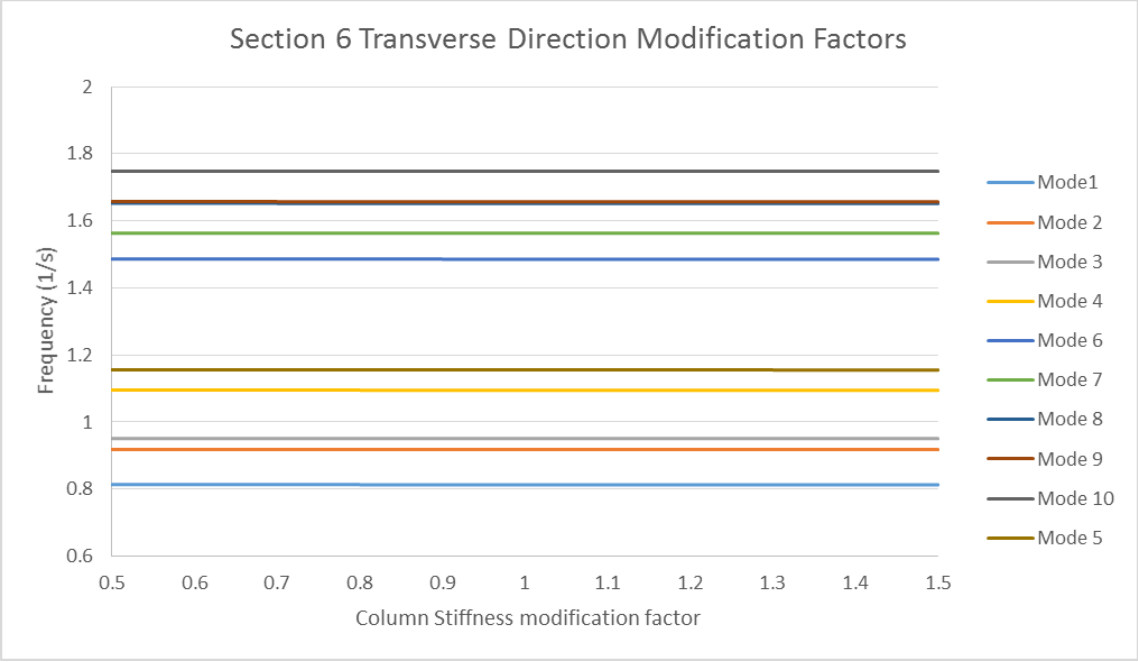
Section 6 Transverse Direction Modification Factors
Frequency (1/s)
2
1.8
1.6
1.4
1.2
1
0.8
0.6
0.5 0.6 0.7 0.8 0.9 1 1.1 1.2 1.3 1.4 1.5
Column Stiffness modification factor
Mode1
Mode 2
Mode 3
Mode 4
Mode 6
Mode 7
Mode 8
Mode 9
Mode 10
Mode 5